

THE UNIVERSITY OF CALGARY

Mechanical Models of Skeletal Muscle

by

Michael G. Anton

A THESIS

SUBMITTED TO THE FACULTY OF GRADUATE STUDIES
IN PARTIAL FULFILLMENT OF THE REQUIREMENTS FOR THE
DEGREE OF
DOCTOR OF PHILOSOPHY

DEPARTMENT OF MECHANICAL ENGINEERING

CALGARY, ALBERTA

DECEMBER, 1991

© Michael G. Anton 1991



National Library
of Canada

Bibliothèque nationale
du Canada

Canadian Theses Service Service des thèses canadiennes

Ottawa, Canada
K1A 0N4

The author has granted an irrevocable non-exclusive licence allowing the National Library of Canada to reproduce, loan, distribute or sell copies of his/her thesis by any means and in any form or format, making this thesis available to interested persons.

The author retains ownership of the copyright in his/her thesis. Neither the thesis nor substantial extracts from it may be printed or otherwise reproduced without his/her permission.

L'auteur a accordé une licence irrévocable et non exclusive permettant à la Bibliothèque nationale du Canada de reproduire, prêter, distribuer ou vendre des copies de sa thèse de quelque manière et sous quelque forme que ce soit pour mettre des exemplaires de cette thèse à la disposition des personnes intéressées.

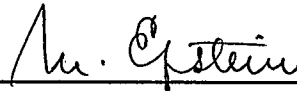
L'auteur conserve la propriété du droit d'auteur qui protège sa thèse. Ni la thèse ni des extraits substantiels de celle-ci ne doivent être imprimés ou autrement reproduits sans son autorisation.

ISBN 0-315-75305-6

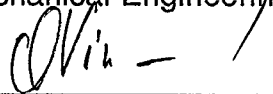
Canada

THE UNIVERSITY OF CALGARY
FACULTY OF GRADUATE STUDIES

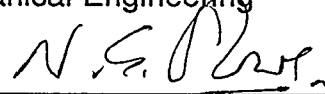
The undersigned certify that they have read, and recommended to the Faculty of Graduate Studies for acceptance, a thesis entitled, "Mechanical Models of Skeletal Muscle" submitted by Michael G. Anton in partial fulfillment of the requirements for the degree of Doctor of Philosophy.



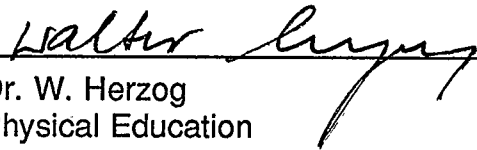
Supervisor, Dr. M. Epstein
Mechanical Engineering



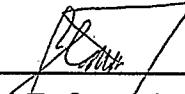
Dr. O. Vinogradov
Mechanical Engineering



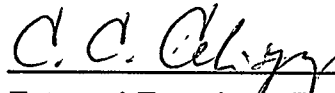
Dr. N.G. Shrive
Civil Engineering



Dr. W. Herzog
Physical Education



Dr. J.F. Stanislav
Chemical and Petroleum Engineering



External Examiner, Dr. C.C. Celigoj
Mechanical Engineering
Technical University of Graz, Austria

December 19, 1991

Abstract

Geometrical muscle models are typically based on kinematic constraints, that is, the modes of muscle deformation are preset. Whereas kinematically based models have been shown to predict muscle behaviour accurately, the contribution of the kinematic constraints to the favourable model predictions can only be assessed by eliminating them from the model definition. To this end, a muscle model has been developed which is based on a constitutive description of muscle tissue and the theory of deformable continua (continuum muscle model). Consequently, muscle deformations result from the solution of the structural problem posed, and the internal stress distributions become accessible. The continuum muscle model has been explored by using the Finite Element Method.

In order to establish a connection with the traditional approach to muscle modelling, the continuum muscle model has been preceded by a model which is based on kinematically constrained deformation modes. Paying special attention to physical consistency and simplicity, this model incorporates consistent equilibrium considerations which relate the external muscle forces to the internal

fibre forces, and the equations describing the model are expressed by a closed set of nonlinear algebraic equations. Keeping with the presently accepted view of muscle structure and function, the assumptions underlying both models are that (a) muscle fibres are one-dimensional entities and that (b) the mechanical muscle behaviour is a reflection of the active and passive muscle fibre characteristics exclusively.

Model predicted muscle force-length curves have shown a notable dependency on the parameters which describe the muscle geometry and on the geometrical boundary conditions. In general, the muscle optimal force is predicted for a muscle configuration which is different from the one at which the muscle fibres assume optimal length. On account of the continuum formulation novel considerations regarding intra-muscular pressure have been possible.

A number of disparities have been observed between model predictions and experimental results which are tied to the underlying assumptions of one-dimensional fibre characteristics. Consequently, a reexamination of mechanical muscle tissue characteristics versus single muscle fibre characteristics seems to be indicated.

to Sylviane, Myriam and Marcelo

Acknowledgements

Many thanks to

Dr. Marcelo Epstein, for his patience, for the generous sharing of his time and insights, and most of all for being a friend.

Dr. Walter Herzog, for co-supervising my research work and for giving me access to his experimental knowledge of muscle behaviour.

Dr. Benno Nigg, director of the Human Performance Laboratory, and all his staff for having me as a guest for one year.

Herzlichen Dank an meine Familie, ganz besonders an meine Eltern, für ihre Unterstützung.

Et un grand merci également à ma belle-famille.

Thank you also to all those who helped me in many ways, particularly

Antonio Guimaraes
Dr. John Matyas
Tim Leonard
Cathy Fisher
Brad Stephens

Mike Johnson
Nick Vogt
Roy Bechtold
... and all those in room PE 207

Table of Contents

Approval Page	ii
Abstract	iii
Dedication	v
Acknowledgements	vi
Table of Contents	vii
List of Tables	x
List of Figures	xi
1 Introduction	1
2 Review of Background Material	7
2.1 Continuum Mechanics	7
2.1.1 Kinematics	8
2.1.2 Stress State and Equilibrium Condition	11
2.1.3 Constitutive Relations	13
2.2 The Finite Element Method	14
2.3 The Structure of Skeletal Muscle	16
2.4 Muscle Models	19
2.4.1 Functional Muscle Models	20
2.4.2 Geometrical Muscle Models	24

3	Straight Line Geometrical Muscle Model	28
3.1	Initial Considerations	30
3.2	Model Derivation	35
3.2.1	Simplifications and Assumptions Underlying the Model	35
3.2.2	Muscle Model Geometry and Kinematics of Deformation	38
3.2.3	Fibre Force-Length Relation	44
3.2.4	Equilibrium Conditions	53
3.3	Model Exploration and Discussion	58
3.4	Summary and Outlook	80
4	The Continuum Muscle Model	82
4.1	Simplifications and Assumptions	84
4.2	Constitutive Relations	90
5	The Finite Element Implementation	106
5.1	Formulation of a Custom Finite Element	107
5.2	The global Finite Element Muscle Model	120
6	Stress State, Intra-Muscular Pressure and Global Equilibrium	125

7 Finite Element Model Simulations: Trapezoidal Muscle Geometry	141
7.1 Constant Fibre Force	142
7.2 Fibre Stretch Ratio dependent Fibre Force	151
7.2.1 Fibre Force Profile Number 1	151
7.2.2 Fibre Force Profile Number 2	167
7.3 Curved Muscle Fibres	171
8 Finite Element Simulations: Gastrocnemius Geometry	178
8.1 Fibre Force Profile Number 2	179
8.2 Alternate Mode of Muscular Contraction	186
9 Summary and Conclusions	192
Bibliography	196

List of Tables

Table 3.1: Major simplifications and assumptions underlying the straight line muscle model.	37
Table 3.2: Parameter values for initial muscle model simulations.	62
Table 4.1: Major simplifications and assumptions underlying the continuum muscle model.	89

List of Figures

Figure 3.1:	Schematic geometry of pennate muscles.	31
Figure 3.2:	Consequences of muscle deformation and different initial muscle geometries on specific muscle attributes.	33
Figure 3.3:	Muscle model geometry (lateral muscle cross section).	39
Figure 3.4:	General deformation of a muscle fibre or muscle fibre bundle.	43
Figure 3.5:	Fibre force and fibre stress profiles (force profile number 1). . .	46
Figure 3.6:	Active fibre force and stress profiles (force profile number 1). .	49
Figure 3.7:	Alternate active fibre force and stress profiles (force profile number 2).	52
Figure 3.8:	Free body diagrams for the entire muscle and the upper tendon sheath.	55
Figure 3.9:	Active muscle force-length relations of similar muscles with different reference angles of pinnation.	63
Figure 3.10:	Active muscle force-length relations of muscles with alternate geometry.	66
Figure 3.11:	Total muscle force-length curves.	68
Figure 3.12:	Active muscle force-length curves based on fibre force profile number 2.	69
Figure 3.13:	Range in the actual angle of pinnation and the actual angle of pinnation corresponding to the muscle peak force as functions of the reference angle of pinnation.	71
Figure 3.14:	Range in the actual muscle length, the actual muscle length corresponding to the muscle peak force, and the muscle reference length as functions of the reference angle of pinnation.	72
Figure 3.15:	Muscle force at muscle reference length and muscle peak force as functions of the reference angle of pinnation.	73
Figure 3.16:	Muscle work over a complete contraction as a function of the reference angle of pinnation.	74
Figure 3.17:	Influence of trapezoidal muscle cross section and depth change during contraction on the muscle peak force.	78

Figure 4.1:	Fibre second Piola-Kirchhoff stress and Cauchy stress components with respect to local coordinate systems.	99
Figure 4.2:	Force profile number 1.	102
Figure 4.3:	Force profile number 2.	103
Figure 4.4:	The influence of the stimulation parameter, θ , on force profile number 1.	104
Figure 5.1:	Triangular element geometry in reference and spatial configuration, and unit triangle.	109
Figure 5.2:	Element fibre direction in the reference configuration and element reference coordinate system (X' - Y').	112
Figure 5.3:	Multiple equilibrium configurations illustrated for the case of a general non-linear function.	118
Figure 5.4:	Finite element muscle model geometries (not to scale) and finite element mesh.	121
Figure 5.5:	Finite element muscle model geometries (to scale).	121
Figure 6.1:	Tendon sheath curvature in relation to applied loads.	127
Figure 6.2:	Stress state for a volume element adjacent to the tendon sheath.	129
Figure 6.3:	Hydrostatic pressure within the muscle tissue fluid matrix.	131
Figure 6.4:	Shear stresses acting on the muscle body.	136
Figure 6.5:	Muscle model behaviour based on the geometrically linear theory.	137
Figure 6.6:	Lines of constant pressure in the muscle tissue fluid matrix.	139
Figure 6.7:	Nodal reaction forces for nodes along the tendonal boundaries.	140
Figure 7.1:	Muscle geometry and deformations for constant fibre force.	144
Figure 7.2:	Muscle force length curves for muscle with fibre stretch ratio independent fibre forces.	147
Figure 7.3:	Comparison of muscle force length curves.	149
Figure 7.4:	Deformations of a muscle model which is based on fibre stretch ratio dependent fibre forces.	152
Figure 7.5:	Tendon sheath strain.	155
Figure 7.6:	Muscle force length curves for muscle with fibre stretch ratio dependent fibre force (symmetric active force profile).	156
Figure 7.7:	Force displacement history for a component having a nonlinear force length relation with inflection point.	158

Figure 7.8:	Muscle force length curves for muscle with fibre stretch ratio dependent fibre force (symmetric active force profile).	160
Figure 7.9:	Effects of tendon stretch on fibre angle of pinnation and fibre length.	163
Figure 7.10:	Muscle force length curves for muscle with fibre stretch ratio dependent fibre force (asymmetric active force profile). . . .	168
Figure 7.11:	Muscle force length curves for muscle with fibre stretch ratio dependent fibre force (asymmetric active force profile). . . .	170
Figure 7.12:	Muscle with initially curved fibres.	172
Figure 7.13:	Muscle force length curves for muscle with initially curved fibres.	174
Figure 7.14:	Nodal reaction forces for the muscle fluid matrix elements. . .	175
Figure 8.1:	Medial gastrocnemius muscle geometry and deformations. . . .	180
Figure 8.2:	Medial gastrocnemius muscle deformations for supported lower tendon sheath boundary.	183
Figure 8.3:	Muscle force length curves for medial gastrocnemius muscle with supported lower tendon sheath.	185
Figure 8.4:	Muscle deformation, tissue - tendon sheath interaction, and tissue matrix pressure distribution based on the alternate mode of muscular contraction.	189

Chapter 1

Introduction

The contraction of skeletal muscle acting on the skeletal system is responsible for vertebrate locomotion and movement. In the process of muscle contraction muscle cells convert chemical energy into mechanical work; muscle cells produce forces which are channelled by tendinous structures to either side of skeletal articulations, i.e., joints, and induce movement of the skeletal system. Whereas the cause of muscle contraction falls into the domain of biology, the exploration of intra- and extra-muscular force transmission and its dependence on muscle structure falls into the domain of mechanics.

Studying muscles from a mechanical point of view, adds a further facet to the body of knowledge assembled in the fields of bio-chemistry, muscle neurology, physiology, morphology, etc. It is hoped that the integration of information obtained in the different disciplines will result in beneficial contributions to the development of medical procedures, to the field of rehabilitation and to the design of prostheses.

The understanding of muscular function may also be of interest in technical areas, in particular in the field of robotics. Actuators based on muscular-skeletal design principles might improve on current implementations from the perspective of efficiency, motor fine control and failure tolerance.

Stimulated muscle fibres have different characteristics from unstimulated muscle fibres. In particular, stimulation causes muscle fibres to generate forces, whose magnitude depends on the fibre length, and to contract. The mechanics of muscular contraction on a microscopic scale as well as the associated active (stimulated) and passive (unstimulated) muscle fibre characteristics are thought to be well understood both from an experimental and theoretical point of view. The most widely accepted models (or theories) of muscular contraction on a microscopic scale, that is the Cross Bridge Theory and the Sliding Filament Theory, are results of relatively recent research by Huxley [1957, 1974] and Gordon et al. [1966].

By contrast, models of entire muscles have a far longer tradition. The first efforts to investigate muscular function scientifically were undertaken by Giovanni Alfonso Borelli (1608 - 1679) and Niels Stenson (1638 - 1686). Stenson recognized the pennate structure of muscle, that is, the arrangement of muscle fibres at an angle relative to the direction of muscular force exertion. He demonstrated, based on geometrical arguments, that muscles could contract without changing their volume. This assertion contradicted the conviction held by his contemporaries that the

animal spirit entered and inflated the muscle, thus causing the tendency of muscle shortening.

The currently most cited (pennate) muscle models have been proposed by Woittiez et al. [1983, 1984] and Otten [1985, 1987a, 1987b, 1988]. In general, these models are based on kinematic constraints, that is, the mode of muscle deformation is preordained with the imposed mode of muscle deformation showing a close resemblance to the work of Stenson. The models incorporate the present knowledge of active and passive muscle fibre behaviour and are essentially based on the assumptions of one-dimensional fibres with uni-directional fibre activity, non-interaction between neighbouring fibres, and the constancy of muscle volume.

From an analytical point of view, restricting potential muscle deformations by kinematic constraints reduces the number of degrees of freedom inherent to the model and guarantees solutions independent of more detailed considerations concerning the constitutive character of muscle tissue. Because of the lack of general constitutive relations in combination with an adequate theory of deformation, considerations regarding the internal stress state of the muscle and statements pertaining to the adequacy of the imposed deformation modes with respect to local equilibrium of the structure are not possible. Whereas kinematically based models have been shown to predict muscle behaviour accurately, the contribution of the kinematic constraints to the favourable model predictions can only be assessed by eliminating them from the model definition.

It is, therefore, the goal of this thesis, to develop a muscle model which is based on a constitutive description of muscle tissue and on the theory of deformable continua. This continuum muscle model will be used to explore in more detail the relationship between the tissue contractile condition, the muscle tissue stress state and the muscle deformation, and to observe their consequences on the muscle force-length curve.

Muscle tissue will be interpreted as a composite material constituted of a fibrous component, which carries the active and passive characteristics of muscle fibres, embedded in a fluid matrix. Both the physical non-linearity due to nonlinear fibre characteristics and the geometrical non-linearity due to the large deformations innate to muscle contractions will be incorporated into the model. No kinematic constraints will be applied, except for anatomically justifiable boundary conditions. The general approach taken allows for a natural inclusion of muscle tendon sheath elasticity and deformability into the muscle model. Solutions of the structural problem will be sought using the Finite Element Method.

The continuum muscle model will be preceded by a "Woittiez-type" muscle model which is based on kinematically constrained muscle deformation modes (Chapter 3). The purpose of this model is to establish a basis to which the continuum model can be compared, thus highlighting the differences between the two modelling approaches and their predictions. In its formulation, the model is simple enough to be described by a closed set of algebraic equations, yet it

contains most of the prominent features of Woittiez' original model. The transparent form of the equations governing this model allows for certain general observations regarding the model behaviour to be made independently of any numerical analysis. The model will be explored on its own merits with regard to muscle work, optimal muscle forces, active muscle range and the relationship between optimal fibre force and optimal muscle force.

The literature predominantly records models of pennate muscles. In order to compare the predictions of the here presented models to those by other authors, only pennate muscles will be considered in this thesis. The formulation of the continuum muscle model, however, contains no intrinsic limitations which would preclude the modelling of fusiform muscles, that is, muscles where the muscle fibres are aligned with the direction of muscular force exertion.

The primary concern in developing the muscle models is directed towards their internal consistency. Starting with the assumptions underlying the models, the tools of mathematical physics are applied rigorously. Consequently, expected and unexpected model behaviour have to be seen as a direct reflection of the underlying assumptions, and the model behaviour will have to be interpreted as such. The most important assumptions underlying the presented models are, that muscle fibres have one-dimensional active and passive characteristics coincident with their length axis, that there is no direct interaction between neighbouring muscle fibres, and that muscle tissue is incompressible.

In order to avoid confusion in the main body of the text, the following comments should be made: When not stated otherwise, general remarks related to muscle fibres or muscle tissue refer to mammalian muscle, more specifically to cat muscle. Unreferenced model comparisons to experimental results and experimental observations are made with respect to experiments conducted independently of this thesis by Dr. Walter Herzog in his laboratory at the University of Calgary. The term "straight line muscle model" has to be seen in the context of the model developed in Chapter 3 which does, on purpose, not include any generalized constitutive law for muscle tissue. Models on the same level of abstraction which include a more involved description of muscle tissue are absolutely conceivable. Muscle model geometries in this thesis are loosely tied to the cat medial gastrocnemius muscle. The focus of this thesis rests, however, on considerations related to pennate muscles in general. The derivation and analysis of the presented models are restricted to quasi-static situations.

Chapter 2

Review of Background Material

This chapter provides a short summary of material which is relevant to the subject of this thesis. Starting with the concepts underlying the Mechanics of Continua and an outline of the Finite Element Method, the chapter will conclude by giving a brief description of the structure of skeletal muscle and by reviewing muscle models presented in the literature.

2.1 Continuum Mechanics

This section summarizes concepts of Continuum Mechanics. The selection of topics covered corresponds to what will be needed in setting up the proposed continuum muscle model. In particular, the geometrically nonlinear theory of deformation will be covered, because of the large deformations inherent to muscle deformations. The treatment follows Truesdell [1965], Malvern [1969] and Becker [1975].

The following conventions will be adopted throughout this section: tensor entities will be represented alternatively in component form, e.g. x_i , σ_{ij} , and symbolic notation, (\mathbf{x}, σ) . Tensor components will be referred to three-dimensional Cartesian coordinate systems, tensor indices run from 1 to 3, and the same index appearing twice in any given term implies a summation of terms, e.g. $x_i y_i \equiv \sum_{i=1}^3 x_i y_i$. Partial derivatives with respect to coordinates will be abbreviated by the comma operator; $\frac{\partial(\)}{\partial x_i} \equiv (\)_{,i}$.

2.1.1 Kinematics

A body of a finite volume occupies a region in space. The identification of the body particles with their coordinates in three-dimensional euclidean space is termed a configuration. Given a body in its original (reference) and deformed (actual or spatial) state, the deformation can be described mathematically by a mapping from the reference configuration onto the deformed configuration:

$$x_i = x_i(X_J) \quad (2.1)$$

The coordinates x_i refer to the deformed, and X_J refer to the reference configuration. Differentiating Equation 2.1 results in:

$$dx_i = \frac{\partial x_i(X_K)}{\partial X_J} dX_J = x_{i,J} dX_J \equiv F_{i,J} dX_J \quad (2.2)$$

or in symbolical notation:

$$dx = F dX \quad (2.3)$$

The deformation gradient tensor, F , maps a line element in the reference configuration to the corresponding line element in the deformed configuration; the volumetric relation between a reference and actual volume element is given by $dV = \det F dV_0$. F is in itself a measure of deformation. It contains, however, information about rigid body rotations which require special attention in the constitutive relations. According to the polar decomposition theorem, F can be represented by:

$$F = RU \quad \text{or} \quad F = VR \quad (2.4)$$

This describes the decomposition of a general deformation into a rotation and a pure deformation (R being a proper orthogonal rotation tensor and U and V symmetric positive definite stretch tensors).

The right and left Cauchy-Green deformation (or stretch) tensors (C and B) are defined by:

$$C = F^T F = U^2 \quad \text{and} \quad B = F F^T = V^2 \quad (2.5)$$

A deformation, as opposed to a rigid body motion, is characterized by a change of distances between neighbouring material particles. This aspect of the deformation leads to the (classical) strain measures **L** and **E**, the Lagrange and Euler finite strain tensors. Below, only **L** will be discussed, which is defined by:

$$\mathbf{L} = \frac{1}{2}(\mathbf{C} - \mathbf{I}) \quad (2.6)$$

with **I** being the identity tensor.

Relating the reference and spatial configuration to the same coordinate system and introducing a displacement vector **u** through $\mathbf{x} = \mathbf{X} + \mathbf{u}$, one arrives at the strain displacement relation

$$L_{IJ} = \frac{1}{2}(u_{I,J} + u_{J,I} + u_{K,I}u_{K,J}) \quad (2.7)$$

In linear elasticity one assumes that the displacements u_i as well as the displacement gradients $u_{i,j}$ remain small. The quadratic terms in Equation 2.7 as well as the distinction between the referential and spatial coordinate systems can be neglected in this case, and one obtains the geometrically linearized strain tensor:

$$\varepsilon_{ij} = \frac{1}{2}(u_{i,j} + u_{j,i}) \quad (2.8)$$

2.1.2 Stress State and Equilibrium Condition

A material volume which is subjected to surface forces (\mathbf{t}) and body forces (\mathbf{k}) will deform into a new equilibrium configuration. As a consequence, forces will be transmitted internally from one portion of the continuum to another. Using the Method of Sections, the continuum can be separated at any point and the interaction between the two section surfaces can be represented by force and moment resultants \mathbf{f} and \mathbf{m} . Focusing on one section surface, a resultant force $\Delta \mathbf{f}$ and resultant moment $\Delta \mathbf{m}$ will be transmitted over a section surface area element ΔS surrounding a given point P . The Cauchy Stress Principle states that $\lim_{\Delta S \rightarrow 0} \frac{\Delta \mathbf{f}}{\Delta S}$ will have a definite value $\frac{d\mathbf{f}}{dS} = \mathbf{t}^{(n)}$, called the stress vector, and that the moment resultant will vanish in the limit. The stress vector $\mathbf{t}^{(n)}$ depends in general not only on the point P , but also on the orientation of the surface element, which is defined by its unit normal \mathbf{n} .

It can be shown through the force and moment equilibrium of an infinitesimal tetrahedron and parallelepiped that there exists a symmetric stress tensor σ_{ij} , called the Cauchy stress tensor, which completely specifies the stress state at a point. The stress vector on a surface element with unit normal \mathbf{n} at this point is obtained from:

$$t_i = \sigma_{ji} n_j \quad (2.9)$$

Equilibrium considerations on an arbitrary portion of the material volume lead to the equilibrium conditions:

$$\sigma_{ji,j} + k_i = 0 \quad (2.10)$$

where \mathbf{k} refers to a volume force density. These equilibrium conditions are supplemented by the traction boundary conditions

$$\sigma_{ji} n_j = t_i(a_\alpha) \quad (2.11)$$

with a_α being a suitable parametrization of the volume boundary, and suitable geometrical boundary conditions. The Cauchy stress tensor (σ) expresses stresses in terms of the deformed configuration. However, when solving a specific problem, the deformed configuration is initially unknown in general. The deformation is, therefore, most suitably expressed using one of the referential strain tensor (\mathbf{C} or \mathbf{L}). On the other hand, the conjugate entity to the Lagrange finite stress tensor \mathbf{L} is the second Piola-Kirchhoff stress tensor, \mathbf{S} , where the stresses are expressed in terms of the un-deformed geometry. The relation between σ and \mathbf{S} is given by:

$$\sigma = \frac{1}{|F|} \mathbf{F} \mathbf{S} \mathbf{F}^T \quad (2.12)$$

The following equation presents the relation between the second Piola-Kirchhoff stress, \mathbf{S} , and the first Piola-Kirchhoff stress, \mathbf{P} , where the latter will have some significance for the derivation of the constitutive relations in the context of this thesis.

$$\mathbf{P} = \mathbf{F} \mathbf{S} \quad (2.13)$$

If both the displacements and displacement gradients are small, no distinction needs to be made between the reference and the deformed description. In that case, a distinction between Cauchy and Piola-Kirchhoff stresses is not necessary and only one stress tensor will be used, denoted σ .

2.1.3 Constitutive Relations

The constitutive relations establish a relationship between the strain measures and the stresses in a continuum. While the discussion in the previous sub-chapters was independent of any specific material, the constitutive equations rest on the particularities of the materials out of which the continuum of interest is composed; universal constitutive relations, which would be valid for an arbitrary material are not known.

In this thesis, muscle tissue will be treated as a composite (fibre reinforced) material, which is composed of a fluid matrix and contractile fibres. The fibres run in a well defined direction at any point within the continuum. If a strain energy

function, W , is assumed to exist for an isotropic material with one family of fibres, Spencer [1984] demonstrated by the theory of invariants that this energy function can only depend on the following invariants (I_α):

$$\begin{aligned} I_1 &= \text{tr} \mathbf{C}, \quad I_2 = \frac{1}{2}((\text{tr} \mathbf{C})^2 - \text{tr} \mathbf{C}^2), \quad I_3 = \det \mathbf{C} \\ I_4 &= \mathbf{a} \mathbf{C} \mathbf{a} = \lambda^2, \quad I_5 = \mathbf{a} \mathbf{C}^2 \mathbf{a} \end{aligned} \quad (2.14)$$

where \mathbf{a} represents the unit vector in fibre direction, and λ is the fibre stretch ratio. As before, \mathbf{C} denotes the left Cauchy-Green stretch tensor.

By definition, the second Piola-Kirchhoff stress tensor components follow from the strain energy function, $W(I_\alpha)$, through:

$$S_{KL} = \sum_{\alpha=1}^5 \frac{\partial W}{\partial I_\alpha} \left(\frac{\partial I_\alpha}{\partial C_{KL}} + \frac{\partial I_\alpha}{\partial C_{LK}} \right) \quad (2.15)$$

2.2 The Finite Element Method

In the context of solving analytical problems in the theory of continuous media, one usually searches for fields (e.g. stresses and displacements) which are governed by differential (or integral) equations, and which correspond, for example, to the equilibrium state of a continuum under a certain loading and certain boundary conditions. An exact solution is more often than not unobtainable.

Consequently, an approximate solution is usually sought by using a discretization method which reduces the infinite number of degrees of freedom of a continuum to a finite number of degrees of freedom or parameters, and which converges to the exact solution as the number of parameters is increased. Different discretization methods in common use include the power series expansion method, the finite difference method, direct methods of variational calculus (Ritz's method) and the finite element method.

The Finite Element Method divides the continuum into a finite number of simply shaped regions (elements), which are connected at selected points (nodal points). The sought solution to the problem at hand is assumed to be of a certain shape over each element region and to depend uniquely on a finite number of parameters associated with the nodal points (nodal parameters or nodal degrees of freedom).

In the case of a structural problem, the stress and strain distributions over the extent of the continuum are the unknown functions, while the nodal forces and displacements are the corresponding nodal parameters. A physical principle, for example the principle of virtual work, is used to interrelate on an element for element basis the nodal parameters by way of the assumed approximate solutions, which results in a generalized element force-displacement relation. Once these element force-displacement relations are established for all the elements, a general force-displacement relationship for the whole continuum can be obtained using standard matrix methods. The whole procedure results in an algebraic system of

linear equations which has to be solved for the unknown nodal parameters. Once this solution is obtained, the approximate continuous stress and strain solutions are obtained by interpolating the nodal parameters over the element regions.

The finite element method (FEM) exhibits the following advantages over other discretization methods:

- complex geometries can be modelled with relative ease.
- complex loading and boundary conditions are possible.
- a structure being composed of different structural entities can be represented easily.
- elements with different material descriptions can be superimposed to obtain a more complex material behaviour in a region.

2.3 The Structure of Skeletal Muscle

Muscles are the components of the animal body which are capable of active contraction. Three types of muscles are commonly distinguished: skeletal, heart and smooth muscle. Skeletal and heart muscle are characterized as striated muscles, because of the dark and light striations visible in their fibres when they are observed under a light microscope. Skeletal muscles constitute a major part of the animal body and, controlled by voluntary nerve action, they are the foundation of animal locomotion.

Skeletal muscles are composed of a large number of individual fibres which are held together by a sheath of connective tissue, the epimysium. Varying numbers of fibres within a muscle are grouped together to form fibre bundles or fasciculi which again are encased in connective tissue, called perimysium. Each muscle fibre is a single cell with hundreds of nuclei, surrounded by a cell membrane (sarcolemma) and a connective tissue sheath (endomysium). The fibres are elongated, with lengths reaching from several millimetres up to 30 cm, and diameters of 10 to 60 μm .

The cell cytoplasm is arranged into strands of myofibrils, each having a diameter of about 1 μm . When stained by dyes and inspected optically, the myofibrils have a striated appearance with alternating dark and bright regions along their length axis. The myofibrils can be subdivided further into myofilaments which, in turn, are composed of sarcomeres, each of which has a length of approximately 2.5 μm . It is the structure and regular arrangement of the sarcomeres that gives the myofibrils and, in fact, the skeletal muscle fibres their striated appearance; an individual sarcomere extends from the middle of one light region, called Z-Band, to the next within the dark-light striation pattern of the myofibrils. Sarcomeres constitute the smallest contractile unit within a muscle. They are composed of interdigitating thick (12 nm diameter) and thin (5 nm diameter) filaments which shorten by sliding relative to each other under stimulation. The contractile tendency and associated force generation under stimulation is explained by cross-bridges,

which periodically form between the thick and thin filaments, and which pull the thin filaments past the thick filaments.

Isometrically held muscle fibres react to a single stimulation impulse with a force twitch. Two successive impulses, closely spaced in time, lead to a superposition or summation of the twitch responses. As the frequency of stimulation impulses is increased, the superimposed twitch responses fuse into a time-constant fibre force, and the fibre is then said to be tetanized. In general, the fibre force increases along with the stimulation frequency, but it does not increase beyond a certain maximum value.

Skeletal muscle fibres can be classified into slow and fast twitch fibres with further sub-categories; their names are related to the comparative rate of force increase and force decrease in response to a single stimulus. Moreover, the fibre types differ, from a functional point of view, in their fatigue resistance and, perhaps, in their level of force generation. Slow twitch fibres fatigue less rapidly than fast twitch fibres. Most muscles contain a blend of different fibre types, where the actual composition seems to be determined by contractile speed, strength and fatigue requirements on the muscle.

Different numbers of muscle fibres within a muscle constitute a motor unit. A motor unit is defined by a single nerve fibre and all the muscle fibres it innervates. All muscle fibres belonging to a single motor unit are of the same type. The nervous

system regulates the force generated by a specific muscle through the stimulation frequency and by recruiting different numbers of motor units within the muscle.

2.4 Muscle Models

For the presentation below, muscle models will be grouped into functional muscle models and geometrical muscle models. On the one hand, functional muscle models consist of a number of equations (often a single equation) which follow from statistical modelling of experimental data. They may, for example, describe the force-length and/or force-velocity relations of a muscle without attempting to explain these relations by underlying biological and physical principles. The lack of a well founded theoretical basis is evidenced by the fact that these models often contain free parameters, which are available for adjustment when the models are used. On the other hand, functional muscle models describe muscle behaviour by certain "guessed-at" relations which may or may not be related to experimental experience and which contain a certain number of free parameters on purpose. These free parameters are then adjusted, often through optimization procedures, to have the muscle or the musculo-skeletal system behave in a predetermined manner.

Geometrical muscle models take account of the muscle geometry in deriving the equations which describe the muscle behaviour, and they attempt to explain the influence of differing geometrical arrangements and of such structures as tendon sheaths on muscle performance. They depend on relations describing the muscle

fibre behaviour, where these relations are often related to the functional muscle models above, but which are now specific to fibres. A constitutive description of muscle tissue is rarely encountered in the context of these models. Constitutive models of muscle tissue will be summarized in Chapter 4.

2.4.1 Functional Muscle Models

Functional muscle models are commonly employed for investigations which relate more to the musculo-skeletal system than to questions about the inner workings of muscles. In their purest form, these models intentionally ignore any detailed current knowledge about muscle behaviour. They rather centre on a specific actual or perceived functional role of muscles in the musculo-skeletal system. Their mathematical and/or physical description is based on this functional role. In human (and animal) gait, for example, the body's centre of mass follows a sinusoidal trajectory in space, much like a mechanical oscillator moving perpendicularly to its oscillating direction. Several authors [e.g. Alexander 1975, Blickhan 1986, Greene and McMahon 1979, McMahon and Greene 1979] therefore equate the animal body with oscillators of varying complexity. All major muscles involved in the movement are grouped together, and they are assigned suitable spring stiffnesses and parallel (dashpot) viscosities to form an oscillating system with the body mass. The models are reported to have good predictive capacities related to questions regarding optimal running speed, the influence of running surface characteristics on energy consumption during running, etc.

At the same level of abstraction, Anton and Nigg [1990] developed a model for walking and running, where the muscle groups involved were lumped into a single force generator whose time rate of force generation was limited to an experimentally determined value. The time dependent force of the generator was controlled in such a way, as to maintain a certain movement pattern and, in doing so, to minimize the work performed by the generator. The model produced realistic force magnitudes, and, more importantly, the different characteristics in the force-time profile for running and walking were reproduced by exclusively changing the speed of the movement pattern.

Most functional muscle models are derivations of Hill's Equation or Hill's Three-Element Model of muscular contraction. Hill [1938] derived an empiric equation for tetanized (frog sartorius) muscle, which expresses a hyperbolic relation between the muscular contractile velocity and the applied load. Hill's investigation, which was restricted to muscle optimal length, was later generalized by Abbott and Wilkie [1953] to varying muscle lengths. The parameters entering Hill's Equation (especially the maximum isometric force) were thus shown to be dependent on the muscle length. In his paper, Hill also proposed a mechanical model which was intended to "visualize" the basic features of his empiric equation. The model consisted of a contractile element in series with an elastic element (series elastic element). In more recent times, the model has been extended and its elements have been related to the Sliding Filament Theory. The most basic extension to

Hill's original model consists of the addition of a parallel elastic element, and the extended model is usually referred to as Hill's Three-Element Model [Fung 1970]. In this model, the series elastic element is commonly associated with the intrinsic elasticity of the actin and myosin molecules and cross-bridges, while the parallel elastic element is related to connective tissues, cell membranes, etc. Often, a viscous element is added in parallel to Hill's Three-Element Model in order to give the model the velocity dependence of Hill's Equation when the active element is described as being independent of the shortening velocity. However, already in his 1938 paper as well as in later publications [e.g. Hill 1970], Hill objected to the interpretation which attributed the lower fibre tensions for higher shortening velocities to viscous effects.

Hatze [1976] and Audu and Davy [1985] studied a musculo-skeletal motion problem (the minimum time kicking problem formulated by Hatze [1976]) using optimal control algorithms. Different muscles and/or muscle groups were represented by individual Hill Models of varying complexity. The parameters of the equations which describe the behaviours of the Hill Model elements were obtained experimentally, except for a newly introduced stimulation over time function. These stimulation functions were optimized with respect to the minimum time kicking problem and model predictions for the skeletal movement sequences validated against experimental results.

Zajac [1989] added a tendon series elastic element to Hill's Model and investigated its influence on the force length relations of the muscle-tendon actuator. He demonstrated that the tendon elasticity distorts the force length curve of the muscle-tendon actuator to higher actuator lengths with decreasing tendonal stiffnesses.

Herzog [1987] used a modification of the original Hill's Equation to estimate individual muscle forces in situations where different muscles are acting together in various activities. The modifications consisted in adding further parameters which describe the muscle's angle of pinnation, its state of activation, physiological cross sectional area and muscle force constant, i.e., the maximum isometric force a muscle can exert per unit physiological cross sectional area.

Detached from any Hill type consideration, Otten [1987] proposed a three parameter mathematical expression which could be used to approximate closely the experimentally determined isometric force length relations of most muscles. The proposed equation is related to Gauss' equation for normal distribution, and the three parameters influence roundness, skewness and width of its graph. Kaufman et al. [1989] showed that these three parameters are dependent on a single parameter, namely the index of architecture, which they define as the ratio of fibre optimal length to muscle belly optimal length. As a consequence, the general expression given by Otten is made dependent on morphometric data. The

index of architecture was introduced by Woittiez et al. [1983 and 1984] and mentioned in a less formal manner already by Benninghoff and Rollhäuser [1952].

2.4.2 Geometrical Muscle Models

Geometrical muscle models incorporate the muscle geometry in one way or the other into the considerations regarding the behaviour of muscles. The Danish scientist Niels Stenson (1638 - 1686) was first in formulating a mechanical model of muscular contraction, using the mathematical tools of his time; Euclidean geometry. His observations about muscular structure contained the statements that muscles are composed of pennate structures which, in turn, contain fibres of equal length and globally form a parallelepiped between parallel tendons (or tendon sheaths). With his model, Stenson was able to demonstrate that muscles could contract without changing their volume, a concept running totally against the beliefs of his contemporaries. Reaffirming the convictions of ancient greek philosophers, Descartes (1596 - 1650) had stated in his "De Homine" that a substance or "the animal spirit" entered from the brain through hollow nerves to make the muscles swell and contract. (The discussion above was taken from a paper by Kardel [1990]. Please refer to this paper for references of original publications by Stenson.)

In more recent times, Benninghoff and Rollhäuser [1952] discussed the consequences of different angles of pinnation. Their reasoning, which was based on trigonometric considerations of individual fibre deformations, resulted in the

statement that the maximal economical angle of fibre pinnation would be 30° , if the muscle fibres are assumed to shorten by half of their original lengths. Among all possible angles of pinnation, he reported the angle of pinnation of 45° to produce the highest force in a pennate muscle. He also observed that muscles with a high degree of pinnation would produce a higher force over a smaller distance compared to muscles with a low degree of pinnation.

The most widely accepted geometrical muscle model in the literature today is the one by Woittiez et al. [1984]. His three-dimensional model geometry consists of two kite shaped tendon sheaths (with opposite geometrical orientation at top and bottom) which in general are not of equal size and are not parallel. Fibres run between the two tendon sheaths and are allowed to have varying angles of pinnation. The muscle volume is divided into segments for which, at different muscle lengths, muscle fibre forces, shortening velocity etc. are calculated. Through a least square analysis of the instantaneous segment volumes and segment volumes at muscle optimal length, the overall muscle volume is kept close to constant. The segmental muscle fibre forces are added after correcting for the angle of pinnation at different muscle lengths and result in the length dependent total muscle force. They observed a narrow active and steep passive force length relation for muscles with a considerable degree of pinnation. Woittiez reports excellent agreement between the model generated muscle force-length and force-velocity relations and those obtained by experiments on Wistar rats.

Otten presented an initial muscle model in 1985 which he later extended to account for fibre curvature, tendon elasticity and internal muscle pressure [Otten 1985, 1987a, 1987b and 1988]. The model consists essentially of six sub-units in a pennate geometrical arrangement, where each unit is formulated as a Hill type model. The tendon sheaths tie the ends of the sub-units together at either side. Comparing his model predictions to experiments performed on the cat vastus lateralis, Otten obtains good agreement. He observes that the inclusion of tendon elasticity in the model shifts the muscle force length curves to higher lengths. He also observes reasonable agreement between estimated internal muscle pressure and those generated by his model, with the highest pressure being about 120% of muscle fibre stress. (Using his model for pennate muscles, Heukelom et al. [1979] estimated the internal muscle pressure in pennate muscles to about 10 kPa. Based on their respective models, Benninghoff and Rollhäuser [1952], Gans and Bock [1965], and Gans [1982] on the other hand did not see any reason for internal muscle pressure to occur in pennate muscles.)

Dr. M. Epstein and Dr. A. Hoffer, University of Calgary, have recently developed a geometrical muscle model which is based on a constitutive description of the muscle tissue and includes an accurate treatment of the large muscle deformations. The model incorporates nonlinear material characteristics for both the muscle tissue and the tendon sheaths. Tendon sheaths are flexible in bending, and muscle fibres may take on varying angles of pinnation within the muscle. The

model has been used to investigate the sensitivity of model predictions on different constitutive assumptions. Experimentally observed wrinkling of the tendon sheaths could be reproduced with this model under certain loading conditions [private communication].

Chapter 3

Straight Line Geometrical Muscle Model

Geometrical muscle models use the muscle geometry for the derivation of the equations which describe the muscle contractile behaviour. Often, these models approximate both the initial and the deformed muscle geometry by comparatively simple geometrical shapes which are bordered by straight line segments. These muscle models as well as the muscle model to be developed in this chapter will be collectively referred to as "Straight Line Model(s)" (SLM).

The current model as well as similar models in the literature make precise assumptions about the possible modes of muscle deformations. Because these models are not based on a general constitutive theory of muscle tissue, the assumptions are required in order to reduce the number of degrees of freedom inherent to the model and to guarantee a solution. The deformation assumptions are, at times, problematic and their consequences on the muscle predictions cannot be assessed. For example, tendon sheaths are often assumed to remain

straight during muscle activity and deformation; this deformation mode represents the physical reality only under the conditions that tendon sheaths are stiff in bending or that the stresses have an appropriate distribution within the structure. However, the former condition is contrary to physiological evidence and the latter cannot be confirmed within the confines of these models.

Despite the preceding observations, Woittiez¹ et al. [1983, 1984], for example, have achieved excellent agreement between their model predictions and experimental data. Consequently, one may assume that SLM reproduce muscle behaviour to an acceptable degree, and they will be used as a basis of comparison for the Continuum Muscle Model (CM) which will be developed later in this thesis.

The development of the current SLM will be used to lay the foundations for the CM. By exploiting the potential for simplicity inherent to SLM, the mathematical description of the model will result in a closed set of algebraic equations. Due to the transparent form of these equations, certain observations about the muscle model behaviour can be made independently of any numerical analysis. Numerical analysis will, however, be employed for a broadly based exploration of the model behaviour.

¹The presentation and discussion in this chapter are very much focused on the papers by Woittiez et al. [1983, 1984] due to the shortage of similar work in the literature. While other muscle models exist, they usually do not have the broad scope of the approach taken by Woittiez.

3.1 Initial Considerations

A two-dimensional Straight Line Model (SLM) of unipennate muscles will be developed. The basic features of unipennate muscles are schematically presented in Figure 3.1a. Tendon sheaths run along the lower and upper edge (thick lines), while the muscle fibres run between the two tendon sheaths from bottom to top (thin lines). At the lower left and upper right tendon sheath ends, the muscle is connected to bone or tendons (tendons are indicated in Figure 3.1a). Defining the line of action of a muscle as the line which runs between the muscle attachment points, a muscle is termed pennate whenever its fibres intersect this line of action at an appreciable angle. A unipennate muscle has only one predominant fibre orientation. This contrasts with multi-pennate muscles which include fibres with several distinctly different fibre orientations. The general geometry of a bipennate muscle is indicated in Figure 3.1b.

Since fibres are assumed to exert forces exclusively along their longitudinal axis, the degree of pinnation has a direct effect on the magnitude of the force a muscle can produce. A fibre which is nearly aligned with the muscle's line of action contributes almost all of the force it generates to the overall muscle force, whereas a fibre running perpendicularly to the muscle's line of action does not contribute to the external force of the entire muscle. This observation is usually expressed by a cosine relation, in which the amount of fibre force contributed to the overall muscle force is taken to be equal to the fibre force, multiplied by the cosine of the

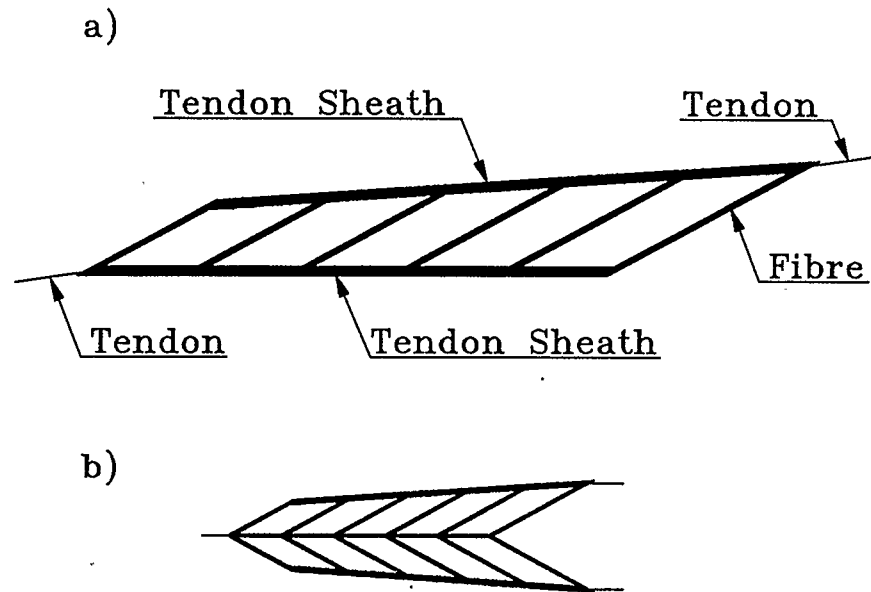


Figure 3.1: Schematic geometry of pennate muscles.

angle spanned between the muscle's line of action and the fibre direction. The cosine relation is used, for example, by Woittiez et al. [1983, 1984] and Scott² and Winter [1991] in their models. Because the value of the cosine function increases with smaller angles, it would appear that less pinnation is beneficial in obtaining higher muscle forces. As will be shown below however, the degree of pinnation also influences the number of fibres which run in parallel between the two tendon

²The treatment by Scott and Winter [1991] simplifies the pennate muscle geometry even further. The whole muscle is represented by a single line element which is arranged at an angle to the muscle tendons. This angle, identified with the angle of pinnation, and the cosine relation is the only geometrical component of the model.

sheaths. More fibres are arranged in parallel in the case of a higher degree of pinnation, and the muscle force increases correspondingly.

The consequences of the changing muscle geometry during muscle deformation on the fibre angle of pinnation as well as the effects of different initial muscle geometries on the number of fibres acting in parallel are illustrated in Figure 3.2. Focusing on Figure 3.2a, a unipennate muscle is displayed with tendon sheaths at the top and bottom, and muscle fibres, indicated by equally spaced lines, running at an angle between bottom and top tendon sheath. For now, the angle of pinnation, γ , will be defined as the angle included between the line of action of the muscle and the general fibre direction. The indices indicate the muscle geometry number 1 (first index = 1) at reference configuration (second index = 0).

When stimulated, a muscle fibre generates a force, whose magnitude depends on the length of the fibre. For a particular length, the fibre force takes on a maximum value which decreases to zero as the fibre is lengthened or shortened from this "optimal length". Furthermore, experimental evidence suggest that muscle tissue and individual muscle fibres are incompressible, that is, their volume does not change during deformation. Consequently, the fibre cross sectional area decreases proportionally when a fibre is stretched and increases when a fibre is shortened. The muscle reference configuration is taken here to refer to a geometry for which all muscle fibres have a length at which they are able to generate a maximum force when stimulated and at which they have a specific cross sectional area.

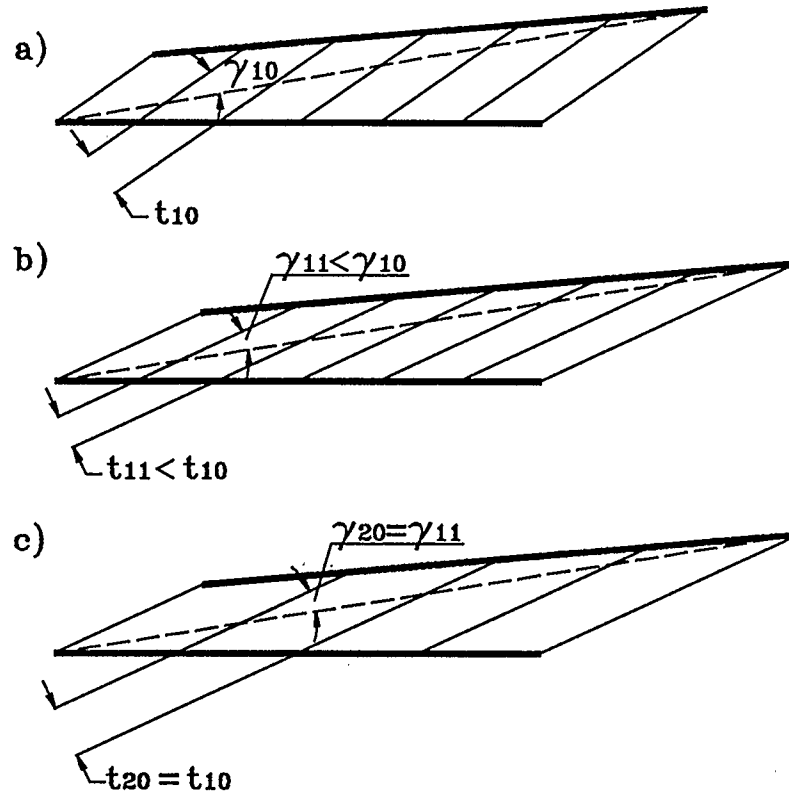


Figure 3.2: Consequences of muscle deformation and different initial muscle geometries on specific muscle attributes.

The areas between any two adjacent lines running in fibre direction in Figure 3.2 are assumed to contain the same number of fibres forming fibre bundles. Alternatively, two adjacent lines may be seen to border one disproportionately thick fibre for the current argument. The thickness of these fibres or fibre bundles is

indicated by t . A unit depth (or thickness) of the muscle perpendicular to the drawing plane is assumed, which will not change during muscle deformation.

Figure 3.2b displays the same muscle as Figure 3.2a in a deformed (stretched) configuration³ (second indices = 1). The deformation results in a decrease of the angle of pinnation and a lengthening of the muscle fibres associated with a corresponding decrease in their thickness. The number of fibres acting in parallel has evidently not changed, but they are now orientated more in the direction of the line of action of the muscle, which allows them to contribute a higher proportion of their current force to the external muscle force (cosine relation). However, the individual fibre forces have decreased during the deformation on account of the fibre force-length relation. For any deformation, the external muscle force will be influenced by these two opposing effects.

A second muscle (first index = 2) with its initial geometry (second index = 0) being equal to the deformed geometry of the first muscle is shown in Figure 3.2c. The muscle and its fibres are now at reference configuration, and the fibres take on their reference cross sectional area and thickness. Therefore, fewer but longer fibres can be fitted in parallel into this muscle volume. Being at optimal length however, each fibre is able to exert a higher active force compared to Figure 3.2b.

³The deformed muscle geometry in Figure 3.2b results from the initial geometry in Figure 3.2a by a stretch in the direction of the line of action of the muscle and followed by a rotation which aligns the lower tendon sheath with the horizontal. The rotation is carried out for purposes of clarity.

The muscle model to be developed will address the trade-off between the force contribution of individual fibres and the number of fibres acting in parallel in relation to the angle of pinnation. Muscles of identical volume but with different initial geometries will be modelled in order to study the dependence of certain muscle characteristics on the initial muscle geometry. Muscle characteristics of interest include the muscle peak force, the deformation range over which a muscle is able to exert a force and the relation between the force-length profiles of muscle fibres and the whole muscle.

3.2 Model Derivation

The equations which describe the current SLM will be derived in this chapter. The section starts by stating the simplifications and assumptions underlying the muscle model. Consequently, the admitted muscle model geometries and kinematics of deformation will be defined. Finally, after looking at different aspects of the muscle fibre force-length relation, the section concludes with the derivation of the equilibrium conditions.

3.2.1 Simplifications and Assumptions Underlying the Model

The simplifications and assumptions which underlie the current model development are similar to those encountered in the treatment by Woittiez et al. [1983, 1984].

Assumptions determine to a large extent how the final model will perform, and they, therefore, constitute an important part of any model.

Table 3.1 groups the current simplifications and assumptions into three categories, where the first category (marked 'R') refers to the initial or reference muscle configuration, the second (marked 'D') to the deformed muscle geometry, and the third group (marked 'A') lists additional assumptions which do not fit into the first two categories. The first category of simplifications and assumptions will be carried over almost unchanged to the development of the Continuum muscle Model (CM) later in this thesis. For the current model, no use is made of constitutive relations, except for fibre force-length relations. Instead, kinematic constraints expressing assumed muscle deformation modes are applied. They constitute the second category in Table 3.1., and they will be replaced by constitutive relations in the context of the CM. Table 3.1 makes reference to optimal and relative fibre length which will be defined in Chapter 3.2.3.

It is worth noting, that the simplifications and assumptions in Table 3.1 describe the tendinous sheath as being rigid both in tension and bending. Fibres, while they are allowed to contract and elongate freely, are also taken to be stiff in bending. These simplifications are counter to physiological evidence. As an aside, the assumed fibre deformation mode implies that the tendon sheaths remain straight during muscle deformation, whereas the converse does not hold. The muscle tissue as a whole is seen to behave as a mere superposition of individual fibres,

-
- R.1 Tendon sheaths are straight.
 - R.2 All muscle fibres are straight, they have identical directions and are at optimum length.

 - D.1 Tendon sheaths remain straight and maintain their original length; at times, they are allowed to change in width.
 - D.2 All muscle fibres remain straight, and they take on identical relative lengths and orientation. All fibres are uniformly stimulated.
 - D.3 The volume of the entire muscle and of any volumetric element of muscle tissue remain unchanged, that is, the muscle tissue is incompressible.

 - A.1 The only origin of forces or stresses is seen in the active and passive fibre force-length property. These forces or stresses act in fibre direction only.
 - A.2 There is a unique functional relation between the fibre force and the relative fibre length.
 - A.3 The muscle has two points of attachment only. There are no other points of contact with surrounding structures.

Table 3.1: Major simplifications and assumptions underlying the straight line muscle model.

modulated by the muscle geometry. The incompressibility of muscles under stimulation has been shown by Abbott and Baskin [1962].

In the context of this chapter, the concept of mechanical stress will be used loosely. Whenever reference is made to stresses, it will refer to distributed loads (forces divided by areas). Due to the absence of a general constitutive theory, stresses are not to be understood as components of a stress tensor.

The final form of the equations below will be independent of the concept of muscle fibres. Nevertheless, muscle fibres will be referred to whenever it helps the

argumentation. In these cases, fibres are assumed to extend over the entire distance between the two tendon sheaths and to possess a thickness being small compared to the dimensions of the muscle.

3.2.2 Muscle Model Geometry and Kinematics of Deformation

The general muscle model geometry, whose cross section takes on a trapezoidal shape, is displayed in Figure 3.3. A uniform muscle thickness or depth, measured perpendicularly to the drawing plane is assumed. Tendon sheaths are located at the top and bottom, and fibres run in parallel between the tendon sheaths in a direction coincident with the boundary fibres indicated at the left and right end. For the derivation of the equations, the muscle is assumed to be attached rigidly (to bone) at the left end of the lower tendon sheath, while the right end of the upper tendon sheath (connected to a tendon) is free to move⁴. The muscle attachment point on the left may be identified with the muscle origin and the one on the right with the muscle insertion. As shown in Figure 3.3, the muscle is freed from its attachment points and force resultants are drawn in their place.

The muscle geometry is described by the following parameters: the lower tendon sheath length, l , the muscle height at the left end, h_1 , the difference in height between the muscle's right and left end, h_2 , the muscle depth, d , the overall

⁴The muscle deformations result from moving the upper right hand apex in the direction of the line of action of the muscle. However, the deformations are described relative to a coordinate system which is attached rigidly to the lower tendon sheath. Thus, the rotation of the tendon sheath in global coordinates is eliminated from the equations.

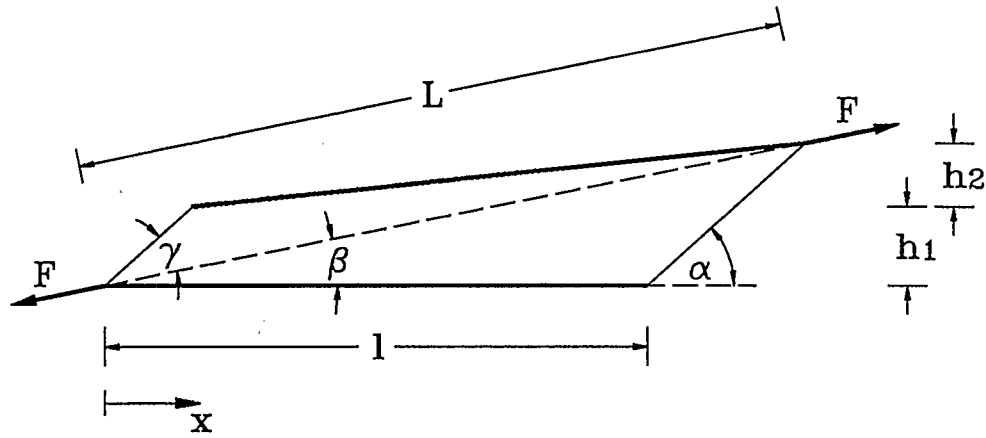


Figure 3.3: Muscle model geometry (lateral muscle cross section).

muscle length (the length of the connecting line between the origin and insertion), L , the angle between the lower tendon plate and the fibre direction, α , the angle between the line of action of the muscle and the lower tendon sheath, β , and the angle between the fibre direction and the line of action of the muscle, γ .

From the possible subsets of independent geometrical parameters which describe the muscle geometry uniquely, the set being composed of l , h_1 , h_2 , d and α will be used below. Following Otten [1988], α will be termed the angle of pinnation in the context of the current model. This contrasts with the treatment by Woittiez et al. [1984] who use γ for this purpose. The angle α has been chosen here because it simplifies the derivation and the final form of the equations below, and because the angle under which the fibres connect to the tendon sheaths has a higher significance than γ . The general trapezoidal muscle geometry contains the

commonly treated muscle geometry of muscles with parallel tendon sheaths by setting h_2 equal to zero.

For the description of the muscle deformation the concepts of initial or reference configuration and deformed or actual configuration have to be distinguished. Initially, the muscle geometry is determined by a set of values for l , h_1 , h_2 , d and α , and the fibres are taken to be at optimal length (see next section). Symbolically this will be expressed by subscripting parameters which describe the reference configuration by 0 (e.g. α_0). The actual configuration is defined by a new set of unsubscripted parameters which, in general, are functions of the geometrical parameters at reference configuration and of the actual angle of pinnation, α . It is a consequence of the simplifications and assumptions made in the previous section that only α is needed from the set of actual parameters to determine uniquely the actual configuration. During the deformation, the angle of pinnation, α , will change, h_1 , h_2 and d will change in general, while l will always remain constant. Values for the dependent parameters, L , β and γ , can be obtained at any configuration.

When the muscle deforms, the fibres will change in length and, on account of the required constancy of volume, their cross sectional area perpendicular to the fibre direction will change accordingly. If the depth of the muscle is taken to remain constant, the fibres can only change their thickness in the drawing plane of Figure 3.2 and Figure 3.3. However, the equations below do allow for a uniform

depth change of the entire muscle, where the amount of depth change is controlled by an additional kinematic constraint and included in the equations by way of a parameter, D . D imposes the ratio of fibre thickness changes in depth direction to the fibre thickness change in the drawing plane of Figure 3.2 and Figure 3.3. A value of $D=0$, for example, implies no fibre thickness change in depth direction, whereas $D=1$ translates into equal fibre thickness changes in depth and drawing plane direction during muscle deformation.

The ratio of the actual fibre length to the reference fibre length, which is commonly called relative fibre length⁵, is denoted by λ . λ will also be referred to as the (fibre) stretch ratio; the fibre forces depend ultimately on the fibre stretch ratio. On the other hand, the absolute fibre length has no significance for the present considerations and will not appear in the equations.

The equations below express the functional dependence of the geometrical parameters which describe the actual muscle configuration on the independent parameters at reference configuration and on the actual angle of pinnation, α . They are derived by trigonometric considerations and incorporate the simplifications and assumptions listed in Table 3.1 under category D.

$$L = \frac{h_1 + h_2}{\sin\beta} \quad (3.1)$$

⁵The fibre reference length will be defined below as being equal to the fibre optimal length.

$$\tan\beta = \frac{(h_1 + h_2)\tan\alpha}{(h_1 + h_2) + l\tan\alpha} \quad (3.2)$$

$$h_i = \lambda \frac{\sin\alpha}{\sin\alpha_0} h_{i0}, \quad i = 1, 2 \quad (3.3)$$

$$\lambda = \frac{1}{\frac{\sin\alpha}{\sin\alpha_0} \left(1 + D \left(\frac{\sin\alpha}{\sin\alpha_0} - 1 \right) \right)} \quad (3.4)$$

If it is desired to express the equations above in terms of γ , that is, the angle between the line of action of the muscle and the fibre direction, then α may be replaced by the term $(\beta + \gamma)$ in the equations above. For $D=0$, which corresponds to a constant muscle depth during muscle deformation, Equation 3.4 simplifies greatly and Equation 3.3 becomes trivial.

Equations 3.1 and 3.2 express trigonometric relations which are obtained directly from Figure 3.3. Figure 3.4 displays a fibre or fibre bundle in its reference and deformed configuration. Equation 3.3 follows by eliminating l_{i0} from the following two equations:

$$\begin{aligned} h_0 &= \sin\alpha_0 l_{f0} \\ h &= \sin\alpha l_f = \sin\alpha \lambda l_{f0} \end{aligned} \quad (3.5)$$

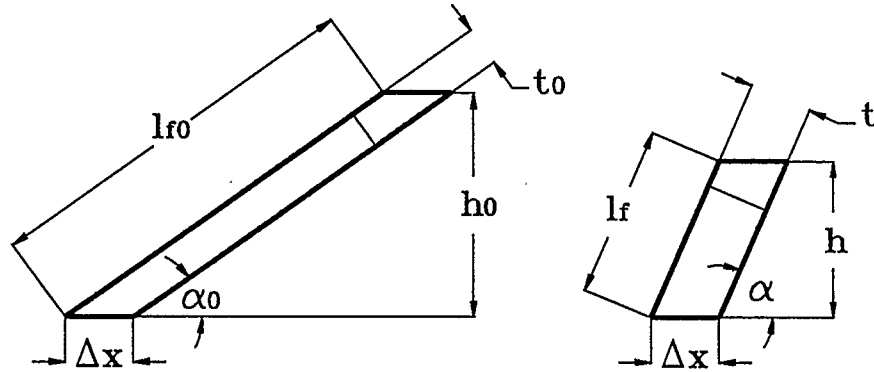


Figure 3.4: General deformation of a muscle fibre or muscle fibre bundle.

Introducing the stretch ratios in fibre thickness direction, λ_t , and depth direction, λ_d , the requirement of volume constancy leads to the relation $\lambda \cdot \lambda_t \cdot \lambda_d = 1$ by way of the following equations:

$$V_0 = l_{f0} t_0 d_0 = l_f t d = \lambda l_{f0} \lambda_t t_0 \lambda_d d_0 = V \quad (3.6)$$

An expression for λ_t is obtained through:

$$\Delta x = \frac{t_0}{\sin \alpha_0} = \frac{t}{\sin \alpha} \rightarrow \lambda_t = \frac{t}{t_0} = \frac{\sin \alpha_0}{\sin \alpha} \quad (3.7)$$

The depth change parameter, D , is introduced through the defining equation:

$$\lambda_d = D(\lambda_t - 1) + 1 \quad (3.8)$$

Substituting Equations 3.7 and 3.8 into the relation $\lambda \cdot \lambda_i \cdot \lambda_d = 1$, Equation 3.4 results after rearranging.

3.2.3 Fibre Force-Length Relation

Experimental evidence indicates that muscle fibre forces depend on the fibre length, the degree of stimulation and the time rate of the fibre length change. While work has been done in the area, the question of how to quantify the amount of stimulation in a mathematically precise sense is not entirely resolved. For that reason no conclusive functional expression which relates the active fibre force to the degree of stimulation is available. However, the fibre force under stimulation reaches a fibre length dependent maximum value, whose magnitude is independent of the degree of stimulation as long as the stimulation is above a specific saturation level. In this case a fibre is said to be maximally stimulated. This thesis deals only with fibres which are either unstimulated or maximally stimulated, and the current chapter focuses on maximally stimulated fibres exclusively. Furthermore, only static or quasi static conditions will be considered, which renders the equations and considerations below independent of the time rate of fibre length changes.

Muscle fibre force-length relations have been established experimentally by bringing individual muscle fibres to different absolute lengths and measuring the forces of maximally stimulated and unstimulated fibres. Figure 3.5 displays the general form of the fibre force-length relations for a stimulated (solid line - total

muscle fibre force) and unstimulated fibre (dotted line - passive muscle fibre force). The difference in force between the total and passive muscle fibre force is commonly called the active fibre force (dashed line). Rather than using the absolute fibre length, the abscissa in Figure⁶ 3.5 displays the ratio of the actual fibre length (l_f) to the fibre optimal length (l_{f0}), that is, the fibre stretch ratio $\lambda = (l_f / l_{f0})$. The ordinate displays the relative fibre force, where the absolute fibre force is divided by the maximum active fibre force. The absolute fibre length at which a fibre reaches its maximum active force is called fibre optimal length. An unstimulated fibre left to itself will take on a length, called resting length, which, in most cases, is close or equal to its optimal length. Fibres will be defined to be at reference length when they take on their resting length which is assumed to be equal to the fibre optimal length. The fibre stretch ratio, λ , is equal to 1 at fibre reference length.

The literature usually gives examples of fibre force-length relations for different species and muscles in the form of Figure 3.5, that is, the relative force is plotted against the stretch ratio. Nevertheless, the expressions "force" and "length" are used when referring to the ordinate and abscissa, respectively. Below, the terms "fibre length" and "fibre relative length" or "fibre stretch ratio" will be used interchangeably when referring to the fibre stretch ratio. When the difference

⁶The reference to fibre stress within the figure caption and the ordinate label "P" will be explained below.

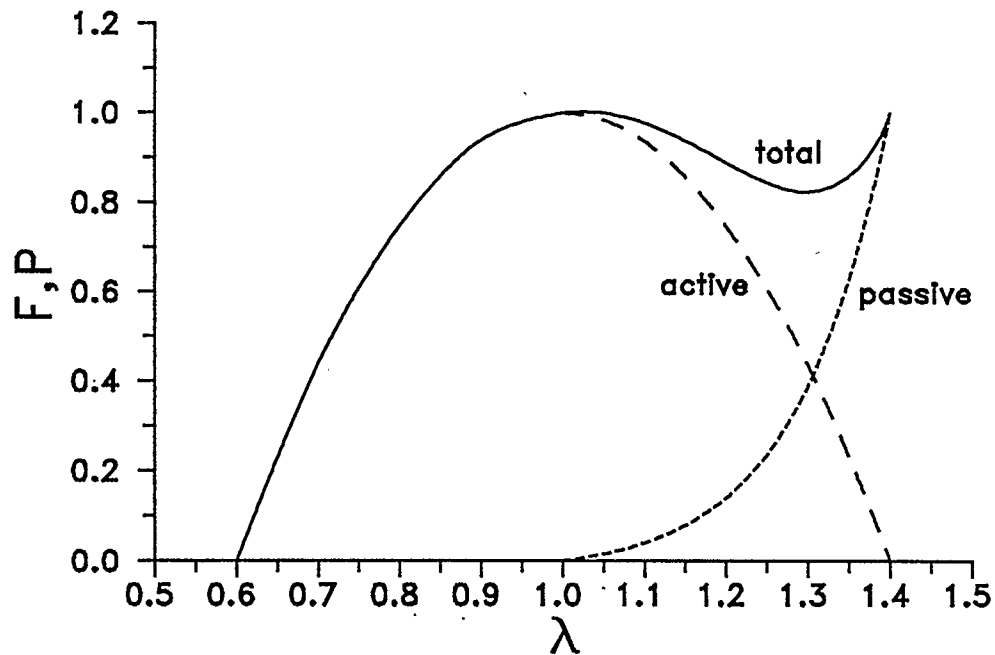


Figure 3.5: Fibre force and fibre stress profiles (force profile number 1).

between absolute and relative fibre forces is of importance, the relative force-length relation will be termed active force profile.

Absolute muscle fibre forces are seldom listed in the literature (data obtained experimentally from frog muscle fibres are given, for example, by Woledge et al. [1985]). Absolute values are mostly given for active muscle tissue peak stresses in the fibre direction. However, these active fibre stresses vary greatly in magnitude; Kaufman et al. [1991], for example, indicate a range from 10 to 100 N/cm² for human muscles. The active stress values are usually obtained from force measurements performed on entire muscles, where the muscle peak force under

maximal stimulation is divided by the average fibre length and where a correction term is applied to account for the angle of pinnation. This procedure implies the acceptance and use of a basic muscle model which relates external muscle forces to muscle tissue stresses.

From a modelling point of view, one is confronted with the situation of knowing the fibre force-length profile which was obtained from a single fibre experiment and which is assumed to remain unchanged for fibres in the tissue compound; however, one does not have access to absolute fibre forces but to a muscle tissue stress. Below, the fibre forces and tissue stresses will be related. At the same time, two different stresses, the first Piola Kirchhoff stress and the Cauchy stress, will be introduced.

If one considers a force profile function $f(\lambda)$ which describes, for example, the total normalized fibre force in Figure 3.5., the absolute fibre force can be expressed by

$$F(\lambda) = \hat{F} f(\lambda) \quad (3.9)$$

with \hat{F} being the force scaling factor. Dividing F by the fibre cross sectional area corresponding to the fibre optimal length results in

$$P(\lambda) = \frac{F(\lambda)}{A_0} = \frac{\hat{F}}{A_0} f(\lambda) = \hat{P} f(\lambda) \quad (3.10)$$

Keeping in mind the reservations made about the stress concept in Chapter 3.2.1, P could be termed the first Piola Kirchhoff stress, being the quotient of the actual fibre force divided by the reference fibre cross sectional area. $F(\lambda)$ and $P(\lambda)$ have the same profile function $f(\lambda)$, but different scaling factors in magnitude and dimensions. $F(\lambda)$ applies to each muscle fibre individually, while $P(\lambda)$, considering the assumptions made about fibre uniformity throughout the muscle, expresses the tissue stress in fibre direction at any point within the muscle body.

During muscle fibre length changes, the fibre cross section is assumed to change in such a way as to keep the fibre volume constant. Dividing Equation 3.9 by the actual fibre cross sectional area, $A(\lambda)$, leads to

$$\sigma(\lambda) = \frac{F(\lambda)}{A(\lambda)} = \frac{\hat{F}}{A(\lambda)} f(\lambda) = \frac{\hat{F}}{A_0} \frac{f(\lambda)}{\lambda} = \hat{P}s(\lambda) = \hat{\sigma}s(\lambda) \quad (3.11)$$

where $\sigma(\lambda)$ might be called the fibre tissue Cauchy stress in fibre direction, that is, the actual force acting in fibre direction per unit cross sectional area perpendicular to the fibre direction in the actual configuration. It follows from the constancy of fibre volume that $A(\lambda)=A_0/\lambda$. The scaling factors \hat{P} and $\hat{\sigma}$ are equal, but the two stress profile functions are different.

Figure 3.6 presents the active force profile $f(\lambda)$ of Figure 3.5 as the solid line which is identical to the first Piola Kirchhoff stress profile. The dashed line corresponds

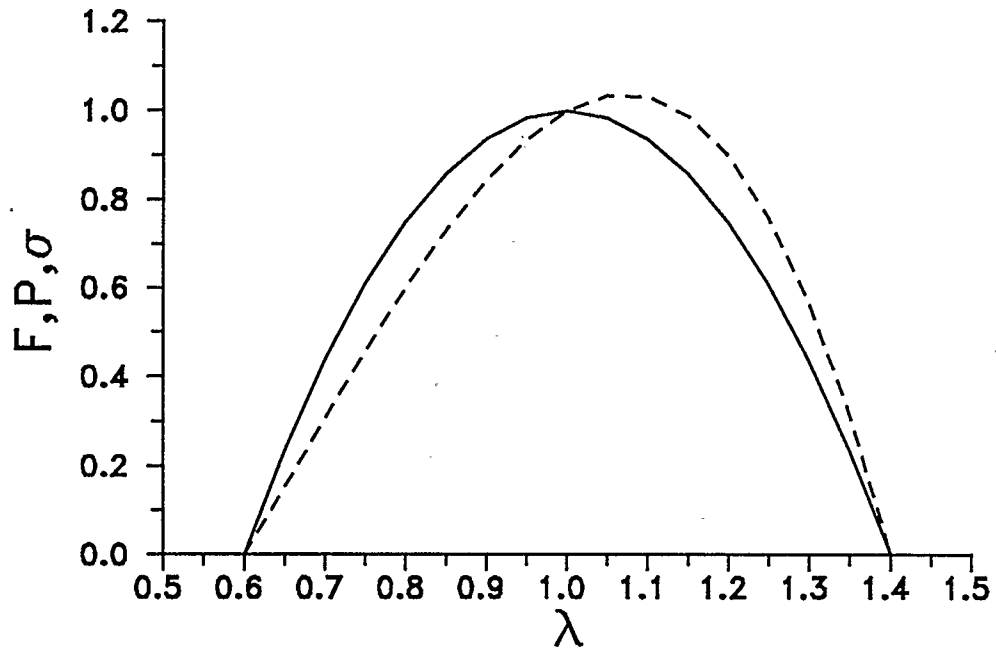


Figure 3.6: Active fibre force and stress profiles (force profile number 1).

to the Cauchy stress profile $s(\lambda)$ in Equation 3.11. Its maximum is shifted to the right and is, at a value of about 1.1, greater than unity. The two curves intersect at $\lambda=1$, which corresponds to the reference configuration, and for which the Cauchy and Piola Kirchhoff stresses are identical.

From a conceptual perspective, the question arises, which of the fibre stresses P and σ is intended to be derived from experiments on entire muscles. Below, stresses reported in the literature will be interpreted as resulting from single fibre experiments, and they will be identified with \hat{P} .

For the derivation of the equilibrium conditions in the next section, it is helpful to introduce the internal energy of fibre tissue per unit volume at reference configuration:

$$W_{\text{int}} = \hat{P} \int f(\lambda) d\lambda \quad (3.12)$$

which, when focusing e.g. on one fibre, follows from

$$\frac{1}{V_{f0}} \int F dl_f = \frac{1}{V_{f0}} \int P A_{f0} l_{f0} d\lambda = \frac{A_{f0} l_{f0}}{V_{f0}} \hat{P} \int f(\lambda) d\lambda \quad (3.13)$$

and where Equation 3.9 and the relation $l_f = \lambda l_{f0}$ have been used. In Equation 3.13, F stands for the fibre force, l_f for the fibre length, V_{f0} for the fibre volume at reference fibre length, and A_{f0} for the fibre cross sectional area at reference fibre length. While Equation 3.13 focuses on one fibre, Equation 3.12 gives the internal energy per unit volume at any point in the muscle. The internal energy density is independent of the location within the muscle, due to the simplification which required all fibres to be in the same state of deformation and activation.

In the current context, the term "internal energy" refers to the capacity of the fibre tissue to produce work and contains an activation energy component resulting from the fibre stimulation as well as a strain energy like component associated with the passive fibre force-length characteristic.

Two force profiles $f(\lambda)$ will be considered in this chapter. Profile number 1, $f_1(\lambda)$, incorporates both an active and passive fibre force-length relation. The active part is taken directly from Woittiez et al. [1984], whereas the passive part has been somewhat modified. The force profiles are displayed in Figures 3.5 and 3.6. The active profile has the form of a parabola centred at $\lambda=1$, and it is positive over the range $\lambda \in (0.6, 1.4)$. The total force profile, that is, the active plus passive force profile, has a local minimum of about 0.84 at $\lambda \approx 1.32$ and attains a value of 1 at $\lambda=1.4$. Equation 3.14 gives the functional description of force profile number 1:

$$\begin{aligned}
 f_1(\lambda) &= f_{1,act} + f_{1,pas} \\
 f_{1,act} &= (-6.25\lambda^2 + 12.5\lambda - 5.25) \\
 f_{1,pas} &= 3.289 \cdot 10^{-6} e^{9.037\lambda} - 0.02766
 \end{aligned} \tag{3.14}$$

The active force profile number 2, Figure 3.7, is a modification of force profile number 1. In principle, it is generated from the previous profile by shifting the location of the active fibre force peak (solid line) to the left and is motivated by the fact that the Cross Bridge Theory predicts, and that measurements taken on sarcomere level show, a more asymmetrical force-length relation. Compared to profile number 1, the range of λ over which the fibre generates an active force and the integral $\int f(\lambda) d\lambda$ over the active range have been kept constant. The latter means that fibres having characteristics described by either profile perform the same amount of work in a contraction covering their active range. Furthermore, the

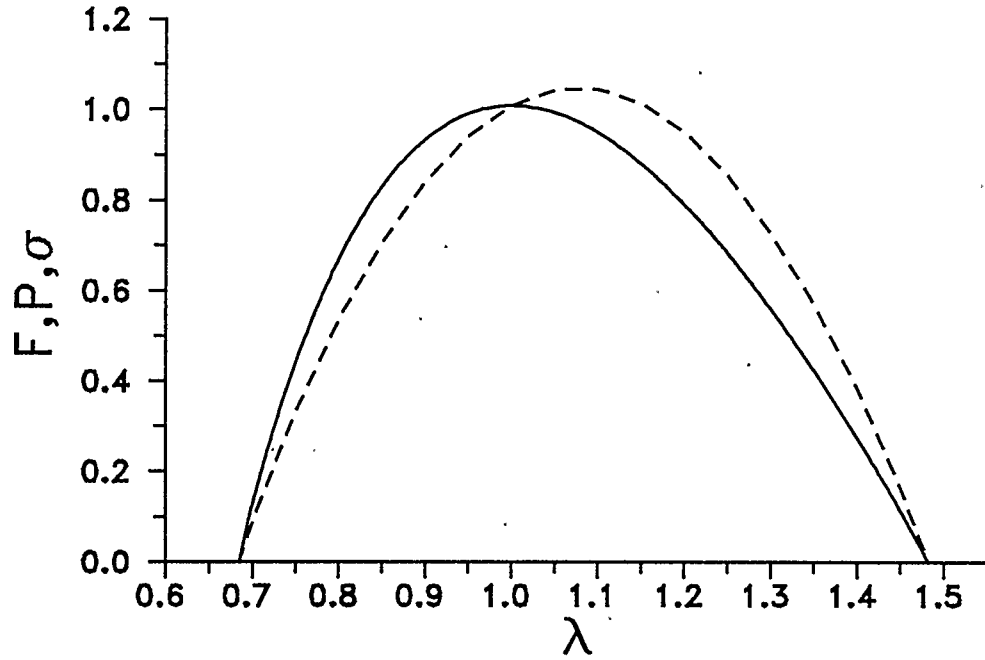


Figure 3.7: Alternate active fibre force and stress profiles (force profile number 2).

active Cauchy stress profile (dashed line) has now a parabolic shape. The curves have been shifted to the right through a coordinate transformation, to keep the force profile maximum at $\lambda=1$. Equation 3.15 presents the equations describing force profile number 2; no passive force profile is included for the considerations in this chapter.

$$f_{2,act}(\lambda^*) = \frac{1}{1.034\lambda^*} (-6.25(\lambda^*)^2 + 12.5\lambda^* - 5.25) \quad (3.15)$$

$$\lambda^* = \lambda - 0.08349$$

3.2.4 Equilibrium Conditions

The equilibrium conditions, which relate muscle fibre forces to the external muscle force, are usually given little attention in deriving the models in the literature. Woittiez et al. [1984], for example, treat this topic in one sentence, saying that "the product of the force of each fibre and the cosine of its angle results in the force contribution of each fibre in the direction of the length axis of the muscle" (in terms of the current model, "angle" refers to the angle γ in Figure 3.3). No attempt has been made to establish the physical merits of this approach and their discussion does not indicate any concern with this kind of approach.

Otten [1988] derived equilibrium conditions for a muscle with parallel tendon sheaths at one particular configuration only by using the methods of sections and by considering the equilibrium of the individual tendon sheaths. He fails, however, to apply the required mechanical rigour. His equations turn out to be essentially correct, but not for the right reasons.

The equilibrium conditions have probably been treated so carelessly because the muscle, even on the abstraction level of a straight line model, turns out to be a statically indeterminate system, which may not have been realized. Figure 3.8. presents the free body diagram of an entire muscle with parallel tendon sheaths and two alternative free body diagrams for the upper tendon sheath alone. Looking at the entire muscle held at two opposing points only, equilibrium is solely possible

if the forces have a common line of action⁷, opposite direction and the same magnitude (Figure 3.8a).

The upper tendon sheath of the muscle, sectioned and redrawn in Figure 3.8b, is in equilibrium if both the force equilibrium condition (closed force polygon) and moment equilibrium (the lines of action of all forces intersect at one point) are satisfied. It was one of the simplifications made for the model that all fibres are always in the same contractile state, that is, all fibres generate an equal amount of force. Therefore, one can substitute one resultant force for the distributed fibre forces, whose line of action intersects the tendon sheath at mid-length with a direction parallel to the general fibre orientation. In addition to the line of action, the magnitude of this fibre force resultant, F_F , is known in dependence of the fibre stretch ratio λ . The line of action of the external muscle force, F_M , is also known from the considerations made above. To establish static equilibrium, a closed force polygon has to be drawn at the intersection of the line of actions of F_F and F_M . Closing of the force polygon is only possible by introducing an additional force, F_A , which has been drawn with a vertical line of action in Figure 3.8b. This choice of direction for F_A is, however, in no way unique, which is illustrated by the free body diagram in Figure 3.8c, displaying another force system in static equilibrium. The

⁷In the current model with two muscle attachments at the origin and insertion only, the line of action of the muscle forces is identical to the line which joins the muscle origin and insertion. In keeping with commonly accepted terminology, the latter has previously been defined as the line of action of the muscle. It should, however, be noted that in the case of additional muscle boundary conditions (e.g. supported tendon sheath) the external muscle forces may have different lines of action neither being coincident with the "line of action of the muscle".

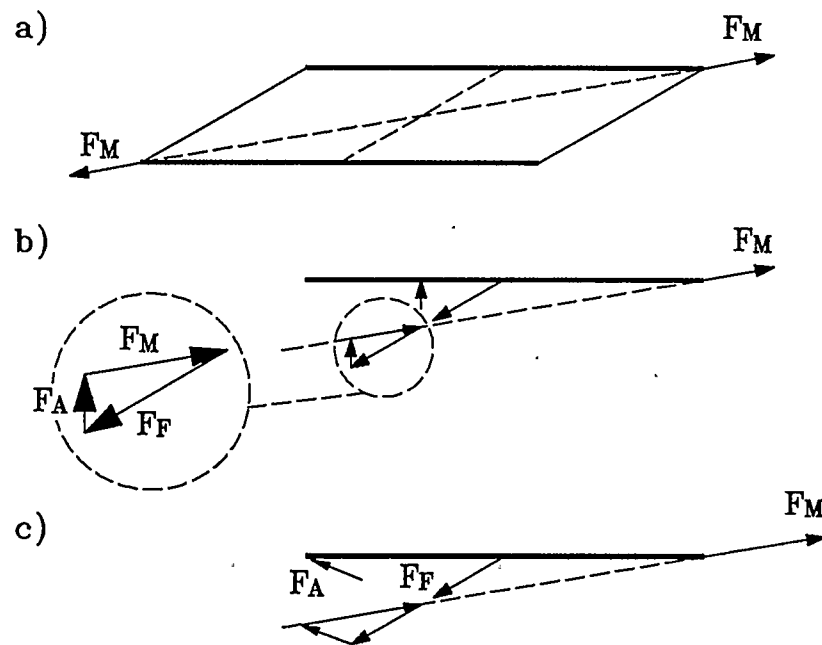


Figure 3.8: Free body diagrams for the entire muscle and the upper tendon sheath.

direction of F_A is important, as it influences directly the magnitude of F_M ; the magnitude of F_M in Figure 3.8c is larger than the one in Figure 3.8b.

Otten [1988] assumes F_A to have a vertical line of action by alluding to pressure forces or pressure stresses that have been shown to exist in muscles. However, the simplifications and assumption underlying his model and the current model, in particular the absence of any general constitutive law, do not contain a convincing basis for this choice. By drawing the free body diagram for a trapezoidal muscle

geometry, one sees at once that F_A cannot be perpendicular to both the bottom and top tendon sheaths. All that can be said about F_A is that it is a consequence of the imposed kinematic constraints. It should also be noted that the line of action of F_A does not intersect the tendon sheath at mid length.

The decision, which one of F_A 's possible line of actions to choose, has to be built on a physical foundation, instead of an arbitrary assumption. This will be achieved below by using the principle of virtual work. In the context of the current model, the principle equates the incremental internal energy change to the incremental work performed by the muscle force, F_M , for any incremental deformation of the muscle consistent with the kinematic constraints.

It follows from the free body diagram of the entire muscle, Figure 3.8a, that F_M is collinear with the line of action of the muscle along which the muscle's length, L , is measured (Figure 3.3). The external muscle work can therefore be written as:

$$W_{\text{ext}} = \int F_M(L) dL \quad (3.16)$$

and the principle of virtual work can be stated as follows:

$$\delta \left[\int_{V_0} w_{\text{int}} dV - W_{\text{ext}} \right] = 0 \quad (3.17)$$

The volume integration limits are independent of the kinematic variables so that the integration and variation may be interchanged. Using Equations 3.12 and 3.16, Equation 3.17 is transformed into

$$\int_{V_0} \hat{P} f(\lambda) \delta \lambda dV - F_M(L) \delta L = 0 \quad (3.18)$$

and further

$$\left[\hat{P} f(\lambda) \frac{d\lambda}{d\alpha} \int_{V_0} dV - F_M(L) \frac{dL}{d\alpha} \right] \delta \alpha = 0 \quad (3.19)$$

By the standard argument of variations, that, given $\delta \alpha \neq 0$, the terms enclosed in parenthesis in Equation 3.19 must be zero, the following equilibrium conditions are found after integrating and differentiating with respect to α and extensive trigonometric transformations (Equations 3.2 through 3.4 are used in the process):

$$F_M = \frac{\hat{P}}{2} \left[\frac{2h_1 + h_2}{h_1 + h_2} \right] d_0 l_0 \sin \alpha_0 \frac{(1 + D) \cos \alpha}{\cos \beta + D \cos \alpha \cos(\alpha - \beta)} f(\lambda) \quad (3.20)$$

Equation 3.20 expresses the muscle force, F_M , in terms of the geometrical parameters at reference configuration (parameters subscripted by 0), the actual angle of pinnation, α , the actual angle between the lower tendon sheath and the line of action of the muscle, β , the first Piola Kirchhoff stress scaling factor, \hat{P} , the

fibre force profile function, $f(\lambda)$, and the kinematic parameter controlling muscle depth changes during contraction, D . By virtue of the Equations 3.2 through 3.4, the variables β and λ in Equation 3.20 can be expressed in terms of α , that is, F_M is a function of α exclusively. In essence, F_M is determined by the functional form of the fibre force profile, which at this point can be an arbitrary function, scaled in magnitude by a constant (parameters subscripted by zero and \hat{P}) and modulated by trigonometric functions of the variables α and β . Combining Equations 3.1 and 3.20, the muscle force, F_M , can be calculated in dependence of the muscle length, L . Mathematically, the model is completely described by Equations 3.1 through 3.4 and Equation 3.20.

3.3 Model Exploration and Discussion

The derivation of the equations above has been based on a muscle geometry with a lateral cross section of the shape of a parallelogram or trapezium (Figure 3.11) and with an uniform depth. The three-dimensional representation of such a muscle with parallel tendon sheaths consists of a parallelepiped with rectangular tendon sheath geometries much like the model Stenson worked with in the 17th century (see Kardel [1990]). However, the equations describing the current model represent a larger class of muscle geometries: the limiting factors on the muscle and tendon geometries are the initial simplifications which require all muscle fibres always to have identical angles of pinnation and identical relative lengths. In other words, any muscle geometry may be chosen, as long as the geometry permits a

deformation which is conform to the kinematic Equations 3.2 through 3.4. This condition is fulfilled, whenever the orthogonal projection of the upper tendon sheath in Figure 3.3 into the plane of the lower tendon sheath, results in an identical shape to the lower tendon sheath. In particular, the tendon sheaths may have a variable depth along the muscle length axis, and the upper tendon sheath may be curved in the plane of Figure 3.3. If a different admissible muscle geometry is to be modeled, the final form of Equation 3.20 will change in that, going from Equation 3.19 to Equation 3.20, the volume integration term will take on a different form. For example, assuming tendon sheaths of an elliptical shape, and identifying l_0 and d_0 with the major and minor principal axes of the lower tendon sheath, only the term $d_0 l_0$ in Equation 3.20 would change to $\pi/4 d_0 l_0$.

When limited to the case of uniform fibre angles of pinnation, the muscle geometry employed by Woittiez et al. [1984] in their model is also contained in the current description. Woittiez et al. used kite-like shapes to represent the tendon sheath geometries with the kites at the top and bottom of the muscle geometry having opposite orientation. In this geometry, the muscle fibres running between the tendon sheaths do not have, in general, a direction which is in parallel to the lateral mid-plane of the muscle. A longitudinal cross section of the three-dimensional muscle geometry takes on the shape of a symmetric trapezium. However, this feature has not been translated into the mathematical treatment of the model by Woittiez et al. Rather, the trapezium is transformed into a rectangle by averaging the widths of the top and bottom tendon sheaths for each cross

section. The tendon sheath geometry, as seen through the mathematical implementation of Woittiez et al., consists of a rectangle ending in two triangles along the muscle length axis and is an admissible geometry for the current model.

According to Equations 3.1 through 3.4 and Equation 3.20, muscles of different shapes with identical parameter values for h_{10} , h_{20} , l_0^8 , d_0 and α_0 will exhibit the same muscle force-length relation. Because the model behaviour is to a large extent independent of the absolute model geometry, exploring a simple geometry (with rectangular tendon sheath geometries) will be representative of other geometries. The relative independence of the current model on geometry is not due to an inadequate mathematical treatment, but it is a consequence of the simplifications made at the outset which are similar to those made by other authors. It is rather thanks to the modelling approach taken here, that the independence on geometry becomes readily perceptible.

As a consequence of the discussion above, one could conceive unrealistic muscle model geometries which would lead to the same results as a simple geometry. Therefore, caution is necessary when interpreting results from SLM. However, the good agreement obtained by Woittiez et al. [1984] between model predictions and experimental data supports the idea that there is a correspondence between muscle and model behaviour. The current model will be explored on this basis.

⁸If a more general geometry than the one underlying the derivation of the equations in the previous section is to be used, then the parameters should describe the lateral muscle cross section in a plane which contains the muscle tendons or muscle attachment points.

Whereas a one to one correspondence could be established from a geometrical point of view between the treatment by Woittiez et al. [1984] and the current model, this is not true for the predicted muscle force in dependence of the changing angle of pinnation. Setting $D=0$, the term $\cos(\alpha)/\cos(\beta)$ in Equation 3.20 corresponds to the term $\cos(\gamma)$ in the treatment by Woittiez et al. Therefore, changes in muscle force are here predominantly governed by the angle between the fibre direction and the lower tendon sheath orientation, whereas they depend there on the angle between the fibre direction and the direction of the line of action of the muscle. Realizing that γ is always smaller than α , the model by Woittiez et al. consistently predicts a higher force than the current model. It must be stressed, however, that the equilibrium equation for the current model has been derived by using a physical principle, while the one used by Woittiez et al. has been assumed. Using the model by Woittiez et al., one will predict non-zero forces for a muscle with all its fibres running perpendicular to the tendon sheaths which does not make physical sense.

The current model will be explored below by starting from a simple base geometry with parallel tendon sheaths which will be modified progressively. The geometrical parameters (Table 3.2) are chosen so that they may be taken as a rough approximation of the cat gastrocnemius muscle, with the exception of the reference angle of pinnation, α_0 , which will be freely varied. Anatomical observations would

$$h_{10} = 0.8 \text{ cm}$$

$$h_{20} = 0.0 \text{ cm}$$

$$d_0 = 2.5 \text{ cm}$$

$$l = 8.0 \text{ cm}$$

$$(\text{Muscle Volume, } V = 16 \text{ cm}^3)$$

$$D = 0.0$$

$$\hat{P} = 25 \text{ N/cm}^2$$

$$\alpha_0: \text{variable}$$

Table 3.2: Parameter values for initial muscle model simulations.

limit the choice for the reference angle of pinnation⁹ to an upper limit of about 25° [Benninghoff and Rollhäuser 1952, Wickiewicz et al. 1983, Woittiez et al. 1984]. The first Piola Kirchhoff stress scaling factor, \hat{P} , will be given a value of 25 N/cm² for the remainder of this sub-section¹⁰ [Woledge et al. 1985]. The following conventions will be adopted: Parameters subscripted by 'max' will refer to a configuration for which the fibres are at their maximal active length ($\lambda=1.4$ for fibre force profile number 1). Correspondingly, the subscript 'min' refers to a configuration of fibre minimal active length. The subscript 'peak' refers to a configuration where the muscle reaches its maximum force; this configuration will, in general, be different from the configuration at which the muscle fibres are at

⁹Angles of pinnation in the literature are mostly identified with the angle γ in Figure 3.3.

¹⁰Otten [1988] uses a fibre stress value of 23 N/cm².

optimum length. The latter corresponds to the reference configuration for which the subscript '0' will be used.

Figure 3.9 displays muscle force-length curves for five muscles with similar, but different geometries. The five geometries are described by the same geometrical parameters given in Table 3.2. They differ, however, in their reference angle of pinnation, α_0 , which takes on the values of 15° , 20° , 30° , 40° and 50° , respectively. The fibre force-length characteristic is given by the active part of force profile

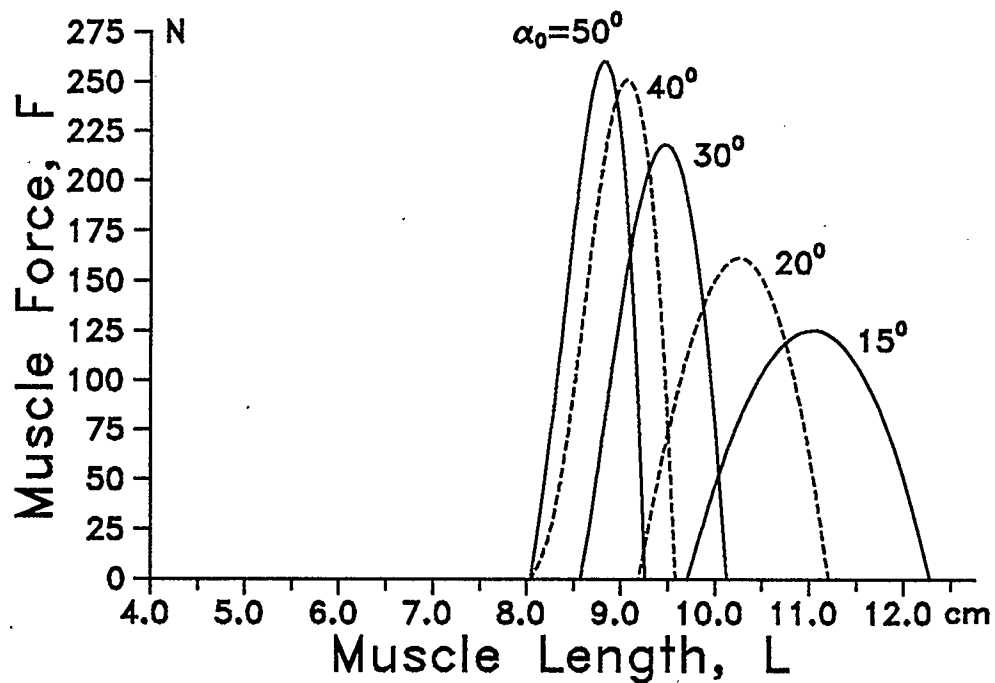


Figure 3.9: Active muscle force-length relations of similar muscles with different reference angles of pinnation.

number 1. With increasing reference angle of pinnation, the peak muscle force increases steadily while the active muscle range, that is, the interval in muscle length over which the muscle is able to generate an active force, decreases. It will be shown below, that the peak muscle force will start to decrease again for higher reference angles of pinnation than those considered at present. The higher muscle peak forces for increasing reference angles of pinnation can be explained by the fact, that more and more fibres are acting in parallel and that this effect overcompensates for the fibre directions becoming increasingly misaligned with the line of action of the muscle. The individual muscle fibres become shorter with an increasing reference angle of pinnation which decreases their absolute active range and subsequently the active range of the muscle.

The interrelation between muscle peak force and active range can also be seen as a consequence of the fixed amount of work a muscle can potentially perform. A unit volume of muscle fibre tissue can be seen to have a specific potential to perform work when the fibres contract completely from maximum to minimum fibre length. All of the muscles above, containing the same amount of tissue volume, should be able to perform an equal amount of work over a complete muscle contraction. Simplifying the concept of work to the product of force times distance, a higher muscle peak force has to be compensated by a smaller range over which a muscle force can be exerted.

In agreement with the argument above, the integral of the muscle force with respect to the muscle length over the active muscle range results in the same value for the curves corresponding to $\alpha_0 = 15^\circ$, 20° and 30° . Muscles with reference angles of pinnation of $\alpha_0 > 38^\circ$, however, deform during the contraction to a configuration in which the fibres attain an actual angle of pinnation of 90° . In this configuration, which will be termed "neutral configuration", no external muscle force is present, even if the fibres themselves are still at a relative length at which they are able to produce a force under stimulation¹¹. The curves in Figure 3.9 for $\alpha_0 = 40^\circ$ and 50° both end at the same minimum muscle length corresponding to the neutral configuration. The muscle force-length integral results in these cases in a smaller value than for the other curves; the "work potential" contained in the muscle tissue cannot be fully realized due to geometric effects.

While the muscle force-length curves differ in peak force and range, their shapes are similar. The symmetric fibre force-length curve is re-scaled to muscle level and slightly distorted (the peak muscle force is shifted slightly to the right relative to the mid-point of the active range of each individual curve).

Figure 3.10 displays the active muscle force-length curves for five muscles with a modified base geometry. Compared to the previous example, the modifications consist in doubling the muscle height ($h_1 = 1.6$ cm) and dividing the tendon plate

¹¹That an actual angle of pinnation of $\alpha = 90^\circ$ results in a zero muscle force, can be seen directly from Equation 3.20; the term " $\cos \alpha$ " evaluates to zero in this case.

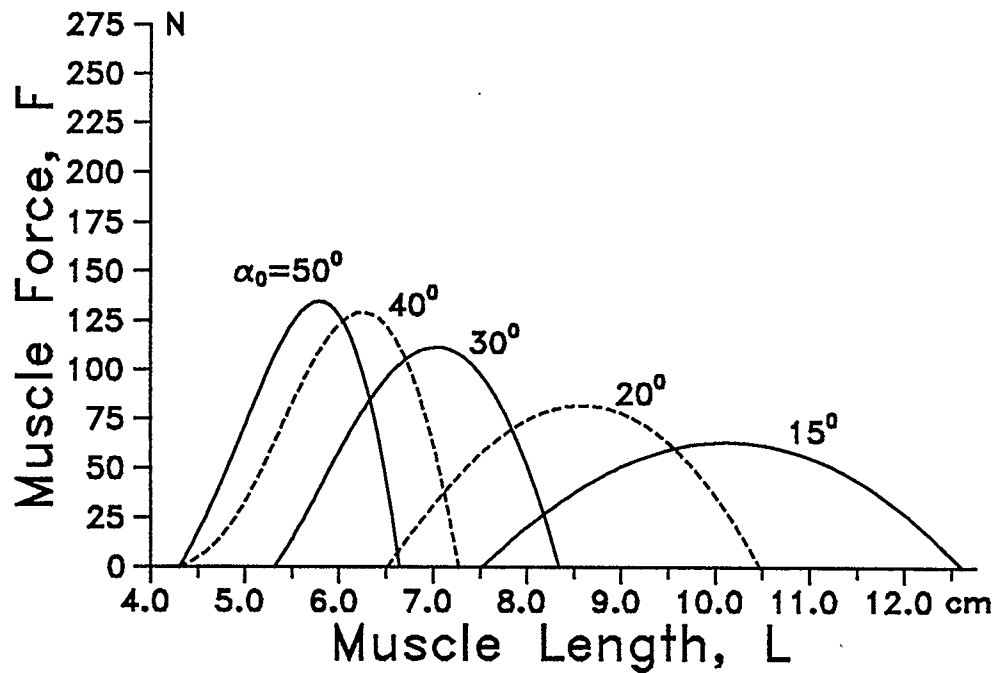


Figure 3.10: Active muscle force-length relations of muscles with alternate geometry.

length, l , by two ($l = 4$ cm); the muscle volumes remain unchanged at 16 cm^3 . The axes of Figure 3.9 and Figure 3.10 are drawn to the same scale. Compared to Figure 3.9 the same characteristics, that is, increasing force and decreasing range for increasing reference angles of pinnation, are observed. While having different absolute force and length values, the curves are similar in both cases. The change in geometry has an effect of scaling alone, and nothing has changed in principle by going from the base geometry to the modified geometry.

The literature attributes a major importance to the "index of architecture" which is defined by the ratio of the mean fibre length at muscle optimal length and the muscle optimal length itself¹² [Kaufman et al. 1989 and 1991, Woittiez et al. 1984, Benninghoff and Rollhäuser 1952]. According to this view, the index of architecture is sufficient to characterize a pennate muscle in its force-length behaviour. However, the force-length curves for $\alpha_0 = 40^\circ$ in Figure 3.10 and $\alpha_0 = 15^\circ$ in Figure 3.9 are almost identical (at different absolute muscle lengths), even though they result from muscles with notably different geometries and with notably different fibre length to muscle length ratios. This observation seems to defy any importance of the index of architecture¹³. However, it may well be that nature does adhere to a "design concept" for which the index of architecture constitutes a significant parameter. If this is the case, the current model does not grasp the underlying reasons for this "design concept", and, by implication, muscle models similar to the current one do not either.

Including the passive fibre forces in the fibre force profile number 1 and using the muscle base geometry leads to the muscle force-length curves shown in Figure 3.11. The curves are only plotted up to the maximum muscle lengths ($\lambda = 1.4$). The ratio of the force magnitudes corresponding to the relative maxima

¹²The muscle optimal length is typically defined as the muscle length at which a muscle can exert maximum force. Additionally, it is commonly assumed that muscle fibres are also at optimal length in this case.

¹³In reversing the argument, different muscles with identical indices of architecture can be constructed whose predicted force-length relations are significantly different.

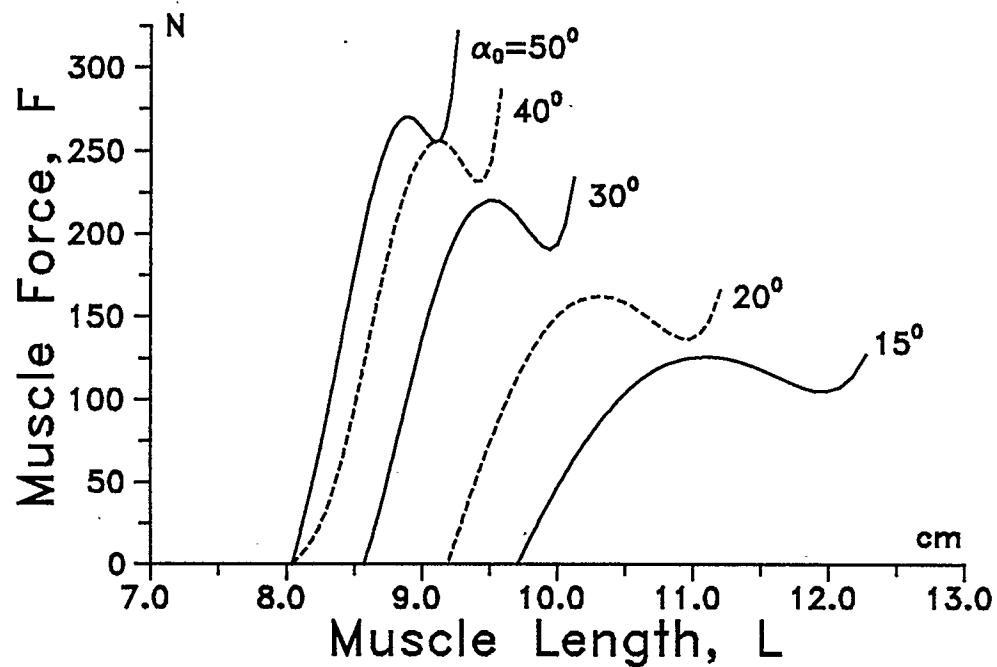


Figure 3.11: Total muscle force-length curves.

and minima of each individual curve decreases for increasing angles of pinnation. Also, the muscle forces at maximum muscle length for each curve increase beyond the relative force maxima. This contrasts with the input fibre force-length relation which has a well defined local minimum value of 84% of the fibre force at optimum fibre length and for which the force at maximum fibre length is equal to the force at fibre optimal length. Consequently, one should proceed with caution when inferring fibre characteristics from experimentally obtained muscle force-length curves.

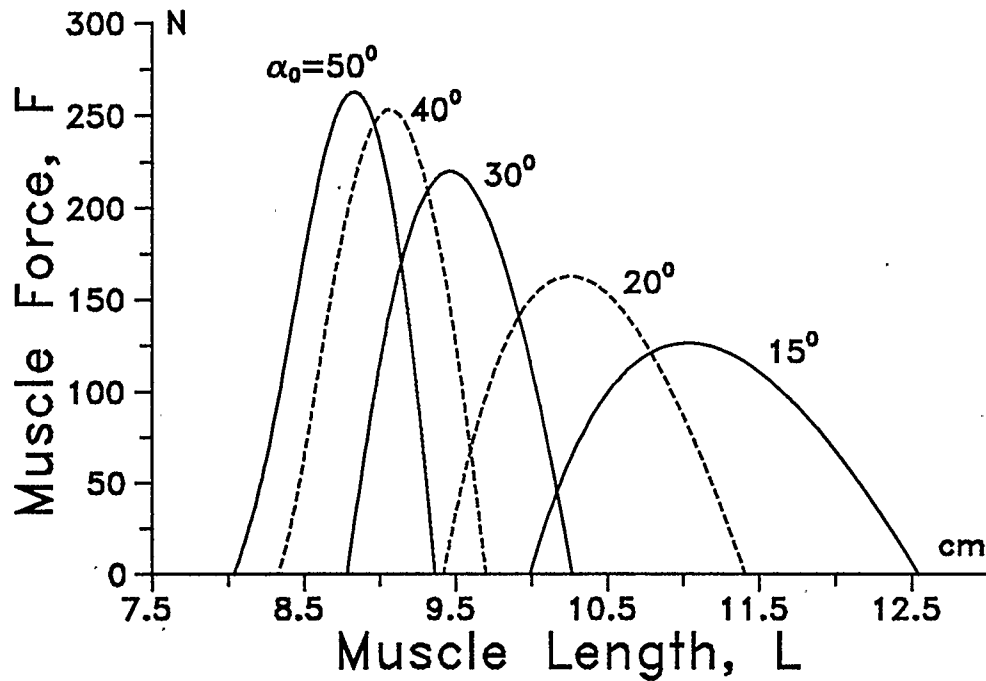


Figure 3.12: Active muscle force-length curves based on fibre force profile number 2.

Figure 3.12 displays muscle force-length curves for muscles which are described by the base geometry and which take the fibre force profile number 2 as input. The relative shift of muscle peak forces to higher muscle lengths is readily perceptible; despite the asymmetric character of the fibre force profile number 2, the muscle force-length curves become symmetric for higher reference angles of pinnation. For the current case, only the curve corresponding to $\alpha_0 = 50^\circ$ reaches the neutral configuration at its shortest length. Finite element simulations of the continuum

model in the following chapters will be based to a large extent on the fibre force profile 2.

So far, entire muscle force-length curves have been considered for discrete values of the reference angle of pinnation, α_0 . The curves have been generated for muscle models which were described by different sets of geometrical parameters and distinct fibre force profiles, thus giving a good idea of the effects of parameter changes. More detailed aspects, for example where the muscle peak force occurs relative to the fibre force-length curve, cannot be inferred from these curves. Selected parameters of interest will now be monitored and displayed individually for an increased number of different muscle geometries, where the geometries differ only in their respective reference angle of pinnation, α_0 (Figures 3.13 through 3.16). The geometric parameters listed in Table 3.2 as well as the active part of fibre force profile number 1 underlie the following considerations. A subset of the parameters displayed in Figures 3.13 through 3.16 can be cross-referenced to Figure 3.9.

Figure 3.13 displays the minimum and maximum actual angle of pinnation (α_{\min} , α_{\max}) as well as the actual angle of pinnation corresponding to the configuration at which the muscle peak force is exerted (α_{peak}). The curved appearance of the line representing α_{peak} shows that the actual angle of pinnation at which a specific muscle exerts its peak force does not coincide with the reference angle of pinnation, α_0 , at which the fibres are at optimal length. The difference between α_0

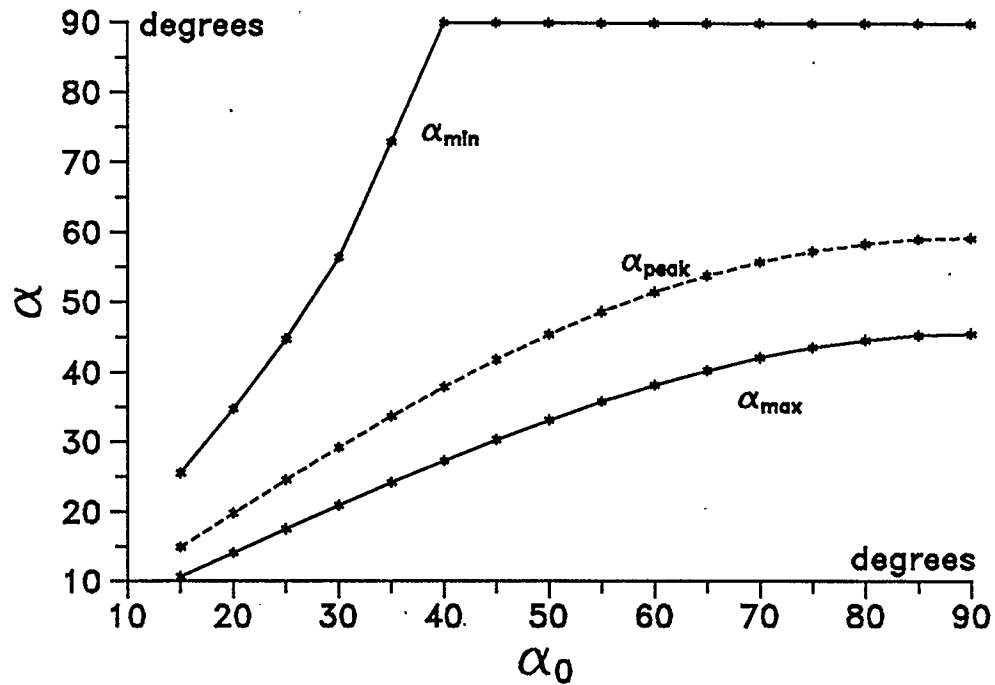


Figure 3.13: Range in the actual angle of pinnation and the actual angle of pinnation corresponding to the muscle peak force as functions of the reference angle of pinnation.

and α_{peak} increases for higher α_0 . Muscles with a higher reference angle of pinnation than 38° reach the neutral configuration during contraction ($\alpha = 90^\circ$).

Figure 3.14 presents selected muscle lengths of interest. The muscle lengths corresponding to the muscle reference configurations (L_{ref}), that is, the muscle lengths for which the muscle fibres assume optimal length, and the lengths at which the muscles exert their peak force, L_{peak} , diverge more and more with increasing α_0 . Again, muscle configurations for muscle peak forces are not identical with configurations for maximum fibre forces. The minimum and maximum

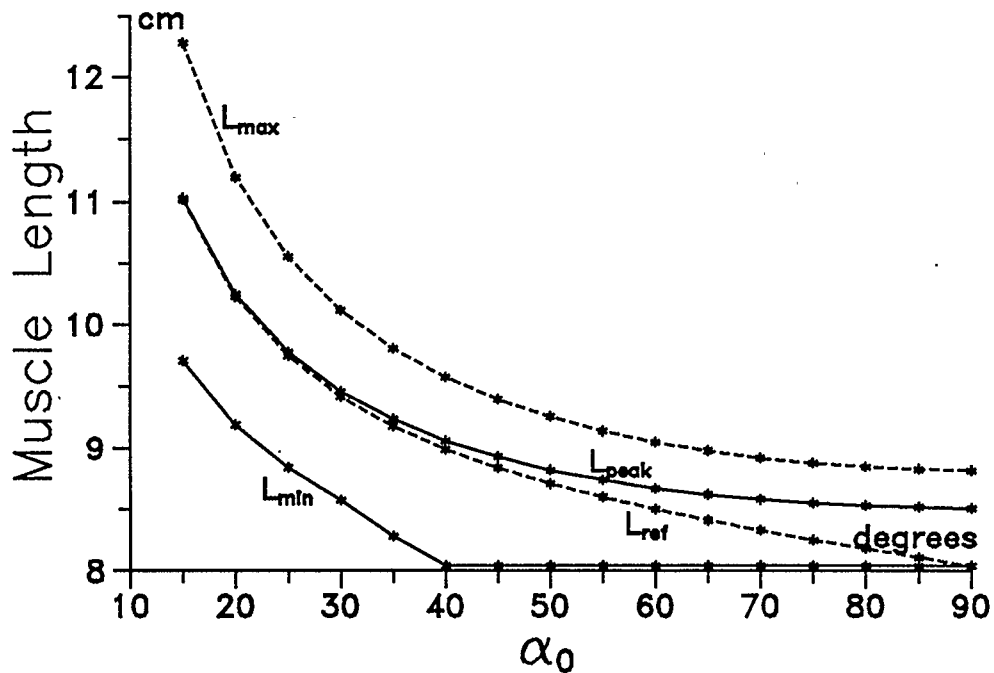


Figure 3.14: Range in the actual muscle length, the actual muscle length corresponding to the muscle peak force, and the muscle reference length as functions of the reference angle of pinnation.

active muscle lengths are indicated by L_{\min} and L_{\max} . The line representing L_{peak} is not located half-way between the lines corresponding to L_{\max} and L_{\min} , but it approaches the line representing L_{\max} . This emphasizes the fact that the symmetric input fibre force-length curve is transformed into a skewed force-length curve at muscle level.

The muscle peak force and the muscle force at reference configuration are shown in Figure 3.15. The absolute highest muscle force is obtained for a muscle with a reference angle of pinnation of about 52° . For higher reference angles of pinnation,

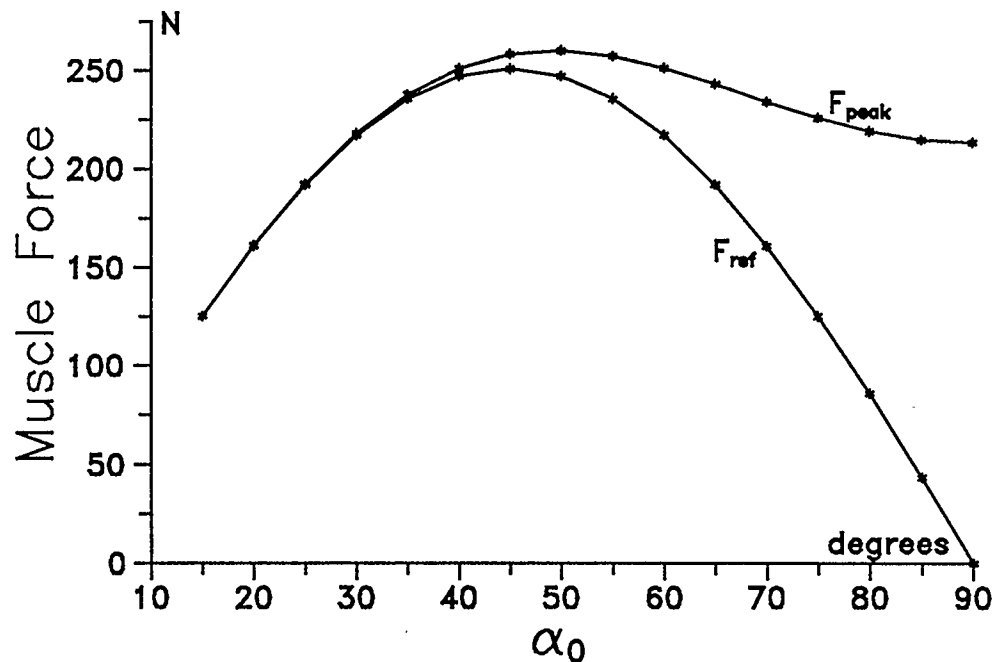


Figure 3.15: Muscle force at muscle reference length and muscle peak force as functions of the reference angle of pinnation.

the muscle peak forces decrease again, and the muscle forces corresponding to the muscle reference configurations fall back to zero.

Finally, Figure 3.16 indicates the amount of work muscles can perform over a full contraction. For a muscle with $\alpha_0 < 38^\circ$, all muscle fibres are able to contract completely, and the muscle is therefore able to produce the maximum amount of work. For higher reference angles of pinnation than 38° , a muscle reaches the neutral configuration during contraction before its fibres have shortened to their minimum length. Consequently, the work which can be produced externally to the muscle is reduced.

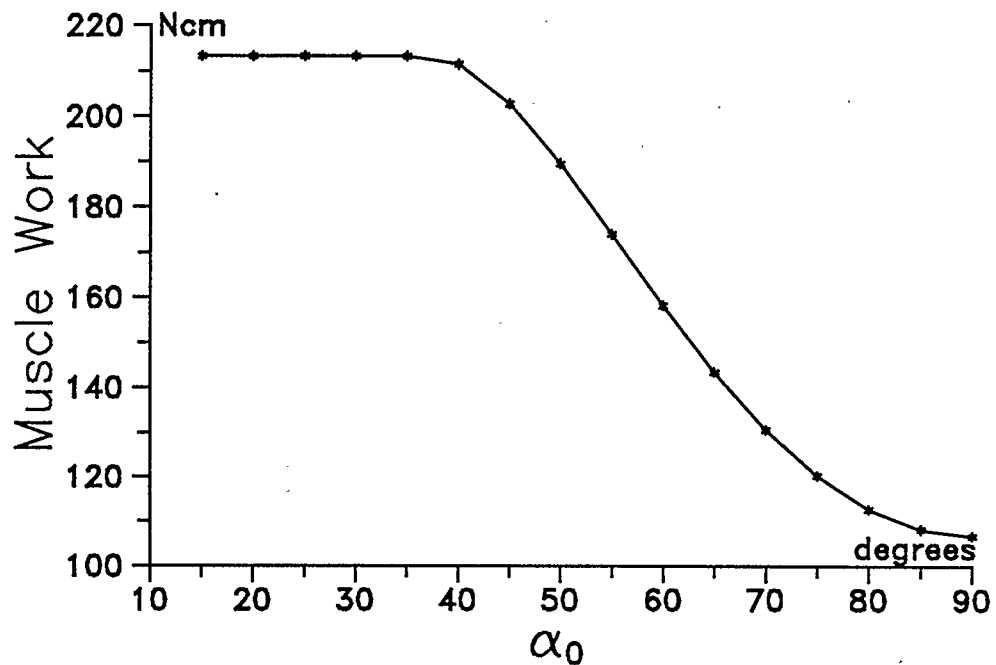


Figure 3.16: Muscle work over a complete contraction as a function of the reference angle of pinnation.

It has been pointed out above, that from all the muscles described by the geometric parameters in Table 3.2, the muscle with the reference angle of pinnation of 52° produces the highest force (Figure 3.15). Furthermore, it follows from Figure 3.13 that this force maximum is exerted at an actual angle of pinnation of close to 45° . At this actual angle of pinnation the muscle fibres assume a relative length for which the Cauchy stress, introduced in Chapter 3.3, peaks. In the context of the current model, this "optimal" angle of pinnation of 45° cannot be explained further. However, the discussion of the CM (Chapter 6) will take this issue up and consider it in the context of the stress state within the muscle

structure. Benninghoff and Rollhäuser [1952] indicated an "optimal" angle of pinnation of 45° . However, no distinction was made between the reference and actual angle of pinnation.

The advantage of a pennate muscle design over a fusiform design is commonly attributed to the pennate muscles being able to produce a comparatively higher force on account of the fact that more contractile material is arranged in parallel between the tendon sheaths [Gans and Bock 1965, Fung 1970]. Following this argument and considering exclusively the generated muscle forces as an optimization criteria, the current model suggests that pennate muscles should exhibit a rather high degree of pinnation (up to 57°). However, anatomical and experimental evidence suggest that angles of pinnation in unstimulated muscles at resting length seldom exceed 25° [Wagemans 1989, Wickiewicz et al. 1983, Benninghoff and Rollhäuser 1952]. Considering the model results presented above, arguments may be made in favour of smaller degrees of pinnation. For example, it has been shown that muscles with angles of pinnation being greater than about 38° can only perform a portion of the work over a full contraction which is potentially contained within the tissue volume. Still, an angle of pinnation of 38° is significantly greater than the angle of 25° indicated anatomically.

Wagemans [1989] performed ultrasound measurements to explore the structural changes of the human gastrocnemius muscle under maximal voluntary contractions. Herzog [1991] used the original results by Wagemans and performed

data analyses in order to quantify the structural changes in terms of angles of pinnation, muscle height and muscle depth. The analysis revealed that the unstimulated muscle assumed angles of pinnation between 25° and 37° depending on the externally controlled muscle length, whereas the contracted muscle took on angles of pinnation close to 45° independent of the muscle length before the contraction was carried out. Relating the results from Wagemans [1989] and Herzog [1991] to the current model, the following observations can be made: Assuming an anatomically realistic reference angle of pinnation of 25° , the current model predicts the peak force to occur very close to this precise angle. During contraction an angle of pinnation of about 45° is attained by the muscle (Figure 3.13). However, by that time the muscle force level will have decreased to close to zero. This is contrary to the observations by Wagemans that there is not only an active force at this configuration, but that, in fact, the maximum muscle force is reached for this angle of pinnation.

The current model does predict the maximum muscle force for an actual angle of pinnation of close to 45° (Figures 3.14 and 3.15). However, this actual angle of pinnation is associated with a reference angle of pinnation of 52° which is not at all comparable to the observations made by Wagemans. Still, it is felt, that the agreement between model predictions and experimental observations regarding the optimal angle of pinnation are more than a mere coincidence, and this agreement certainly constitutes a suitable starting point for further investigations. With respect to the current model, it seems that certain aspects of muscular

contraction are grasped by the underlying assumptions whereas others are not. In particular, it may be worth investigating whether the kinematics of tissue deformation, more precisely the deformation of the contractile microstructures are as strictly linked to the global muscle deformations as assumed.

In interpreting the geometric parameters in Table 3.2 as an approximate description of the cat gastrocnemius muscle, the following comments can be made by comparing the current model predictions to experimental results by Herzog et al. [1990]: Assuming a reference angle of pinnation of 25° , the current model predicts a muscle peak force of about 190 N (Figure 3.15) and a range of close to 1.9 cm (Figure 3.14). These values, when referred to larger sized muscles, compare favourable to the results by Herzog et al. who obtained muscle peak forces between 150 N and 210 N, and a normal range of muscle movement of about 1.9 cm. For the current model, the range of 1.9 cm covers the entire extent of muscle activity, that is to say that the muscle force in this range starts at zero, achieves its peak value and then returns again to zero (compare to Figures 3.9 and 3.12). The experiments by Herzog et al., however, resulted in muscle force-length curves which start with a small but non-zero force for the shortest muscle configuration and terminate with a force magnitude slightly below the muscle peak force at the longest muscle configuration¹⁴. Therefore, it may be assumed that

¹⁴It should also be mentioned in this context that muscle force length-curves analogous to Figure 3.11 are normally not observed in experiments (the curves in Figure 3.11 are based on the total fibre force profile number 1 which includes passive fibre forces). Contrary to the current model predictions, experiments do not show a renewed force increase for muscle lengths being higher than the length corresponding to the local force minima (e.g. Herzog et al. [1990] and Muhl [1982]).

the muscle range investigated by Herzog et al. of 1.9 cm corresponds to a significantly smaller muscle length interval in the current model, and that the match between experimental results and model predictions is, therefore, less perfect. By exploiting the uncertainties in model parameter values (e.g. the maximum active fibre stress, the shape of the fibre force profile, and the model geometric parameters which describe the complex physical muscle geometry) a match could be reestablished. A simple fitting procedure, however, does not enhance the understanding of basic concepts associated with muscular contraction.

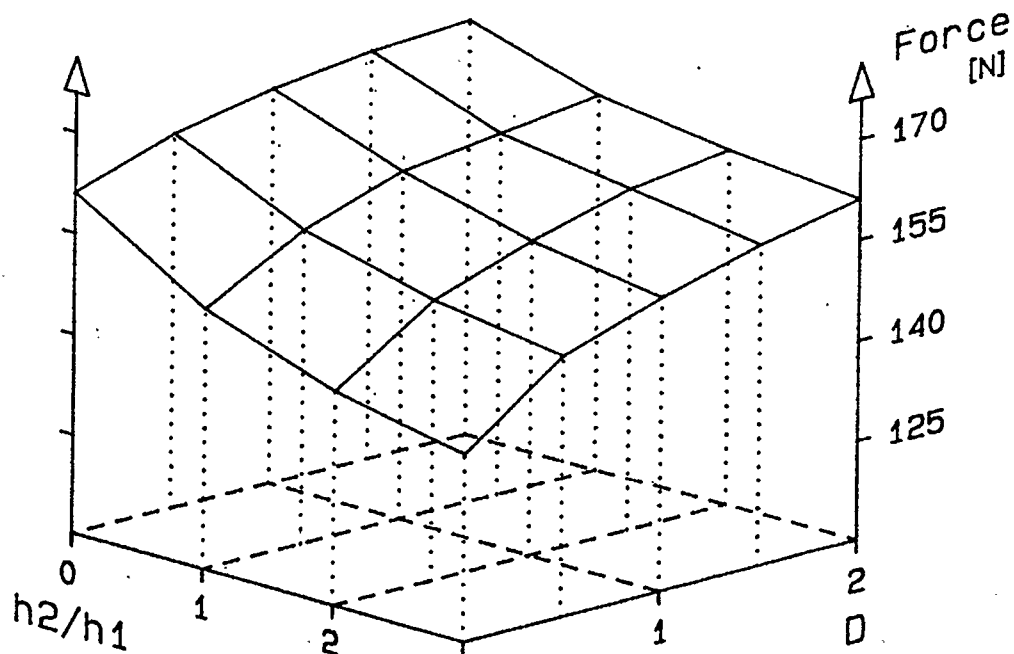


Figure 3.17: Influence of trapezoidal muscle cross section and depth change during contraction on the muscle peak force.

So far, only muscle geometries with parallel tendon sheaths and cases with constant muscle thicknesses during deformation have been considered. The muscle cross section geometry may take on a trapezoidal shape by assigning non-zero values to h_2 (Figure 3.3), and the muscle can be allowed to thicken during contraction by assigning non-zero values to the parameter controlling the amount of depth change, D (Equation 3.4). A thickening of the muscle is associated with a decrease in the distance between the tendon sheaths. This general deformation pattern should be expected, because the fibres are assumed to pull between the tendon sheaths. The effects of trapezoidal muscle cross sections as well as the degree of thickness change during muscle contraction for muscles of equal volume on the muscle force at muscle reference length are displayed in Figure 3.17. A muscle geometry with parallel tendon sheaths described by the muscle length, $L_0 = 10$ cm, lower tendon plate length, $l = 8$ cm, and muscle height parameters $h_{10} = 0.7$ cm and $h_{20} = 0.0$ cm has been chosen as the starting point. Increasing values for the ratio h_2/h_1 describe muscle geometries with an increasingly trapezoidal cross section. Figure 3.17 indicates, that the muscle force decreases in a nonlinear way for increasing h_2/h_1 values. The muscle force increases with increasing values for D , that is for higher muscle deformations in thickness direction. It is important to realize, that for a fixed h_2/h_1 value the muscle geometry is also determined. Still, depending on the parameter D the muscle force changes. This is a consequence of the "quasi" three-dimensional deformation of the muscle

and this effect is neglected when the muscle equilibrium condition is derived from a free body diagram with an assumed orientation of F_A in Figure 3.8.

3.4 Summary and Outlook

A geometrical straight line muscle model for parallel fibred pennate muscles has been developed in this section which is described by a closed set of non-linear algebraic equations. In the derivation process of this model, the equilibrium condition has been based on a physical principle, and the technique employed to derive the equations revealed that the final equations can be easily adapted to describe more complex muscle geometries. Comparing muscles of similar geometry but varying reference angles of pinnation, α_0 , predicted peak muscle forces increased to an absolute maximum at $\alpha_0 = 52^\circ$. Furthermore, the absolute force maximum is reached under an actual angle of pinnation of $\alpha = 45^\circ$. While Wagemans [1989] did observe maximum muscle forces at an actual angle of pinnation of close to 45° , the current model does not reproduce all aspects of her experimental observations.

The mathematical derivation of the equations governing the presented model did not make use of approximations and logical jumps so that any deficiency in model predictions must be associated with the underlying simplifications and assumptions. Judging from the current scientific literature, there is little reason to doubt that the muscle contractile behaviour has its origin exclusively in contracting muscle fibres. The kinematic simplifications which, in essence, require both tendon

sheaths and the muscle fibres to be rigid in bending are obviously too severe, and they will be abandoned in the development of the continuum muscle model in the following chapters.

Chapter 4

The Continuum Muscle Model

Geometrical straight line muscle models (SLM), similar to the one presented in Chapter 3, are predominantly motivated by mathematical simplicity rather than the attempt to describe the physical reality appropriately. Instead of obtaining the muscle deformation as the result of internal fibre forces and tissue material behaviour, the mode of the muscle deformation is imposed by kinematic constraints. The shape of muscle geometries is restricted from the outset by the need for closed form analytic expressions which relate the fibre elongations to the overall muscle deformation. Certain types of questions, for example, the influence of different tendon sheath flexibilities on muscle performance, cannot be investigated with these models.

The straight line approach to muscle modelling guarantees a solution in the form of a muscle force-length relation which results from global equilibrium considerations. However, the global considerations completely bypass any local

equilibrium considerations. It is of no concern, whether the imposed deformation shapes lead to configurations which ensure a local equilibrium of the structure; in fact this question cannot be settled in the context of these models due to the absence of more detailed constitutive relations.

Different ways of relaxing the simplifications and assumptions made at the outset of Chapter 3 could be envisioned. The relaxation of these simplifications and assumptions leads, in general, to an indeterminacy of the mathematical equations which underlie the model. Rather than being a drawback, the resolution of these indeterminacies by physically meaningful principles adds to the quality of the results obtained. An analytical treatment of the model and closed form solutions become, however, more and more unlikely.

The theory of continua will be chosen here as an approach to a more detailed muscle modelling and numerical solutions will be sought with the help of the Finite Element Method. Special difficulties to be overcome in the modelling process lie in the fact that the muscle tissue will have to be described as an anisotropic, active and nonlinear material (physical non-linearity). Because of the large deformations inherent to muscle deformation, the geometrically nonlinear theory of deformation has to be employed as well.

A Finite Element program package, Ansys (Version 4.3) by Swanson Analysis Systems Inc., Houston, has been used for the finite element modelling. Since the built-in capabilities of this package did not allow an adequate representation of

muscle tissue behaviour a special element, representing the active muscle fibre characteristics, has been formulated and linked into the existing program.

4.1 Simplifications and Assumptions

The search for a description of muscle behaviour on a more detailed level underlies the attempt to use the theory of continua for the purpose of muscle modelling. This approach does not eliminate the need for making simplifications and assumptions during the modelling process. The focus of the simplifications and assumptions will rather be shifted from a global perspective (e.g. predefined modes of global muscle deformation) to local considerations about muscle tissue and tendon behaviour. The global structural behaviour as a consequence of the local assumptions are of particular interest.

The current sub-chapter has to be understood as a compilation of the more significant simplifications and assumptions made, and it is meant to facilitate a comparison of the approach taken in Chapter 3 to the one below. Several topics are merely touched upon here and discussed further in the following chapters.

Simplifications and assumptions for the current model are essentially made on three different levels, namely at the level of the continuum description (CD), the finite element implementation (FEI) and the model generation (MG). Choices made at higher levels have a direct bearing on lower levels. At the CD level, for example, basic decisions have to be made about how to represent the muscle tissue

behaviour in the mathematical language of the theory of continua. Most of these decisions are bona fide assumptions, in the sense that statements regarding their completeness in describing tissue behaviour are difficult. Decisions at the FEI and MG levels are more of the character of simplifications, that is to say that a different and perhaps more detailed description could have been chosen. The simplifications at the FEI level arise from the finite element discretization of the continuous description. The discretization itself is inevitable, if a solution is to be sought using any numerical method; there is, however, a choice as to how the discretization is performed. Because the capabilities of the finite element package used do not allow an adequate description of the muscle fibre characteristics, a new element type had to be implemented. For that reason, the FEI modelling level has to be considered separately for the muscle tissue.

In order to compare the current model to the SLM of Chapter 3, similar cases will be treated. Consequently, relatively simple muscle geometries will be employed at the MG level. These simplifications are completely arbitrary. Different and more complex model geometries could be generated using the finite element implementation which are only limited by the model generating capabilities of the finite element program package used. By contrast, a change in the assumptions about muscle tissue behaviour would require a reworking of the entire modelling process from the CD level down.

It must be emphasized that the basic assumption underlying the remainder of this thesis concerns the applicability of the theory of continua to muscle modelling. The great success of the theory of continua in describing a vast number of phenomena in a wide range of circumstances seems to make this remark superfluous. Nevertheless, a basic point should be made about how a material - muscle tissue in the present case - is "seen through the eyes" of the continuum description. As one traverses muscle tissue on a microscopic scale, one encounters many different structures (e.g. thick and thin filaments, collagen fibres, sarcolemma, etc.), each having different mechanical properties. The continuum description does not attempt to reproduce this complexity; rather the mechanical behaviour at each point of the continuum is seen as an average of all the structures in a small volume surrounding this point in the real world structure. This is often compared to a smearing out or blurring of finer details, and it is this feature which allows the tools of calculus to be employed for the analysis of real life entities. However, it cannot be excluded that some essential features of the material are getting lost in the process of smearing out microscopic details. Special approaches in the theory of continua (e.g. the theory of micromorphic continua, higher order constitutive relations etc.) are able to describe certain types of more complex material characteristics, but they will not be used in the context of this thesis.

For the current treatment, muscle tissue is assumed to be adequately described as a simple material. This means in particular, that the stress at a given point is

completely determined by the state of the deformation at this point. The equations for equilibrium and strain measures in the form given in Chapter 2.1 are applicable.

It is further assumed that there exists a strain energy function (potential function) for muscle tissue which depends exclusively on the strain measures and an additional parameter associated with the degree of stimulation. Due to the directionality of the contractile property of the fibres, muscle tissue will be described as a transversely isotropic fibre reinforced material. No dynamic effects will be taken into account, the analysis will be based on statics exclusively.

The discussion above is also applicable to tendon sheath tissue, except for the parts which concern the contractile properties of the muscle tissue. Tendon sheath tissue is seen as a two dimensional entity with tensile stiffness but no bending stiffness.

Muscles will be represented in two dimensions as plane strain models. The models are taken to represent the mid-plane of a muscle containing its line of action and thus the two opposite tendon attachment points. Muscle fibres run within the model plane. For the treatment of three-dimensional structures in a two-dimensional idealization, Ansys, the finite element package used, offers only the plane strain and plane stress assumptions. Because there will be stresses in the muscle thickness direction (normal to the model plane) and because these stresses take on a major importance for the model performance, the plane strain assumption

appears more appropriate. A more general treatment of the third dimension should certainly be envisioned for future applications.

The finite elements which represent the muscle body, will be implemented as triangular three-noded elements with two translational degrees of freedom per node. The deformation shape functions allow each individual element to experience a homogeneous deformation only. This results in the strains being constant over the domain of a single element and leads to non-conforming elements. No provision has been made to allow for initial strains. Consequently, the model reference configuration corresponds to a stress free configuration and constitutes a trivial equilibrium configuration when no muscle tissue stimulation is present.

Muscle geometries at reference configuration are approximated by straight lines extending over a large part of the muscle geometry. Fibres run straight and parallel over macroscopic portions of the model geometry, but not necessarily over the entire extent of the muscle geometry. The fibre density, that is the number of fibres penetrating a unit area perpendicular to the fibre direction, will be constant over macroscopic areas of the muscle geometry. A uniform stimulation will be applied to all the elements representing the muscle tissue. Tendon sheaths will have a uniform tensile stiffness over their entire lengths. No restrictions concerning the deformed configuration are imposed, except for the boundary conditions (e.g. at the tendon attachment points).

Modelling Level

- Muscle tissue is described as a simple (first order) fibre reinforced material. A strain energy function is assumed to exist, which only depends on the strain measures and a stimulation parameter.	CD
- Tendon sheath tissue has tensile stiffness only.	CD
- Constitutive relations are considered for statics only.	CD
- Finite elements representing the muscle tissue are implemented as two dimensional triangular plane strain (three-noded) elements with two translational degrees of freedom per node. The individual elements are restricted to a homogeneous deformation. No provisions for initial strains are made.	FEI
- Tendon sheaths are represented by two-noded spar elements with two translational degrees of freedom per node. No moment is transmitted from one tendon element to its neighbours.	FEI
- The reference muscle geometry is approximated by straight line segments of macroscopic extent. At muscle reference configuration, the fibre density is kept constant and fibres run straight and parallel over large segments of the muscle geometry. The same tissue stimulation parameter value is used for all elements representing the muscle tissue. The tensile stiffness of the tendon sheaths will be uniform over their lengths.	MG

Table 4.1: Major simplifications and assumptions underlying the continuum muscle model.

Table 4.1 summarizes the major simplifications and assumptions underlying the continuum muscle model presented in this chapter and the finite element implementation presented in the next chapter. The modelling level at which these simplifications and assumptions are made - continuum description (CD), finite

element implementation (FEI), model generation (MG) - is flagged out at the right hand side.

4.2 Constitutive Relations

The purpose of this sub-chapter is to establish a material description for muscle tissue which can be used in conjunction with the continuum mechanical approach to muscle modelling. Considerations made in Chapter 3.2.3 regarding the fibre force-length relations are carried over, and they will be supplemented only to the extent necessitated by the application of the theory of continuum mechanics. Tendon sheaths will be described by an elementary elastic material law. They will, therefore, not be considered at this point in time.

When discussing muscle behaviour, either in the context of a muscle model or in a more informal manner, the literature commonly regards a muscle as the sum of its parts. Muscles are seen to behave as a composition of a large number of individual fibres, with the force-length relations of individual fibres being transferred to the whole muscle. A possible interaction between fibres in the tissue context is excluded by this point of view. In the case of pennate muscles, an influence of the muscle geometry on muscle performance is acknowledged, but this influence is perceived to simply constitute a rescaling of the fibre force-length curve to the muscle scale. As a case in point, Hill's three element model for muscular contraction [Hill 1938] has been interpreted to describe adequately both the

contractile behaviour of a single fibre as well as that of entire muscles¹ (e.g. Fung [1981]). The possibility that fibre tissue might exhibit additional characteristics compared to single fibre behaviour, which in turn might be important to whole muscle performance, is rarely considered.

The following arguments may be listed in support of the notion which regards muscle function as a simple extension of individual fibre performance: the building blocks of muscles are certainly individual fibres. Single fibres can be identified in a muscle and they can, in principle, be isolated while keeping them fully functional. The microscopic active components of muscles, the sarcomeres, seem to be functionally parcelled by fibres, which is to say, that under stimulation, either all or none of the sarcomeres in a single fibre become active. Sarcomeres are aligned with the fibre length axis and shorten in this direction during contraction. One can therefore assume that muscle tissue, too, has a contractile direction coincident with the local fibre direction. Furthermore, considerations about muscle function on the basis of fibre characteristics do not lead to immediate contradictions when they are compared to experimental results. However, as manifested in the discussion part of Chapter 3, muscle models based on single fibre properties do not reproduce all aspects of muscle behaviour correctly.

¹Hill's original equation was established for whole muscles. Extensions to this equation, e.g. Hill's three element model, introduce additional parameters which are seen to be related to fibre microstructures, and numerical values of these parameters are often determined by applying the model to single fibre experiments.

A large variety of experiments has been performed on single muscle fibres, especially on amphibian. Muscle fibre behaviour is relatively well understood and the wide acceptance of the cross bridge and sliding filament theory (Huxley [1957, 1974], Gordon et al. [1966]) puts this understanding on a theoretical foundation. While there are considerable variations in the reported values of absolute active fibre force (which are not necessarily obtained from experiments on individual fibres) and active fibre range, the main features of fibre force-length curves are undisputed.

The muscle fibre force is usually thought to originate due to the thick and thin filament interaction at the sarcomere level and to be passed on along the fibre length axis from sarcomere to sarcomere. An interesting dissenting opinion is held by Vain [1990], who suggests, that the primary active component of fibres consists in a tendency to thicken. The local thickening tendency would then lead to a stretching of the collagen fibre network, and the resulting forces would be passed on over short distances to the sarcolemma and endomysium, with these connective tissue structures, instead of sarcomere to sarcomere connections, transferring forces in fibre length direction.

Any attempt to determine active muscle tissue material properties on a small representative tissue volume specimen directly in an experimental set-up would be invalidated from the outset; this kind of procedure implies a sectioning of muscle fibres and, because of individual fibres acting as a unit under stimulation, it would

alter the properties of the tissue sample in an unpredictable manner. It is also doubtful, whether a lifelike stimulation of the specimen could be achieved.

Facing these difficulties, researchers have restricted themselves to measure only passive muscle tissue properties directly. Demer and Yin [1983] and Yin et al. [1987], for example, performed biaxial stretch experiments on thin canine cardiac muscle tissue sheets, with the stretch being applied both in fibre direction and transverse to fibre direction. Their experimental results were used by Lanir [1983] and Lanir et al. [1988] to validate a general three-dimensional constitutive model of passive cardiac muscle tissue. However, the question remains open, whether active tissue characteristics are merely overlaid on the passive characteristics, or whether active muscle tissue should be regarded from a constitutive point of view as a different material compared to passive tissue.

Efforts aimed at gaining a deeper understanding of active muscle tissue material properties seem to be restricted to indirect experimental procedures, complemented by theoretical considerations. Truong [1974] performed wave propagation measurements on whole stimulated muscles and matched the experimental results with a constitutive model which describes active muscle tissue as a viscoelastic material. Part of Truong's experimental data has been reinterpreted successfully by Anton and Epstein [1989] using a perfectly elastic but nonlocal material model. The fact that two completely different material models - and there may still be others - reproduce the same experimental data, indicates

that the issue of finding an adequate constitutive law for active muscle tissue is far from settled. Incidentally, both interpretations mentioned above use a one dimensional tissue description, which excludes material properties transverse to fibre direction.

The validity of any constitutive model can, in principle, only be asserted in a relative sense by the number of different experimental phenomena which are reproduced by the model in question. Realizing that not all direct experiments which may be desired for a constitutive validation are practically possible, a different emphasis is put on muscle modelling: a notion of how muscle tissue might work is translated into a constitutive law on which a muscle model is built. The model predictions for entire muscles can then be compared to experimental observations of entire muscles, which are, in a relative sense, easier to obtain. Comparing predicted and experimentally observed muscle behaviour will give an indication about the adequacy of the constitutive law and thus about the assumed underpinnings of muscle tissue behaviour. In this sense, the currently predominant notion of muscle tissue being a superposition of individual muscle fibre behaviour will be tested here.

The constitutive law below pictures muscle tissue as a composite or fibre reinforced material. One-dimensional active and passive muscle fibre characteristics, which are attributed to the solid muscle tissue components (e.g. thick and thin filaments) are identified with the one dimensional fibres in the

constitutive model. The fibres are imagined to be suspended in a fluid matrix. The fluid matrix, in turn, represents the water content in muscle tissue and provides the near incompressibility of the material. Fluid matrix and fibres deform together, that is, no relative motion between fibres and fluid takes place. Stating it differently, a control volume under deformation consists at all times of the same material points representing the same collection of fluid and fibre particles. Fibres do not interact directly, they do however interact indirectly through the fluid matrix.

It will be assumed that a strain energy function exists for muscle tissue and the left Cauchy-Green stretch tensor, \mathbf{C} , will be employed as the measure of deformation. Spencer [1984] has shown that the strain energy function, W , of a general fibre reinforced material with one family of fibres can only depend on the following invariants (I_α):

$$\begin{aligned} I_1 &= \text{tr} \mathbf{C}, & I_2 &= \frac{1}{2}((\text{tr} \mathbf{C})^2 - \text{tr} \mathbf{C}^2), & I_3 &= \det \mathbf{C} \\ I_4 &= \mathbf{a} \mathbf{C} \mathbf{a} = \lambda^2, & I_5 &= \mathbf{a} \mathbf{C}^2 \mathbf{a} \end{aligned} \quad (4.1)$$

where \mathbf{a} represents the unit vector in fibre direction. λ has the significance of the stretch ratio of a line element being aligned with the fibre direction and will therefore be termed fibre stretch ratio. By definition, the second Piola-Kirchhoff stress tensor components follows from the strain energy function, $W(I_\alpha)$, through:

$$S_{KL} = \sum_{\alpha=1}^5 \frac{\partial W}{\partial I_{\alpha}} \left(\frac{\partial I_{\alpha}}{\partial C_{KL}} + \frac{\partial I_{\alpha}}{\partial C_{LK}} \right) \quad (4.2)$$

Commonly, the term "strain energy function" is associated with energy being passively stored in a continuum in connection with its deformation (elastic strain energy). In the present application, a more general view is taken; the active characteristics of muscle tissue will be included in the strain energy function. Here, the term "(generalized) strain energy function" implies only, that there exists a unique functional dependency of the strain energy, W , on the strain measures, \mathbf{C} .

The invariants I_1, I_2 and I_3 determine the isotropic characteristics of the matrix material. In the present case, where the matrix material is assumed to behave as an incompressible fluid, I_3 is really needed only in the expression for the strain energy function which describes the muscle tissue material law. In anticipation of what will be possible to implement in the finite element program package used, the strain energy function chosen will describe a (solid) Mooney-Rivlin material which depends on the invariants I_1, I_2 and I_3 [Mooney 1940]. Constants in the actual expression for the strain energy function will be chosen so that the material law approximates that of a fluid as closely as possible. The active and passive unidirectional fibre characteristics enter the strain energy function by means of the invariant I_4 . The invariant I_5 , which accounts for a more general interaction between fibres, for example under shear deformation, will not be included in the strain

energy function, because such an interdependence is here assumed not to exist.

By assumption, the strain energy function takes on the additive form:

$$W = W_m(I_1, I_2, I_3) + W_{fa}(I_4; \Theta) + W_{fp}(I_4) \quad (4.3)$$

In equation 4.3, the subscript "m" refers to the contribution of the matrix and "f" to that of the fibre characteristics. The fibre part is, as in Chapter 3.2.3, split further into an active (subscript "a") and passive part (subscript "p"). Θ has the significance of a stimulation parameter and will be discussed in more detail below.

The functional form of W_m , which incorporates the Mooney-Rivlin material law, is given by the following expression [Kohnke 1989]:

$$W_m = A(I_1 - 3) + B(I_2 - 3) + C \left(\frac{1}{(I_3)^2} - 1 \right) + D(I_3 - 1)^2$$

$$C = \frac{A}{2} + B \quad (4.4)$$

$$D = \frac{1}{2} \left(\frac{A(5\nu - 2) + B(11\nu - 5)}{1 - 2\nu} \right)$$

The finite element available within Ansys which will be used to represent the tissue matrix characteristics is based on this particular functional form of W_m . The independent parameters in Equation 4.4, which are input quantities to the finite element muscle model, are A, B and ν . ν controls the degree of compressibility, while A and B influence the elastic response to stretch and shear deformations.

In the finite element models, A and B will be set to 0.125 N/cm^2 and ν will be set to 0.4995 . These values have to be seen in the context of the other material parameters introduced below and have been chosen so that the matrix material behaves as much as possible like an incompressible fluid while still guaranteeing convergence of the finite element model.

The fibre characteristics are introduced into the strain energy function in Equation 4.3 by way of the invariant I_4 . Considering how the second Piola-Kirchhoff stress tensor is derived from the strain energy function (Equation 4.2), and how the second Piola-Kirchhoff stress tensor and the Cauchy stress tensor are interrelated (Equation 2.12), the following observations can be made: let the reference configuration at a certain point within a continuum be described with respect to a rectangular cartesian coordinate system with the X_1 - axis pointing along the fibre direction, and let the spatial configuration be described with respect to a rectangular cartesian coordinate system with the x_1 - axis pointing along the deformed fibre direction. The only non-zero stress tensor components will then be S_{11} for the second Piola-Kirchhoff stress tensor, P_{11} for the first Piola-Kirchhoff stress tensor and σ_{11} for the Cauchy stress tensor. A graphical picture of this situation is given in Figure 4.1 for the second Piola-Kirchhoff stress and the Cauchy stress. Furthermore, the second Piola-Kirchhoff stress depends only on $I_4 = \lambda^2$ (λ being the fibre stretch ratio). Under the assumptions made above regarding the coordinate systems of reference and spatial configuration, I_4 is equal to the component C_{11} of the left Cauchy-Green deformation tensor, \mathbf{C} .

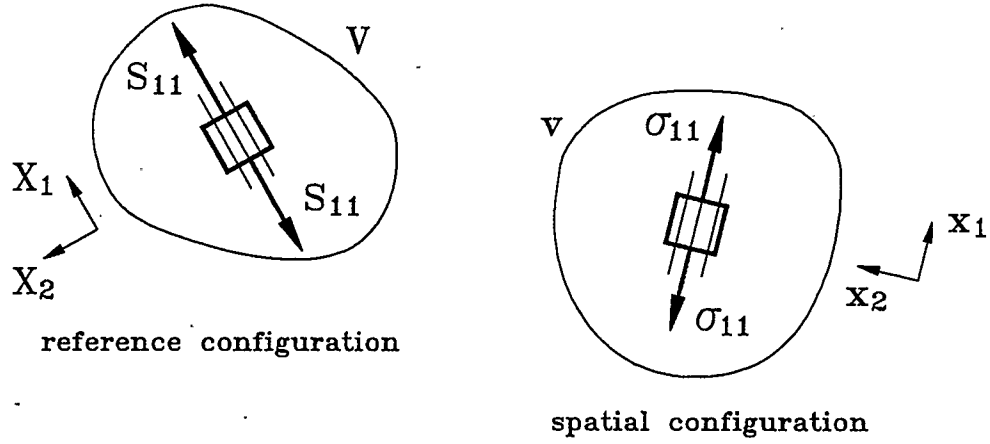


Figure 4.1: Fibre second Piola-Kirchhoff stress and Cauchy stress components with respect to local coordinate systems.

The second Piola-Kirchhoff stress-strain relation for the fibre part can, therefore, be directly given in a simpler and more intuitive way, which corresponds to a one-dimensional description:

$$S_{11} = S_{11}(\lambda^2) = S_{11}(I_4) \quad (4.5)$$

This procedure makes the relationship of the following discussion to the one in Chapter 2.3.2 readily apparent. The stress-strain relations to be developed below are integrable and the contribution to the strain energy function, W , coming from the fibre part of the material, W_f , can be formally obtained through:

$$W_f = \frac{1}{2} \int S_{11}(\lambda^2) d\lambda^2 = \frac{1}{2} \int S_{11}(I_4) dI_4 \quad (4.6)$$

Thus, a description which is independent of any specific coordinate system is recovered.

According to the discussion in Chapter 3.2.3, there is a direct correspondence between the functional dependency of the fibre force and the first Piola-Kirchhoff stress tensor. This similarity persists in the current context with the special choice of coordinate systems made above, and the first Piola-Kirchhoff stress tensor, P_{11} . In Chapter 3.2.3 a "force profile function" was introduced, which will also be used here; in the current context, the force profile will depend on the stimulation parameter, θ , in addition to its dependence on λ :

$$f(\lambda; \Theta) = f_a(\lambda; \Theta) + f_p(\lambda) \quad (4.7)$$

The total force profile is split into an active and passive part. Furthermore, the force profile is taken to be dependent on λ , instead of $\lambda^2 = I_4$. The final expressions for different force profile functions can, however, be made dependent on λ^2 by a simple variable transformation. The non-zero first Piola-Kirchhoff stress tensor component, P_{11} , follows through scaling with the factor \hat{P} , which will be set to 25 N/cm²:

$$P_{11} = \hat{P} f(\lambda; \Theta) \quad (4.8)$$

It has to be recalled, that the force profile functions are obtained, in principle, from single fibre experiments. It is one of the assumptions made here that the functional dependency remains the same within the muscle tissue setting. Using Equation 2.13 and being conscious of the special set of coordinate systems chosen, the non-zero second Piola-Kirchhoff stress tensor component, S_{11} , is obtained from Equation 4.8:

$$S_{11} = \frac{\hat{P}}{\lambda} f(\lambda; \Theta) \quad (4.9)$$

Below, the mathematical expressions for the force profiles employed in the following chapters are listed, and their graphical representations are given in Figures 4.2 and 4.3:

Force profile number 1:

$$\begin{aligned} f_{1,a} &= \Theta (-6.25\lambda^2 + 12.5\lambda - 5.25) \\ f_{1,p} &= 3.289 \cdot 10^{-6} e^{9.037\lambda} - 0.02766 \end{aligned} \quad (4.10)$$

Force profile number 2:

$$f_{2,a} = \Theta \frac{1}{1.034\lambda^*} (-6.25(\lambda^*)^2 + 12.5\lambda^* - 5.25) \quad (4.11)$$

$$f_{2,p} = 1.838 \cdot 10^{-6} e^{9.447\lambda^*} - 0.01059$$

$$(\lambda^* = \lambda - 0.08349)$$

Both force profiles have an equal range for their active components, that is, the λ -interval for which the active part of the force profile function is different from zero is 0.8. The integral of the active force profiles with respect to λ over their

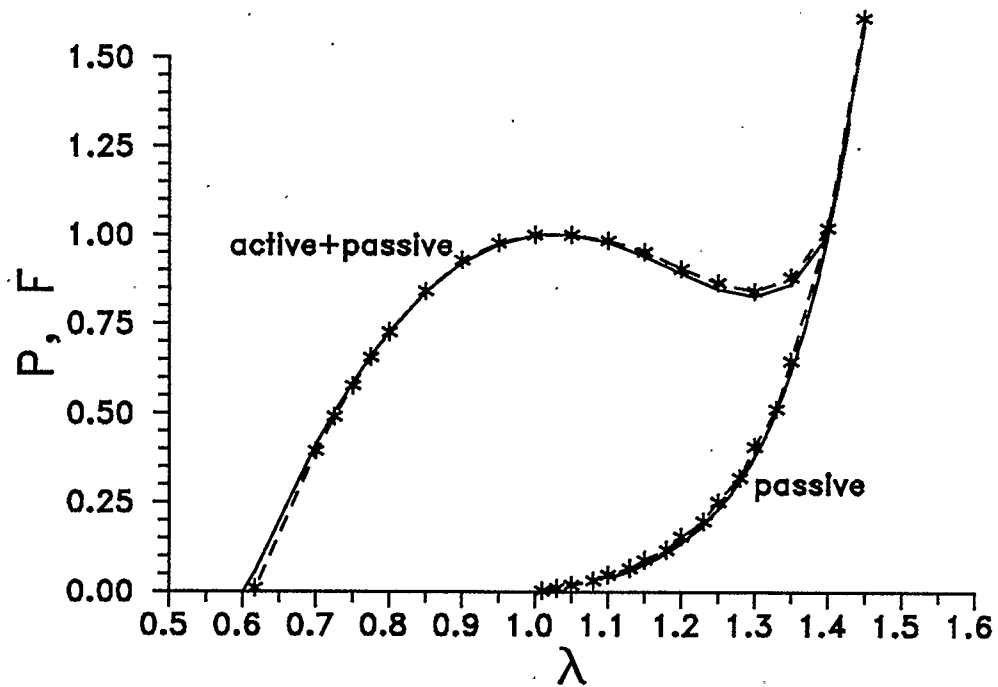


Figure 4.2: Force profile number 1.

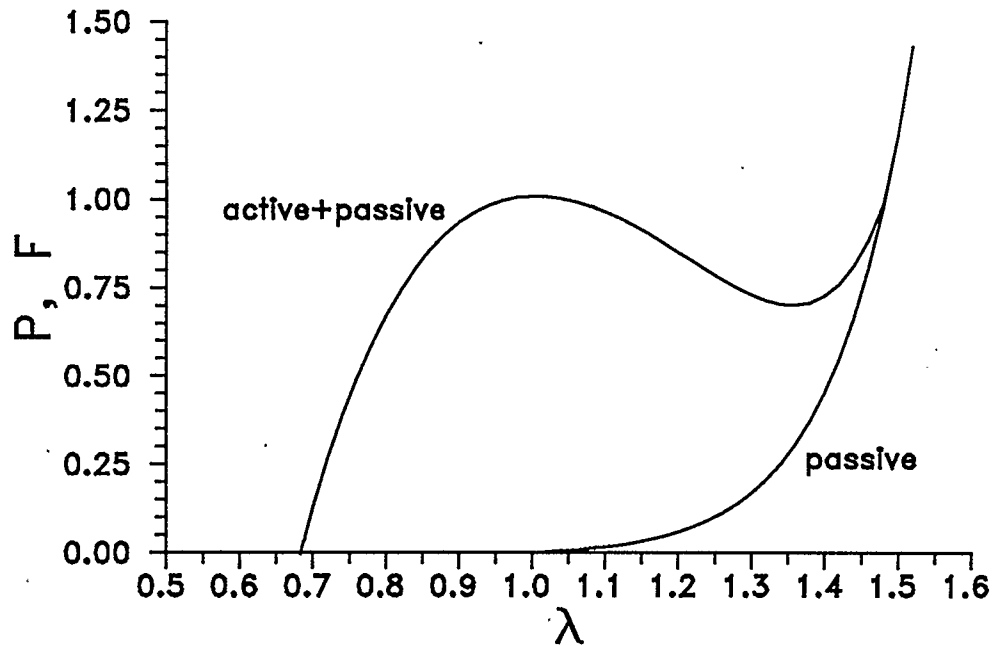


Figure 4.3: Force profile number 2.

respective active range is also equal. The two force profiles reach their active peak at $\lambda = 1$, which will be equated here to the fibre optimal length. Passive fibre profile components are only defined for $\lambda > 1$.

Force profile number 1 describes in its active component the fibre force-length relation used by Woittiez et al. [1983, 1984]. In Figure 4.2, the active and passive force profiles are displayed with solid lines. The dashed lines with star markers show the results from a finite element simulation of a thin strip of "tissue material", where the finite element implementation described in the next chapter has been used. The closeness of the lines indicates that the intended tissue behaviour has

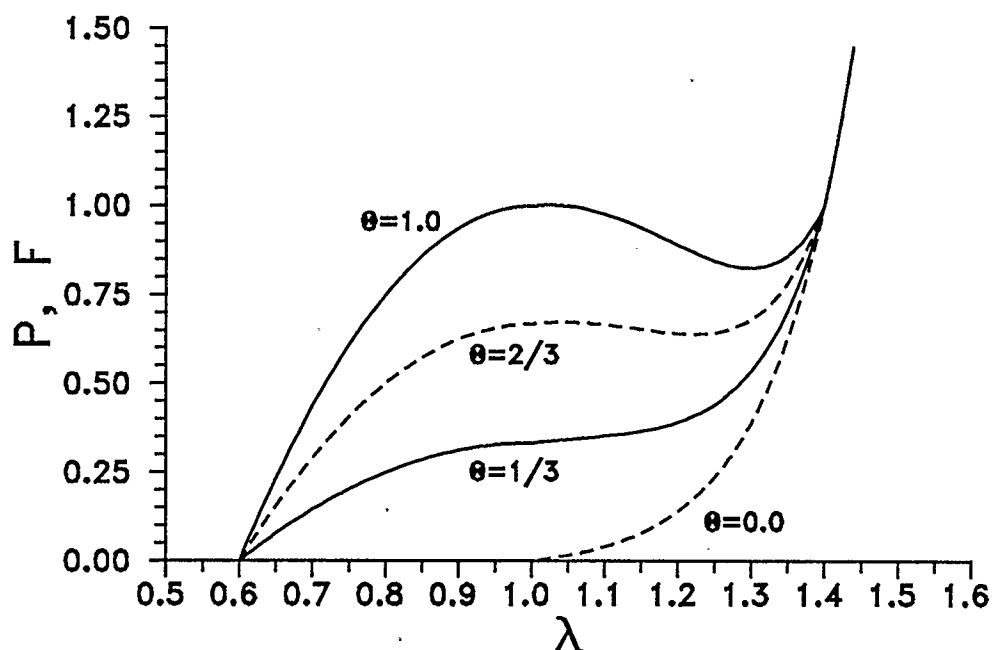


Figure 4.4: The influence of the stimulation parameter, θ , on force profile number 1.

been successfully implemented into the finite element description. Small differences for small and large values of λ are due to the fact, that the tissue (fluid) matrix has not been implemented as a simple fluid element.

Using the fibre force profile number 1 will lead in the finite element analysis to a relative shift of the active peak in the muscle force-length curve to the right. Fibre force profile number 2 compensates for this effect to some degree, in that the force profile active peak is shifted to the left. This shift is achieved by an asymmetric active part of the force profile. This profile also reflects the asymmetric nature of experimentally determined muscle fibre force-length profiles.

The stimulation parameter, θ , enters the active parts of the force profile functions as a multiplicative factor. Its influence on the total force profile of type 1 is illustrated in Figure 4.4. The particular mathematical form is not intended to mirror the actual muscle tissue or fibre response to a partial stimulation. In fact, it is doubtful whether one single parameter would suffice to describe the degree of stimulation adequately. In the context of this thesis, the muscle behaviour will be investigated for $\theta = 1$, which will be identified with maximal stimulation. Because of the nonlinear nature of the equations underlying the current muscle model, the finite element solution will have to be obtained by iterations and in incremental steps of internal loading or stimulation. It is solely for this reason, that the stimulation parameter, θ , has been introduced here.

The material description of muscle tissue to be used in the continuum model has been presented in this chapter. How the adopted material description is realized within the finite elements and the global finite element muscle model is the subject of the following chapter.

Chapter 5

The Finite Element Implementation

It is intended to simulate muscular contraction by using the Finite Element Method. To this end, models have to be generated whose elements are based on the constitutive description set out in Chapter 4. Ansys (Version 4.3), the finite element package used, contains an element which is based on the large deformation theory and which incorporates the isotropic material law of Equation 4.4. However, there is no large deformation element available which includes the active and anisotropic characteristics of muscle tissue. Therefore, an element will be formulated below (custom element) which adds the anisotropic characteristics to the isotropic element. After formulating the custom element, the muscle finite element models to be used in subsequent chapters will be described.

5.1 Formulation of a Custom Finite Element

The custom finite element will be formulated as a triangular two-dimensional plane strain element with three nodes, one node being placed at each triangle vertex. Nodal parameters are the translational displacement degrees of freedom and nodal forces in the coordinate X- and Y-directions. The element will be formulated entirely based on numerical methods, in particular, the element (tangent) stiffness matrix will be established by numerical differentiation. Taking this approach makes it inherently easier to modify the element implementation, which is of advantage for experimenting with different material laws, for example. In contrast to the notations used so far, the element formulation will make use of the Gibbs vector and matrix notation.

A new equilibrium configuration of the entire finite element muscle model under changing (internal) loading and boundary conditions will be sought by using an iterative approach which is based on the Newton-Raphson Method. In principle, the equations for the entire finite element model can be put into the following form:

$$[\mathbf{K}]_n \{\Delta \mathbf{U}\}_n = \{\mathbf{F}^a\}_n - \{\mathbf{F}^c\}_n \quad (5.1)$$

where the index n refers to the current (n^{th}) iteration. The matrix $[\mathbf{K}]_n$ represents the global (tangent) stiffness matrix, the vector $\{\Delta \mathbf{U}\}_n$ the displacement increment for the current iteration, the vector $\{\mathbf{F}^a\}_n$ the applied load vector, and the vector $\{\mathbf{F}^c\}_n$ denotes the force correction vector which, in the current case, will be assembled

from the nodal element force vectors $\{\mathbf{F}^e\}_{n-1}$ resulting from the solution of the preceding iteration. The total displacement after the n^{th} iteration will be given by:

$$\{\mathbf{U}\}_n = \{\mathbf{U}\}_{n-1} + \{\Delta\mathbf{U}\}_n \quad (5.2)$$

Equation 5.1 is assembled from the individual element stiffness matrices and force correction vectors. It is, therefore, necessary to derive expressions for the custom element stiffness matrix, $[\mathbf{K}^e]_n$, and the nodal force vector of the custom element, $\{\mathbf{F}^e\}_n$, based on the spatial element configuration. The element nodal coordinate vector, $\{\mathbf{X}\}$, and the nodal displacement vector, $\{\mathbf{U}\}$, corresponding to the preceding iteration are the base information provided. They are represented as follows:

$$\begin{aligned} \{\mathbf{X}\}^T &= \{\tilde{X}_1, \tilde{X}_2, \tilde{X}_3, \tilde{X}_4, \tilde{X}_5, \tilde{X}_6\} = \{X_1, Y_1, X_2, Y_2, X_3, Y_3\} \\ \{\mathbf{U}\}^T &= \{\tilde{U}_1, \tilde{U}_2, \tilde{U}_3, \tilde{U}_4, \tilde{U}_5, \tilde{U}_6\} = \{U_{1X}, U_{1Y}, U_{2X}, U_{2Y}, U_{3X}, U_{3Y}\} \end{aligned} \quad (5.3)$$

The vectors $\{\mathbf{X}\}$ and $\{\mathbf{U}\}$ are of dimension six according to the number of the nodal degrees of freedom. Vector components superimposed by a tilde, for example \tilde{X}_i , are generic placeholder with the actual value of their index fixing their relative position within the vector. The plain vector components (no superimposed tilde) give additional information as to their meaning. X_1 , for example, represents the X-coordinate of node number one, and U_{1X} represents the displacement of node number 1 in X-direction.

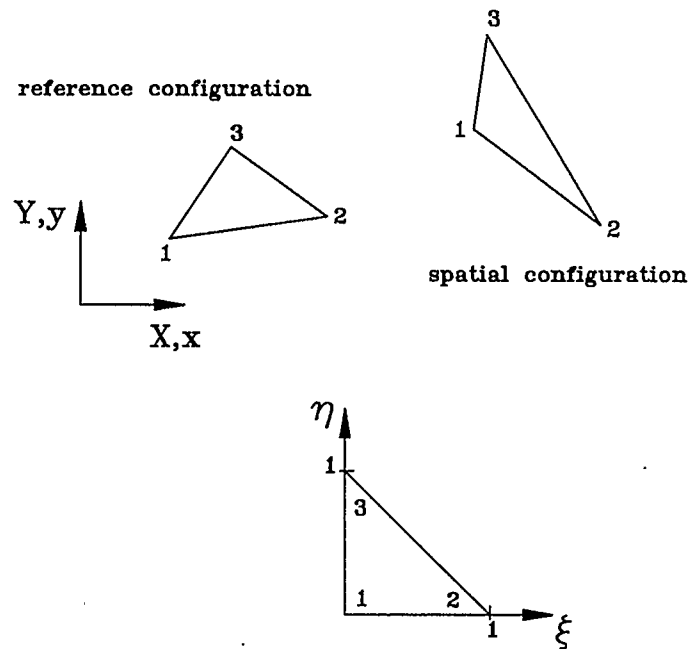


Figure 5.1: Triangular element geometry in reference and spatial configuration, and unit triangle.

Figure 5.1 displays a triangular element in its reference and in its spatial (deformed) configuration. Both configurations are described with respect to the same cartesian coordinate system; in order to avoid confusion, the reference coordinates are given in upper case letters (X, Y) and the spatial coordinates in lower case letters (x, y). The triangular element region in both configurations can be mapped one-to-one onto the unit triangle displayed at the bottom of Figure 5.1. For the case of the triangle in reference configuration, the transformation equations are given by:

$$\begin{aligned}
 X &= X_1 + (X_2 - X_1)\xi + (X_3 - X_1)\eta \\
 Y &= Y_1 + (Y_2 - Y_1)\xi + (Y_3 - Y_1)\eta
 \end{aligned}
 \tag{5.4}$$

Identical relations, with the coordinates written in lower case, hold for the triangle in spatial configuration. An area element is transformed according to:

$$\begin{aligned}
 dA &= dx dy = J d\xi d\eta \\
 J &= (X_2 - X_1)(Y_3 - Y_1) - (X_3 - X_1)(Y_2 - Y_1)
 \end{aligned}
 \tag{5.5}$$

Furthermore, the following relations are obtained from Equation 5.3 which will be needed below:

$$\begin{aligned}
 \frac{\partial \xi}{\partial X} &= \frac{Y_3 - Y_1}{J} & \frac{\partial \eta}{\partial X} &= -\frac{Y_2 - Y_1}{J} \\
 \frac{\partial \xi}{\partial Y} &= -\frac{X_3 - X_1}{J} & \frac{\partial \eta}{\partial Y} &= \frac{X_2 - X_1}{J}
 \end{aligned}
 \tag{5.6}$$

Given the displacement shape functions according to the following equations:

$$\begin{aligned}
 N_1(\xi, \eta) &= 1 - \xi - \eta \\
 N_2(\xi, \eta) &= \xi \\
 N_3(\xi, \eta) &= \eta
 \end{aligned}
 \tag{5.7}$$

the transformation from reference to spatial configuration can be cast into the following form which is dependent on the nodal displacements U_{ix} and U_{iy} , and where "i" refers to the nodal numbers from 1 to 3:

$$\begin{aligned}
 x &= X + u_x(X, Y) = X + \sum_{i=1}^3 U_{iX} N_i(\xi, \eta) \\
 y &= Y + u_y(X, Y) = Y + \sum_{i=1}^3 U_{iY} N_i(\xi, \eta)
 \end{aligned}
 \tag{5.8}$$

The shape functions restrict the element region to a homogeneous deformation, that is, lines are mapped into lines by the transformation. Consequently, the originally triangular element region is mapped onto another triangular region with straight edges (Figure 5.1). Differentiating Equation 5.8 results in the deformation gradient, $[\mathbf{F}]$. The equation below exemplifies this step for the deformation gradient component F_{xx} :

$$F_{xx} = \frac{\partial x}{\partial X} = 1 + \sum_{i=1}^3 U_{iX} \left(\frac{\partial N_i}{\partial \xi} \frac{\partial \xi}{\partial X} + \frac{\partial N_i}{\partial \eta} \frac{\partial \eta}{\partial X} \right)
 \tag{5.9}$$

Using Equations 5.7 and 5.8 the components of the deformation gradient, $[\mathbf{F}]$, can now be expressed in terms of the nodal coordinates and nodal displacement parameters:

$$\begin{aligned}
F_{xx} &= 1 + \frac{1}{J} (U_{1X}(Y_2 - Y_3) + U_{2X}(Y_3 - Y_1) + U_{3X}(Y_1 - Y_2)) \\
F_{xy} &= \frac{1}{J} (U_{1X}(X_3 - X_2) + U_{2X}(X_1 - X_3) + U_{3X}(X_2 - X_1)) \\
F_{yx} &= \frac{1}{J} (U_{1Y}(Y_2 - Y_3) + U_{2Y}(Y_3 - Y_1) + U_{3Y}(Y_1 - Y_2)) \\
F_{yy} &= 1 + \frac{1}{J} (U_{1Y}(X_3 - X_1) + U_{2Y}(X_1 - X_3) + U_{3Y}(X_2 - X_1))
\end{aligned}
\tag{5.10}$$

As a consequence of the assumed displacement shape functions, N_i , the deformation gradient components are constant over the domain of each element.

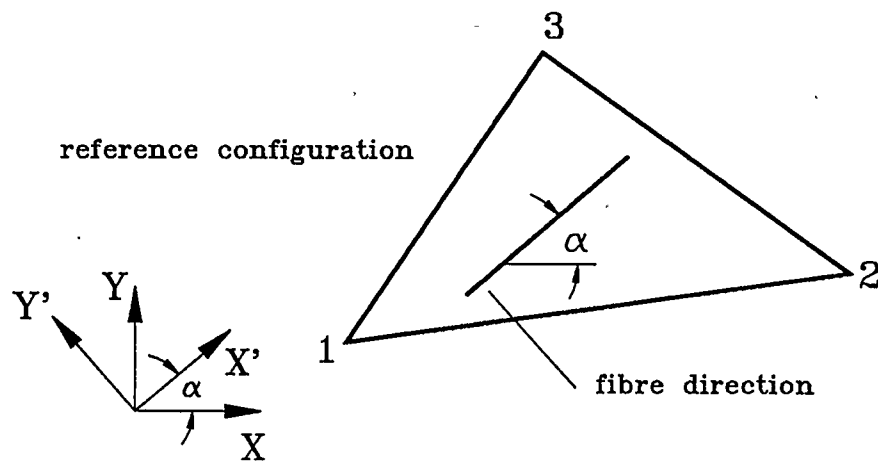


Figure 5.2: Element fibre direction in the reference configuration and element reference coordinate system (X' - Y').

The one-dimensional fibre characteristics have a definite and constant direction in each element, these fibre characteristics being assumed to be aligned with the element plane. The fibre direction is uniquely determined by specifying the angle, α , which is included between the "fibre"-direction and the X-axis of the global coordinate system (GCS). Figure 5.2 illustrates this point. Furthermore, Figure 5.2 shows a primed coordinate system (X' - Y') which will be called element coordinate system (ECS). The X' -axis of the ECS points in fibre direction. The fibre stretch ratio, λ , is obtained by observing how a line element, being identified here with its unit tangent vector, $\{\mathbf{n}\}$, will be stretched under the deformation described by the deformation gradient, $[\mathbf{F}]$, in Equation 5.10:

$$\lambda = \frac{|[\mathbf{F}]\{\mathbf{n}\}|}{|\{\mathbf{n}\}|} \quad (5.11)$$

$$\lambda = \sqrt{(F_{xx}\cos\alpha + F_{xy}\sin\alpha)^2 + (F_{yx}\cos\alpha + F_{yy}\sin\alpha)^2}$$

$$\{\mathbf{n}\}^T = \{\cos\alpha, \sin\alpha\}$$

The second Piola-Kirchhoff stress tensor, with its components referred to the element coordinate system (X' - Y'), is now obtained by using Equation 4.9 and a suitable force profile function, for example Equations 4.10 and 4.11. In addition, the value of the stimulation parameter, Θ , is needed at this point as input:

$$[\mathbf{S}]_{ECS} = \begin{bmatrix} \frac{\hat{P}}{\lambda} f(\lambda; \Theta) & 0 \\ 0 & 0 \end{bmatrix} \quad (5.12)$$

Using the following transformation equation, the Cauchy stresses referred to the global coordinate system are obtained:

$$[\sigma]_{GCS} = \begin{bmatrix} \sigma_{xx} & \sigma_{xy} \\ \sigma_{xy} & \sigma_{yy} \end{bmatrix}_{GCS} = \frac{1}{\|[\mathbf{F}]\|} [\mathbf{F}][\mathbf{Q}][\mathbf{S}]_{ECS}[\mathbf{Q}]^T[\mathbf{F}]^T \quad (5.13)$$

$$[\mathbf{Q}] = \begin{bmatrix} \cos\alpha & -\sin\alpha \\ \sin\alpha & \cos\alpha \end{bmatrix}$$

The transformation matrix, $[\mathbf{Q}]$, transforms the second Piola-Kirchhoff stress tensor from its representation in the ECS to its representation in the GCS. It is now necessary to relate the nodal forces to the Cauchy stresses. Given the nodal force vector, $\{\mathbf{F}\}$, and a virtual nodal displacement vector, $\{\delta\mathbf{u}\}$, in the deformed configuration

$$\begin{aligned} \{\mathbf{F}\}^T &= \{\tilde{F}_1, \tilde{F}_2, \tilde{F}_3, \tilde{F}_4, \tilde{F}_5, \tilde{F}_6\} = \{F_{1x}, F_{1y}, F_{2x}, F_{2y}, F_{3x}, F_{3y}\} \\ \{\delta\mathbf{u}\}^T &= \{\delta\tilde{u}_1, \delta\tilde{u}_2, \delta\tilde{u}_3, \delta\tilde{u}_4, \delta\tilde{u}_5, \delta\tilde{u}_6\} = \\ &\quad \{\delta u_{1x}, \delta u_{1y}, \delta u_{2x}, \delta u_{2y}, \delta u_{3x}, \delta u_{3y}\} \end{aligned} \quad (5.14)$$

and introducing the stress vector, $\{\sigma\}$, and the virtual (linear) strain vector, $\{\epsilon\}$,

$$\begin{aligned}\{\sigma\}^T &= \{\sigma_{xx}, \sigma_{yy}, \sigma_{xy}\} \\ \{\delta \epsilon\}^T &= \{\delta \epsilon_{xx}, \delta \epsilon_{yy}, \delta \gamma_{xy}\}\end{aligned}\tag{5.15}$$

the Principle of Virtual Work for the element under consideration can be stated as follows:

$$\int \{\delta \epsilon\}^T \{\sigma\} dx dy - \{\delta \mathbf{u}\}^T \{\mathbf{F}\} = 0 \tag{5.16}$$

It is important to realize that the Principle of Virtual Work as stated above relates to the deformed element, that is, to the spatial configuration. Using the transformation Equations 5.4 with the nodal coordinates of the deformed configuration and assuming again the displacement shape functions of Equation 5.7, Equation 5.16 can be transformed into

$$\{\delta \mathbf{u}\}^T \left(\int [\mathbf{B}]^T \{\sigma\} dx dy - \{\mathbf{F}\} \right) = 0 \tag{5.17}$$

where $[\mathbf{B}]$ represents the operator matrix which relates the nodal displacements to the linear strains based on the displacement shape functions chosen. Varying the nodal displacement vector components individually the following expressions for the nodal forces are obtained:

$$\{F\} = \frac{1}{2} \begin{Bmatrix} (y_2 - y_3)\sigma_{xx} + (x_3 - x_2)\sigma_{xy} \\ (x_3 - x_2)\sigma_{yy} + (y_2 - y_3)\sigma_{xy} \\ (y_3 - y_1)\sigma_{xx} + (x_1 - x_3)\sigma_{xy} \\ (x_1 - x_3)\sigma_{yy} + (y_3 - y_1)\sigma_{xy} \\ (y_1 - y_2)\sigma_{xx} + (x_2 - x_1)\sigma_{xy} \\ (x_2 - x_1)\sigma_{yy} + (y_1 - y_2)\sigma_{xy} \end{Bmatrix} = \{F^e\}_n \quad (5.18)$$

Equation 5.18 represents the element nodal forces which are passed on to main finite element routines.

The element stiffness matrix, $[K^e]$, is derived column by column through numerical differentiation. To this end, the procedure outlined above will be applied with incremented and decremented displacement vectors

$$\begin{aligned} \{U^{+i}\} &= \{U\} + \{\Delta U_i\} \\ \{U^{-i}\} &= \{U\} - \{\Delta U_i\} \end{aligned} \quad (5.19)$$

where $\{\Delta U_i\}$ designates an incremental displacement vector with all its components set to zero, except for the i^{th} component which will have a value of $\Delta U = |\{\Delta U_i\}|$. $\{U\}$ represents the displacement vector corresponding to the solution of the previous iteration. With the incremented and decremented displacement vectors, new nodal force vectors are obtained

$$\begin{aligned}\{F^{+i}\} &= \{F(\{U^{+i}\})\} \\ \{F^{-i}\} &= \{F(\{U^{-i}\})\}\end{aligned}\tag{5.20}$$

and the i^{th} column of the element stiffness matrix, $\{K_i^e\}$, is derived from the following expression:

$$\{K_i^e\} = \frac{1}{2\Delta U} \{ \{F^{+i}\} - \{F^{-i}\} \}\tag{5.21}$$

Subsequently, the element stiffness matrix itself, $[K^e]$, is assembled by combining all stiffness matrix columns according to

$$[K^e] = [\{K_1^e\}, \{K_2^e\}, \{K_3^e\}, \{K_4^e\}, \{K_5^e\}, \{K_6^e\}]\tag{5.22}$$

Due to the particular nonlinear character of the force profile functions used, the element stiffness matrix, $[K^e]$, will, in general, not be positive definite (after the singular displacement modes are removed). The implications of this fact are best shown using a one-dimensional analogy. Figure 5.3 displays a portion of a nonlinear force-displacement (F-u) relation, represented by the thick curve, for a one-dimensional mechanical component which, in the current context, can be taken to represent a muscle fibre under maximal stimulation. Imagine the fibre to have a configuration corresponding to U_i , and to be loaded by an applied force of magnitude F_a . The intersection of the lines for constant U_i and F_a is not located on

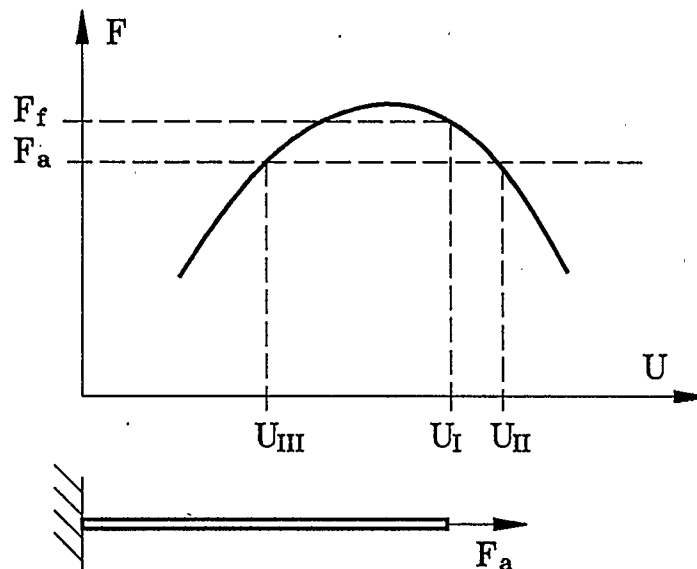


Figure 5.3: Multiple equilibrium configurations illustrated for the case of a general non-linear function.

the force-displacement curve, and it does, therefore, not constitute an equilibrium configuration. There are two possible equilibrium configurations corresponding to the displacements U_{II} and U_{III} . However, only the equilibrium configuration corresponding to U_{III} is physically indicated, because the higher internal force F_f , overcompensates the applied force, F_a , and leads to a decrease in length and smaller values of U . Use of the iterative Newton-Raphson method to search for an equilibrium configuration

$$U_{n+1} = U_n - \frac{F_f(U) - F_a}{F'_f(U)} \bigg|_{U=U_n} \quad (5.23)$$

$$F'_f(U) = \frac{dF_f(U)}{dU}$$

will result in a convergence to U_{II} instead of U_{III} when the solution process is started from U_I . The desired solution can, however, be obtained by using the absolute value of the force derivative in the denominator of Equation 5.23.

$$U_{n+1} = U_n - \frac{F_f(U) - F_a}{|F'_f(U)|} \bigg|_{U=U_n} \quad (5.24)$$

In accordance with the considerations above, a matrix norm is defined, $||[K^e]||$, by transforming $[K^e]$ to diagonal form with the transformation matrix $[T]$, taking the absolute values of the diagonal matrix elements, and transforming the resulting matrix back by the inverse transformation, $[T]^{-1}$:

$$||[K^e]|| = [T] \ ||[T]^{-1}[K^e][T]|| \ [T]^{-1} \quad (5.25)$$

The modified element stiffness matrix is subsequently passed on to the main finite element routines for incorporation into the global stiffness matrix.

5.2 The global Finite Element Muscle Model

A general presentation of the typical finite element muscle models used for performing the simulations in subsequent chapters is given below. All parameter values indicated will be valid for the remainder of this thesis, except where stated otherwise.

The finite element muscle models (Figure 5.4) are generated as plane strain two-dimensional models using fibre tissue elements (small triangular regions in Figure 5.4) and tendon sheath elements along the upper and lower edges of the geometries. Each tissue element consists of two superimposed elements: an isotropic fluid-like element representing the muscle tissue fluid matrix and an anisotropic custom element representing the muscle fibre characteristics. Tendon sheath elements are represented by large deflection spar elements. As a consequence of the plane strain assumption, no thickness changes of the muscles will occur. The models are taken to represent the mid-section of a muscle which contains the line of action of the muscle. Fibres are assumed to run within the model plane. Results, such as the total muscle force for example, have to be interpreted as "per unit thickness" information.

Figure 5.4 displays two different geometries; a trapezoidal geometry at the top for which the results can be compared directly to those in Chapter 3, and a more involved geometry at the bottom, whose shape approximates the lateral cross section of the (cat) medial gastrocnemius muscle. As displayed, the geometries

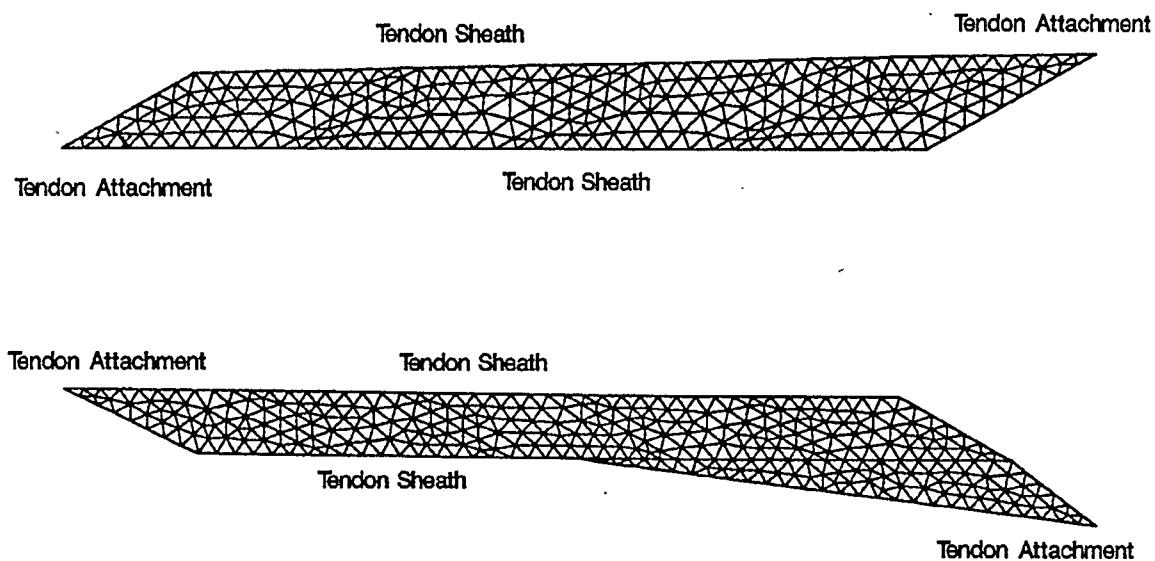


Figure 5.4: Finite element muscle model geometries (not to scale) and finite element mesh.

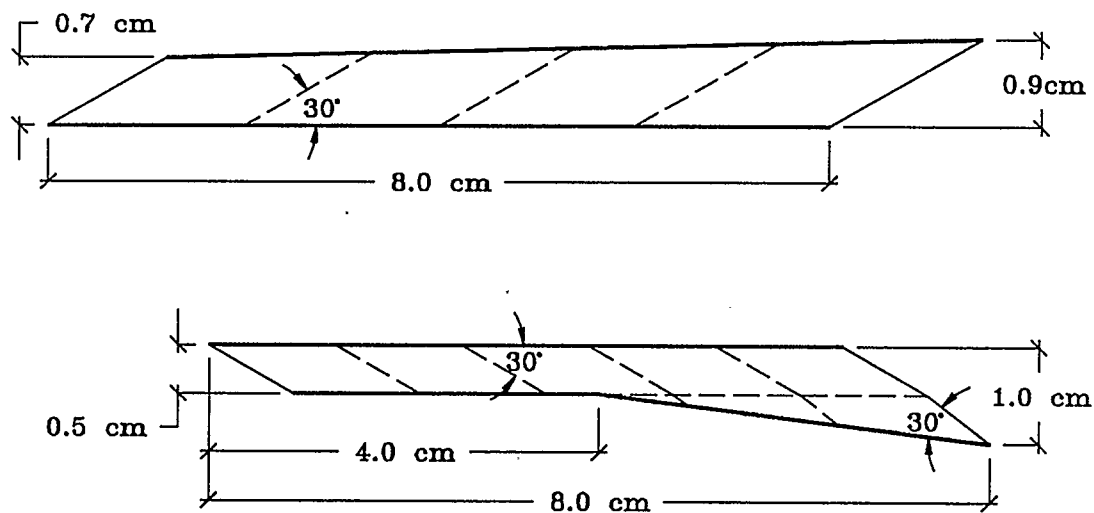


Figure 5.5: Finite element muscle model geometries (to scale).

represent the reference and stress free state. While the geometry at reference configuration is outlined by straight line segments, restrictions regarding the deformed geometry are made only to the extent of suitable boundary conditions. Figure 5.5 provides the exact dimensions of the geometries to be analyzed.

The trapezoidal geometry (TG) is defined by a lower tendon sheath length of 8 cm, the vertical heights of 0.7 cm at the left and 0.9 cm at the right. These dimensions result in a muscle cross sectional area of 6.4 cm^2 . Tendons are assumed to attach at the lower left and upper right hand side of the tendon sheaths, but they are not part of the model. The muscle length, which is defined by the length of the line connecting the two tendon attachment sites, is 9.6 cm. Muscle fibres run at a uniform angle of 30° relative to the lower tendon sheath. The triangular muscle tissue elements are generated so that their edges form straight lines from lower to upper tendon sheath at three locations within the muscle, which coincide with the general fibre direction. The muscle boundary lines at the right and left are also coincident with the fibre direction. The lines which are coincident with the fibre direction facilitate the tracking of the changing fibre directions during muscle deformations.

The medial gastrocnemius geometry (GG) at the bottom of Figure 5.5 can be divided into the "head" section at the right hand side and the "neck" section at the left hand side. For the model generation, the neck part is extended all the way to the right forming a parallelogram, and supplemented by a triangular region at the

bottom right to form the muscle head. The top parallelogram region has a horizontal length of 6.5 cm and a vertical height of 0.5 cm. The bottom triangular region at the right extends a vertical distance of 0.5 cm below the parallelogram and intersects the bottom line of the parallelogram approximately at half-length. The right hand edge of the triangular region, which coincides with the fibre direction in that region, is adjusted so that fibres form an angle of 30° with adjoining tendon sheaths within the entire geometry. Tendon sheaths run along the entire boundaries at top and bottom. Tissue elements are again generated in such a way that element edges form straight line segments coinciding with the fibre direction. In the head section, the fibre direction changes abruptly as one moves from the bottom to the top tendon sheath. Tendons are assumed to attach at the top left and at the bottom right. The muscle length is 8.1 cm and the muscle cross sectional area is 4.1 cm^2 .

Material property values are set to $A = B = 0.125 \text{ N/cm}^2$, $\nu = 0.4995$ (Equation 4.4), and $\hat{P} = 25 \text{ N/cm}^2$ (Equation 4.9). From Yamada [1970] a tendon sheath stiffness of 1200 N/cm^2 has been obtained by taking the initial slope of the stress strain relation for cat tendinous tissue. This translates into tendon sheath spar element specific constants of $E \cdot A = 1200 \text{ N}$, with E being the Young's modulus and A the spar cross sectional area. It is a natural consequence of the current modelling approach that tendon sheath elasticities can be incorporated into the model. The tendon sheath elasticity chosen leads to typical tendon stretches between 4% and 5% for maximum muscle forces.

For the simulations, the model boundary conditions rigidly fix the left hand tendon attachment point, while the right hand tendon attachment point is moved (typically along the line of action of the muscle). Thus, the left attachment point may be identified with the muscle origin and the right attachment point with the muscle insertion. Two different analysis protocols will be followed. According to the first protocol, both tendon attachment points are initially held fixed, while the muscle stimulation parameter, Θ , is gradually increased from 0 to 1. Subsequently the fully stimulated muscle model is lengthened and shortened. Following the second protocol, the muscle is stretched without stimulation ($\Theta = 0$) beyond the active range of the fibres, next, the stimulation is turned on ($\Theta = 1$) and, finally, the muscle is shortened as far as possible. All muscle tissue elements of the model are always uniformly stimulated.

Ansys Version 4.3, the finite element package used for performing the analysis, has the deficiency that the custom elements themselves cannot be made visible on graphical displays. Consequently, no stress plots could be obtained for the muscle tissue as generated. However, stress and nodal force plots are produced for the tissue matrix element by themselves. The matrix stresses will be of interest, because they reveal how the muscle structure works based on hydrostatic pressure within the muscle tissue fluid matrix. The nodal force plots will give an indication as to where and how the muscle fibre component and the muscle fluid component interact.

Chapter 6

Stress State, Intra-Muscular Pressure and Global Equilibrium

Intra-muscular pressure has been experimentally determined by Petrofsky and Hendershot [1984] to be 2.3 N/cm^2 for the cat medial gastrocnemius muscle, and by Otten [1988] to be 13.3 N/cm^2 in the toad gastrocnemius muscle; the respective pressure values differ by a factor of five. Theoretical considerations put the pressure for pennate muscles at 0 N/cm^2 [Benninghoff and Rollhäuser 1952, Gans and Bock 1965, Gans 1982], 1 N/cm^2 [Heukelom et al. 1979], and 13 N/cm^2 [Otten 1988]. In the context of the current continuum model, intra-muscular pressure can be explored as part of the general stress state within the muscle. Different pressure levels can be considered to be reasonable, depending on the point of view. With respect to experimental results, the question arises, which stresses are actually measured in these experiments.

The particularities of the muscle structure in combination with the mode of loading will be shown to have distinctive consequences on the global equilibrium of the structure.

A point of caution needs to be made: the stress state in the muscle structure hinges on intricate interdependencies of global deformations, boundary conditions and boundary effects. In order to make specific arguments below, these complex interactions need, at times, to be simplified. They should, however, be kept in mind.

At present, two assertions in muscle mechanics, which have been implemented into the current continuum model, can be considered to be undisputed: (a) under stimulation, muscle fibres generate a tensile force aligned with their length axis, and (b) muscle tendon sheaths have a negligible bending stiffness. Associated with observation (a) is the common understanding that fibres are pulling on the tendon sheath.

Figure 6.1 illustrates the general effects of a distributed load on the curvature of a short tendon sheath segment, which is assumed to have no bending stiffness at all. The muscle tissue is imagined to be located below the tendon sheath element and its action on the tendon sheath element has been decomposed into distributed loads representing the normal and shear stress components. T represents the tensile force acting on the tendon sheath segment in tangential direction. The

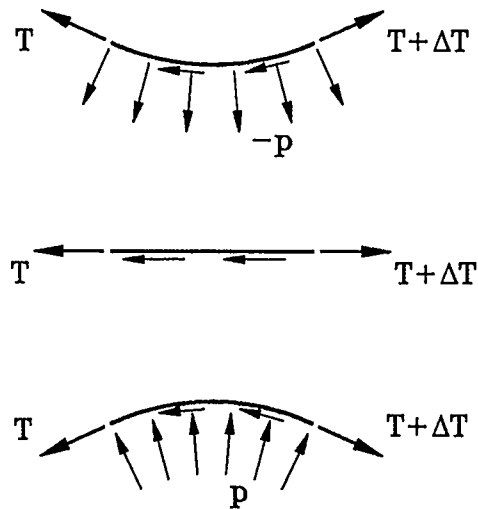


Figure 6.1: Tendon sheath curvature in relation to applied loads.

relation between the radius of curvature, ρ , the distributed load, p , and the tension, T , is given by the following expression:

$$\rho = \frac{T}{|p|} \quad (6.1)$$

A net pulling action by the muscle tissue on the tendon sheath (Figure 6.1, top) would result in a concave tendon sheath curvature. Clearly, this type of tendon sheath curvature is rarely observed on muscles, except, perhaps, for very small regions adjacent to the muscle (tendon) attachment points. What is usually observed, are relatively flat tendon sheaths (i.e. they have a radius of curvature approaching infinity) or tendon sheaths with a convex curvature. This implies however, that the effect of the muscle tissue on the tendon sheath must be of the

nature of pure shear stresses (Figure 6.1, middle) or a combination of shear stresses and pushing stresses (Figure 6.1, bottom), the latter being completely counterintuitive with regard to muscle fibres with an exclusive pulling action.

Figure 6.2 illustrates how equilibrium can be achieved locally in the context of the current constitutive model by inducing a pressure in the matrix part of the muscle tissue. For the following argument, let us assume that we consider the stress state of a muscle tissue volume element which is located directly beneath the top tendon sheath and removed from the tendon sheath end points for the gastrocnemius muscle geometry displayed at the bottom of Figure 5.4. Let us also assume that, for the stimulated muscle, the tendon sheath radius of curvature is infinite at this location (flat tendon sheath), and that the fibre direction forms an angle of 45° with the tendon sheath orientation.

The current constitutive model considers muscle tissue to be a superposition of an incompressible fluid matrix part, and a fibrous part. The stress state associated with the fibrous part only, is indicated for the volume element at the top-left in Figure 6.2 ($\sigma_{I\perp}, \sigma_{I\parallel} = 0$), where two of the edges of the volume element are in parallel with the local fibre direction. This stress state is taken as the base stress state to form Mohr's Circle at the bottom left of Figure 6.2. For a volume element at the same location but with two of its edges in parallel to the tendon sheath (top, second from left), the analogous stress state is arrived at by the appropriate stress tensor transformation (dashed vertical line in Mohr's Circle, bottom left). The - with

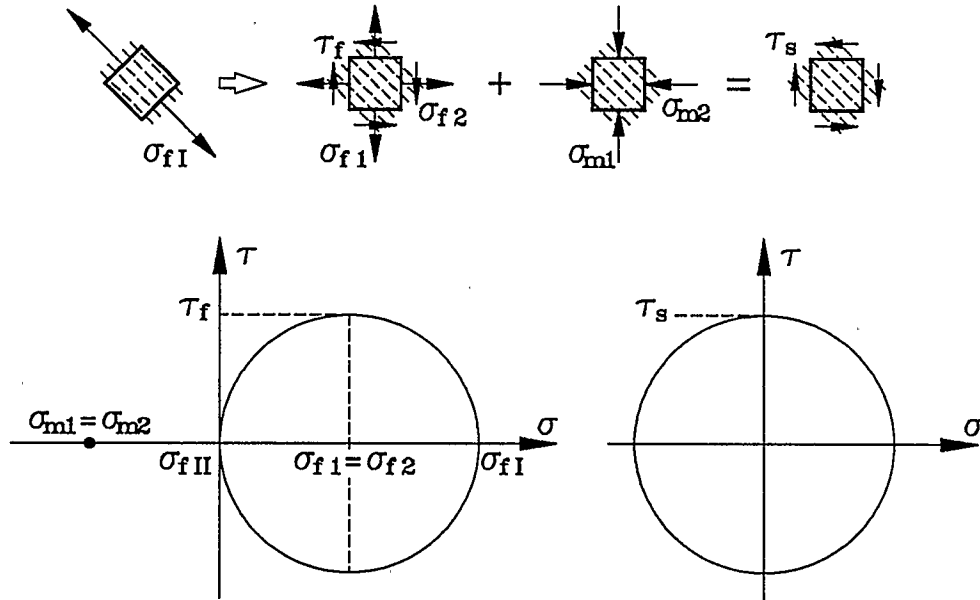


Figure 6.2: Stress state for a volume element adjacent to the tendon sheath.

respect to the tendon sheath orientation - oblique fibre tensile stresses are thus resolved into their normal ($\sigma_{f1} = \sigma_{f2}$) and shear (τ_f) components.

For the current assumption of a flat tendon sheath with no bending stiffness, the discussion above has shown that no normal stress components can be present. To compensate for the normal stress components, the tissue matrix part must, therefore, be put under compression ($\sigma_{m1} = \sigma_{m2} = -\sigma_{f1}$), as indicated in Figure 6.2 (top, third from left, and bottom left). The matrix stresses take on the form of a hydrostatic pressure due to the fluid character of the matrix part. The superposition

of the tissue matrix part and the tissue fibrous part results in a pure shear stress state (τ_s) next to the tendon sheath (Figure 6.2, top right, and bottom right). In summary, matrix hydrostatic stresses will develop in order to achieve local equilibrium; on the other hand, taking the matrix and fibrous part together, no normal stresses are imparted on the tendon sheath.

Let us in the current context define the fibre angle of pinnation from a local perspective as the angle between the fibre direction and the tendon sheath orientation. If the angle of pinnation is not equal to 45° , a more general stress state will result compared to the pure shear stress state above. Still, the matrix hydrostatic pressure will have to adjust in such a way as to cancel the normal stress components induced by the fibrous part. The magnitude of the shear stresses acting on the tendon sheath over the tendon sheath length determines the force acting at the tendon sheath end (or attachment) point. These shear stresses are highest under an angle of pinnation of 45° , if the fibre stresses are taken to be independent of the angle of pinnation. This is conform with the observation in Chapter 3, where the highest muscle force was observed in the case of a muscle with parallel tendon sheaths having an angle of pinnation of 45° (to be precise, this angle of pinnation has to be reached during the muscle deformation, when the Cauchy fibre stress peaks).

Clearly, for the current model the tendon sheaths will not remain absolutely flat along their lengths. The curvature and matrix pressure depend on the global

muscle deformation and boundary effects. Figure 6.3 displays the principal stresses of the muscle tissue fluid matrix for an isometrically held muscle under stimulation. The vector plot is shown for the undeformed muscle geometry, and only the left section of the gastrocnemius geometry is shown; the vertex at the top, left hand side, corresponds to the muscle attachment point. The star shaped vector entities indicate the matrix pressure, with longer vectors indicating relative higher stresses. Matrix pressure is developed in the region where the top and bottom tendon sheaths overlap along the muscle length axis. Close to the muscle attachment point, almost no matrix pressure is present. Consequently, the tissue actually pulls on the top tendon sheath in the normal direction, and the tendon sheath experiences a concave curvature, which will become apparent in deformation plots shown in subsequent chapters.

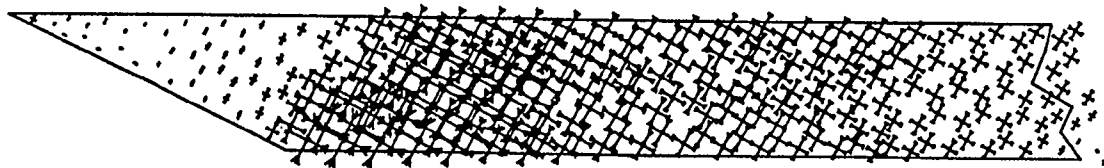


Figure 6.3: Hydrostatic pressure within the muscle tissue fluid matrix.

The considerations made in connection with Figure 6.2 can be extended by including the effects of curvature in relation to the tendon sheath tensile forces. However, a more fundamental consideration relates to the question of what type of global curvature the tendon sheaths will undergo. Focusing on the active character of the fibres and considering the fibre stresses as the primary stresses for stimulated muscle, the matrix stresses can be considered as a reaction to the fibre stresses. Globally, there is no physical foundation for the reactions to be greater than the action. Therefore, the matrix compressive stresses are not expected to overcompensate for the - with respect to the tendon sheath - fibre normal stresses and to bring the tendon sheaths into a globally convex shape. What one can reasonably expect, and - in anticipation of the muscle simulations presented later - what will actually occur for the current muscle model, is that the muscle tissue matrix develops enough compressive hydrostatic pressure to prevent the tendon sheaths from being displaced towards each other. Tendon sheaths will remain close to being straight, not because of kinematic constraints, but because of the mechanics governing the model. There is one notable exception to the last point: depending on the muscle model geometry, the whole muscle may become curved during muscle contraction, with one tendon sheath becoming convexly curved, the other concavely curved. However, during simulations with different muscle geometries, it has never been observed that both tendon sheaths experience a convex curvature.

As a consequence of the discussion above, we are left with the following observations: In order to achieve equilibrium adjacent to the tendon sheath, a compressive hydrostatic pressure is induced in the muscle tissue fluid matrix part. If there is no curvature in the tendon sheath, the matrix stress level depends only on the generated fibre stresses and the angle of pinnation. For example, an angle of pinnation of 45°, results in a matrix hydrostatic pressure of 50% of the fibre stresses, and the percentage value for an angle of pinnation of 25° is 17.8%. The hydrostatic matrix stress level is not dependent on the absolute muscle size. Due to the similarity of conditions along the central part of the tendon sheath, the matrix pressure remains very much the same along the tendon sheath length, with variations being due to changing angles of pinnation, fibre stresses, and tendon sheath radii of curvature.

Assuming an active fibre stress of 25 N/cm² and a fibre angle of pinnation of 25°, the matrix pressure will take on a value in the order of 4.5 N/cm². Looking at the integral muscle tissue (matrix and fibrous parts superimposed), and defining the pressure as $p = -\sigma = -\frac{1}{3}(\sigma_1 + \sigma_2 + \sigma_3)$, with σ_i being the muscle tissue principal stresses, a pressure value of -3.8 N/cm² is arrived at.

The matrix pressure magnitude of 4.5 N/cm² is far closer to the experimental values of 2.3 N/cm² obtained by Petrofsky and Hendershot [1984], than to those obtained by Otten [1988], which are at a level of 13 N/cm². There is, however, still a difference of a factor of two compared to the values given by Petrofsky. In the

experimental setting, the important question that may be asked is, which stresses are actually measured? The matrix hydrostatic pressure may not be directly accessible to experimental measurements, because of interference from the fibrous tissue constituents. Based on the considerations above, any pressure value between 4.5 N/cm^2 and 0.0 N/cm^2 may result from measurements (a negative pressure will certainly not be detected by a pressure probe), depending on the degree of coupling between tissue constituents. On the other hand, starting from the experimental values, conclusions might be drawn about tissue constituent coupling in the context of a more detailed constitutive theory.

The assertion of Benninghoff and Rollhäuser [1952], and Gans and Bock [1965] that there is no reason for intra-muscular pressure to occur in pennate muscles, can be considered to be correct, if seen in the correct context. From their discussions, it appears that they are referring to the normal stress interactions between the muscle tissue and the tendon sheaths, which has here been labelled "distributed load" in conjunction with Figure 6.1. As demonstrated above, the muscle tissue interacts with relatively flat tendon sheaths predominantly by shear stresses. Incidentally, this observation gives the question of how muscle tissue behaves an additional complexion; if, for some reason, experiments related to the exploration of muscle tissue behaviour had been easier to perform on entire muscles than on single muscle fibres, our understanding of how muscle tissue reacts to stimulation might well be that it produces shear stresses on the tendon sheath, rather than a pull in fibre direction.

Otten [1988] also started his arguments from the normal stress interactions between muscle tissue and tendon sheaths, and equated this interaction with muscle pressure. Taking the tendon sheath curvature and tendon sheath tension into account, he arrived at stresses acting normal to the tendon sheath in the order of 13 N/cm^2 , which agreed with his experimental results. Referring to the discussion of Figures 6.1 and 6.2, this would result in fluid matrix pressures, which are even higher than 13 N/cm^2 . However, if the fluid matrix pressure is seen, in principle, as a reaction to the fibre stresses, it is not obvious how this high a pressure could be generated within a muscle.

A very much simplified picture of the stresses acting on the muscle body when the tendon sheaths are removed by the method of sections, is shown in Figure 6.4 for the case of a muscle with parallel tendon sheaths. Whether the muscle tissue stresses are the result of a passive muscle stretch or that of internal stimulation, the main interaction between the muscle tissue and the tendon sheaths consists of shear stresses. While there are shear stresses at the top and bottom boundary, there are no stresses at the right and left end of the muscle, due to the free boundaries. Consequently, the moment generated by the shear stresses at the top and bottom boundaries are not compensated for, and the muscle body is not in equilibrium.

Obviously, the real situation is far more complex, and the moment imbalance is counteracted by the structure through suitable deformations and stress

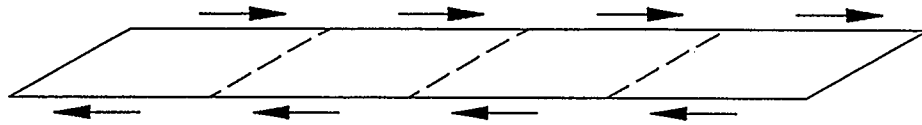


Figure 6.4: Shear stresses acting on the muscle body.

redistributions. Still, the type of loading does impose exceptional demands on the muscle structure. This is best illustrated by the following example, where the model behaviour turns out to be catastrophic. The example also illustrates that the geometrically nonlinear theory of deformation underlying the current modelling approach is not a mere academic exercise.

Figure 6.5 displays muscle deformations for a muscle with parallel tendon sheaths, which has been modelled using finite elements based on the linear theory of deformation. In particular, the incompressibility of the muscle tissue is imposed by constraining the trace of the linear strain tensor to a value of 0. The formulation of these elements incorporates provisions for large deflections based on the "Updated Lagrange" technique. All material properties have been chosen in correspondence to those detailed in Chapter 5.

The model geometry and the finite element mesh are displayed at the top of Figure 6.5. Displacement constraints are applied at the lower left and upper right

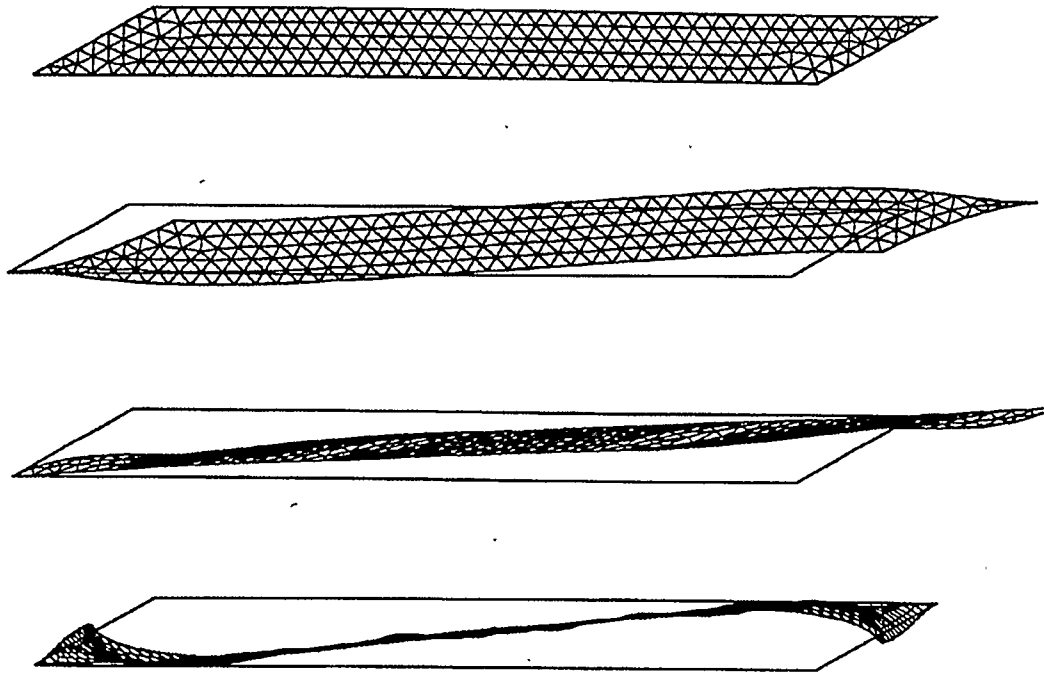


Figure 6.5: Muscle model behaviour based on the geometrically linear theory.

vertices. Figure 6.5, second from top, shows the response of the structure to a passive stretch when no elements are incorporated into the model which represent the tendon sheaths at the upper and lower boundaries of the structure. While the deformation cannot be considered to be physically accurate on account of the elements being based on the linear theory, they do appear quite reasonable. Displacements are shown to scale with the original muscle geometry indicated by the solid lines forming a parallelogram. Stresses (not shown) flow directly between the points of constraint, and the material is in essence stretched uniaxially.

The picture changes dramatically when the same stretch is applied to the previous structure, which now includes spar elements to represent the tendon sheaths (Figure 6.5, third from top). In this case, the muscle volume is put under shear with no corresponding shear stresses being present at the free left and right hand model boundaries. In order to achieve equilibrium, the whole muscle collapses. Incidentally, the incompressibility constraint according to the linear theory is fully observed. A similar behaviour occurs for the same structure when it is isometrically held and when an internal load corresponding to muscle tissue contraction is applied (Figure 6.5, bottom).

The muscle model presented in Chapters 4 and 5 overcomes the deficiencies of the linearized theory. However, it cannot eliminate the peculiar loading of the structure, which is part of the problem definition. The most basic muscle geometry, that is a muscle with parallel tendon sheaths, which has been used extensively in Chapter 3 and by other authors, has the most difficulty in establishing equilibrium. Therefore, the trapezoidal geometry described in Chapter 5 will be used in the following chapters. In general, an asymmetric geometry has more ways in adapting to the imposed loading by asymmetric deformations.

In order to give an impression of how equilibrium is established for the entire muscle structure, Figure 6.6 displays iso-pressure lines for the muscle tissue fluid matrix on the gastrocnemius geometry under an isometric contraction. While the pressure values remain relatively uniform in the midsection, rapid changes in

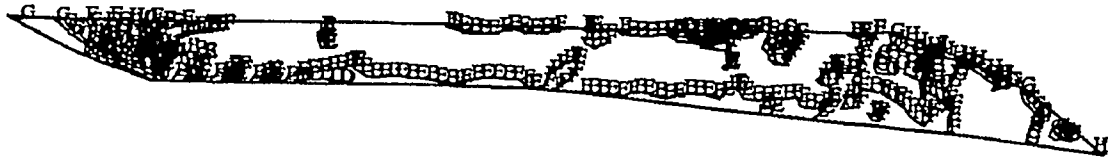


Figure 1. Schematic representation of the experimental design. The subjects were divided into two groups: the control group and the experimental group. The control group received a standard diet, while the experimental group received a diet supplemented with 0.5% of the active ingredient. The subjects were then subjected to a 12-week period of physical training. The results of the study are presented in the form of a bar chart, showing the percentage of subjects who completed the training period without any adverse effects. The control group shows a significantly higher percentage of subjects completing the training period compared to the experimental group.

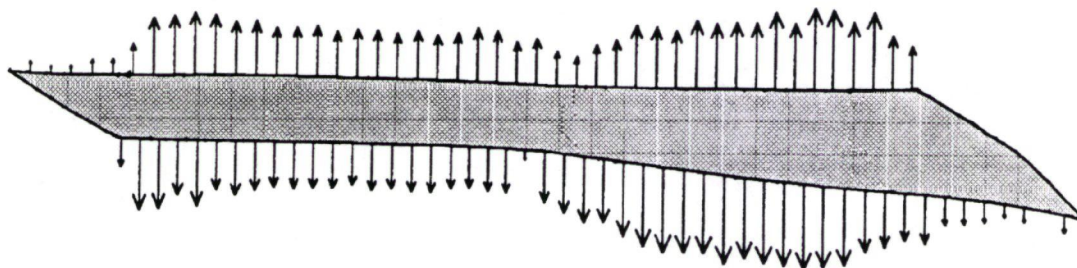


Figure 6.7: Nodal reaction forces for nodes along the tendonal boundaries.

tendon sheaths corresponds to a "buckling" condition and results in a non-convergence of the model. Wrinkling of tendon sheaths under rapid unloading has been observed by Dr. Andy Hoffer at the University of Calgary on the cat gastrocnemius muscle [private communication].

Chapter 7

Finite Element Model Simulations: Trapezoidal Muscle Geometry

In this chapter, the results of finite element muscle model simulations for the trapezoidal muscle geometry described in Chapter 5 will be presented and discussed. The trapezoidal geometry is suitable to be treated with the theory introduced in Chapter 3. Consequently a direct comparison between the Straight Line Model (SLM) and the Continuum Model (CM) will be possible. It will become apparent that the two modelling approaches result in significant differences as far as the muscle force-length curves and the muscle deformations are concerned.

In order to disassociate the influence of the muscle geometry changes and the effect of the nonlinear active fibre force-length relation during muscle deformations, an initial simulation will be based on constant active fibre forces. Subsequently, the fibre force-length profiles number 1 and 2, which have been introduced in Chapter 4, will be included into the model. Finally, the base geometry will be modified

slightly, to include changing muscle fibre orientations within the muscle volume at reference configuration; the intent is to study the behaviour of a muscle model, where the length axes of the muscle fibres in reference configuration form a S-shaped curve. For this geometry, a comparison to the SLM will not be possible.

The muscle geometry and deformation plots presented in this chapter are not scaled uniformly. However, an outline of the muscle geometry at reference configuration is always superimposed on displacement plots, in order to provide a point of reference. Deformations are displayed to scale. The material parameters for the tissue fluid matrix constituent and the tendon sheath stiffness are chosen in accordance with Chapters 4 and 5 (matrix material constants, $A = B = 0.125 \text{ N/cm}^2$, $\nu = 0.4995$, tendonal stiffness, 1200 N/cm^2 , and the active fibre stress, $\hat{P} = 25 \text{ N/cm}^2$).

7.1 Constant Fibre Force

For a given muscle geometry, the muscle force-length curve is essentially influenced by two components which are (a) the fibre stretch ratio dependent nonlinear fibre force-length relation, and (b) the change in fibre orientations as well as geometry changes during muscle deformations. In order to separate the two effects, the simulations in the current section assume a fibre length independent active fibre force. In the context of the CM this is achieved by assuming a strain independent active first Piola Kirchhoff stress of 25 N/cm^2 , where this stress is measured per unit area perpendicular to the fibre direction at the muscle reference

configuration. Furthermore, no passive fibre characteristics are included in the current model. Therefore, the muscle forces resulting from a passive muscle stretch are associated with the resistance to deformations of the muscle tissue matrix part only.

Figure 7.1 presents the muscle geometry in the reference configuration and selected deformed geometries for the current simulation. Within the initial geometry (top), all muscle fibres are assumed to run straight between the tendon sheaths at the top and bottom; the fibre directions are in parallel to the two muscle boundary lines at the right and left. Furthermore, the edges of the triangular finite elements form straight lines at three locations inside the muscle volume which coincide with the fibre direction. Throughout the muscle, the fibre stretch ratio is equal to $\lambda = 1$ in the reference configuration. The muscle is constrained at its origin at the lower left vertex, and stretched or contracted by displacing its insertion at the upper right vertex in the direction of the line of action of the muscle. Initially, a passive stretch is applied, that is, the muscle is elongated without any fibre stimulation (the stimulation parameter, Θ , introduced in Chapter 4 is set to 0). Subsequently, full muscle stimulation is applied ($\Theta = 1$) and the muscle is allowed to contract in incremental steps as far as possible.

In the most stretched configuration, differences in the deformations of the unstimulated and stimulated muscle become apparent. While there is a pronounced bend along the tendon sheaths in the unstimulated muscle, the tendon

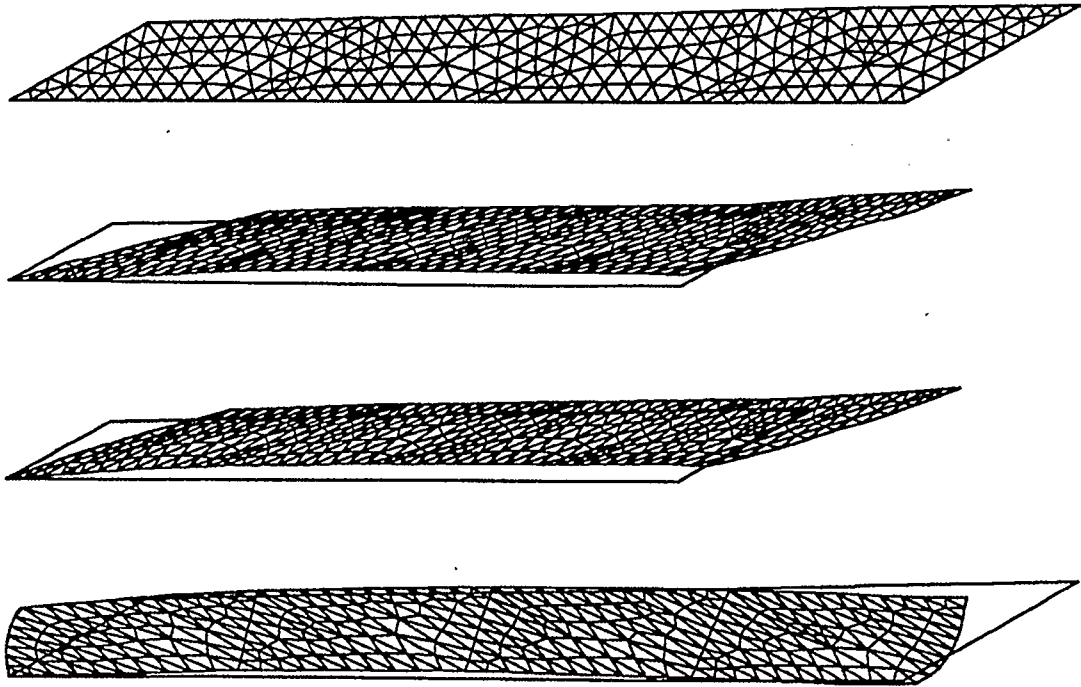


Figure 7.1: Muscle geometry and deformations for constant fibre force. Displayed are the initial muscle geometry (top), the geometry after a passive stretch (second from top), stretched and stimulated (third from top), and fully contracted (bottom).

sheath shapes become more regular in the stimulated case. In the latter case, both tendon sheaths are straight over large portions of their lengths, with concave tendon sheath curvatures close to the muscle attachment locations and at the free tendon sheath ends. Furthermore, the tendon sheaths show an elongation in the stimulated configuration. This can be seen by comparing the positions of the unconstrained tendon sheath ends for the stimulated and unstimulated configuration to the undeformed muscle geometry, shown by solid lines

superimposed to the deformed geometries. The difference in geometries is important from an experimental point of view: the active muscle force-length curve for a muscle is usually determined by measuring muscle forces for the stimulated (total muscle force) and unstimulated muscle (passive muscle force) at different muscle lengths. The differences of the total and passive muscle forces for corresponding muscle lengths are identified with the length dependent active muscle force. The respective muscle forces are then extrapolated to the muscle fibre level and conclusions are drawn about muscle fibre characteristics. It is of importance to realize that, even if the overall muscle length is kept constant, the fibre stretch ratios or relative fibre lengths may be quite different in the stimulated and unstimulated configuration. Due to the fibre stretch ratio independent fibre force in the current analysis, the disparity between fibre stretch ratios in the stimulated and unstimulated configuration will not result in undue consequences. It will, however, have significant consequences for the simulations presented in the following sections which include a stretch ratio dependent fibre force.

In the most contracted configuration (bottom of Figure 7.1), the entire muscle becomes slightly arched, with the upper, longer tendon sheath taking on a convex curvature, while the lower tendon sheath assumes a concave shape. Close to zero muscle force is reached at that configuration. While the SLM attains zero muscle force at fibre angles of pinnation of 90° measured relative to the lower tendon sheath, the CM maximum angle of pinnation is greater than 90° at the muscle origin. As can be observed, the fibre angles of pinnation vary considerably along

the muscle length axis with angles of pinnation being less than 90° over most of the muscle geometry. Fibres at the right and left muscle boundaries become notably curved; fibres removed from the boundaries, however, remain straight for all practical purposes (refer to straight lines coincident with the fibre directions in the central part of the muscle geometry). It can be concluded from the variations in fibre curvature and in fibre angles of pinnation that the strains and, consequently, the fibre stretch ratios vary significantly over the muscle body, which contrasts with the assumptions of uniform fibre deformations in the SLM. That the muscle does not globally reach angles of pinnation closer to 90° at minimum muscle length can be attributed to the small but finite elasticity included in the tissue matrix material description, and the counter-productivity of the fibres having an angle of pinnation of more than 90° .

Figure 7.2 presents the muscle force-length curves resulting from the current finite element simulation. Considering the fact that the fibre description does not incorporate any passive components, the muscle force-length curve for the unstimulated muscle, indicated by "passive", reflects essentially the matrix resistance against deformation. The passive muscle force starts at a muscle length of 9.6 cm, which corresponds to the distance between muscle origin and insertion at muscle reference configuration. Model convergence is only obtained up to the end of the passive force curve shown. A stretch beyond the absolute muscle length of 11.4 cm results in finite element model instabilities. By contrast, the stimulated muscle can be stretched beyond this point, and the simulation has been

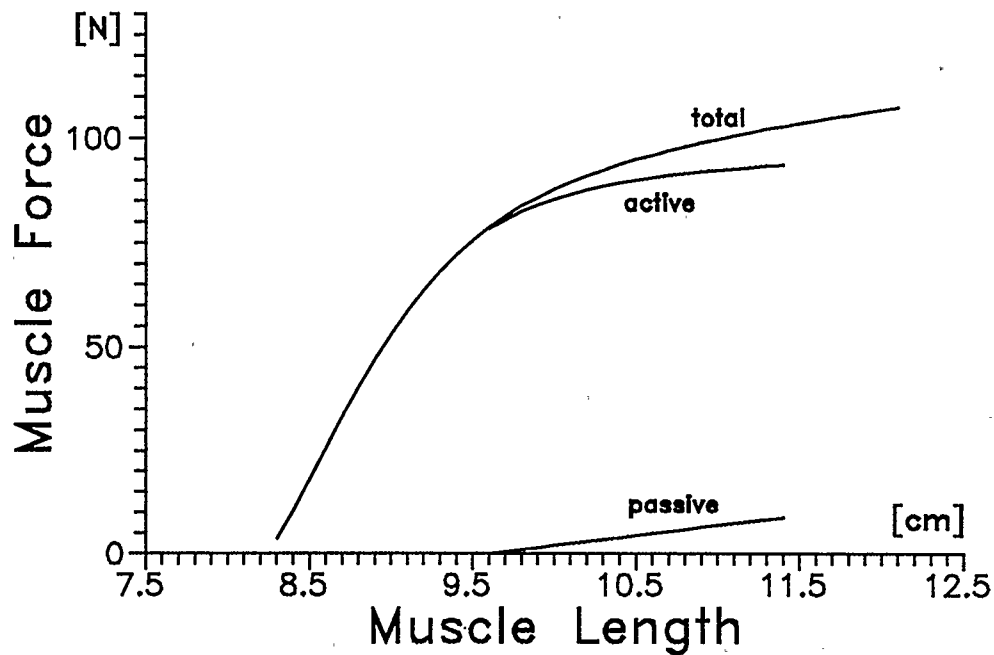


Figure 7.2: Muscle force length curves for muscle with fibre stretch ratio independent fibre forces. Unstimulated - "passive", stimulated - "total", difference of former - "active".

broken off by choice at the end of the total muscle force curve shown. This indicates that the internal fibre forces stabilize the structure. The stretched configurations displayed in Figure 7.1 correspond to the passively attainable muscle length of 11.4 cm. A close to zero muscle force is reached for a muscle length of 8.3 cm.

The difference of the total and passive muscle force curves is here defined and displayed as the active muscle force curve. A passive resistance of the muscle for shortened positions is expected. It is however not possible to obtain the muscle

passive force for shortened muscle configurations. "Pushing" the unstimulated muscle model to shorter lengths than resting length results very rapidly in unstable model performance. Also, the squeezed muscle geometry has only a remote similarity to the stimulated muscle geometry for the same overall muscle length. If the passive force could be obtained, the total and passive muscle forces for corresponding muscle lengths would be related to completely different muscle configurations, which renders the derivation of an active muscle force-length curve based on the difference of active and passive muscle forces at corresponding muscle lengths pointless.

The active muscle force-length curve of Figure 7.2 is reproduced in Figure 7.3 and overlaid with the model predictions of the SLM for the current trapezoidal geometry (hollow squares) and for a similar muscle with parallel tendon sheaths (filled squares). All muscles to be compared have identical volume, equal lower tendon sheath length and angles of pinnation. At the muscle reference length of 9.6 cm, the muscle forces predicted by the CM and the SLM for the trapezoidal geometry practically coincide, with the CM actually producing a slightly higher force, which has to be attributed to the change in configuration between the stimulated and unstimulated muscle (the SLM maintains the unstimulated muscle geometry by definition).

For stretched muscle configurations however, the CM muscle forces do not follow the SLM predictions corresponding to the trapezoidal geometry. Rather, the CM

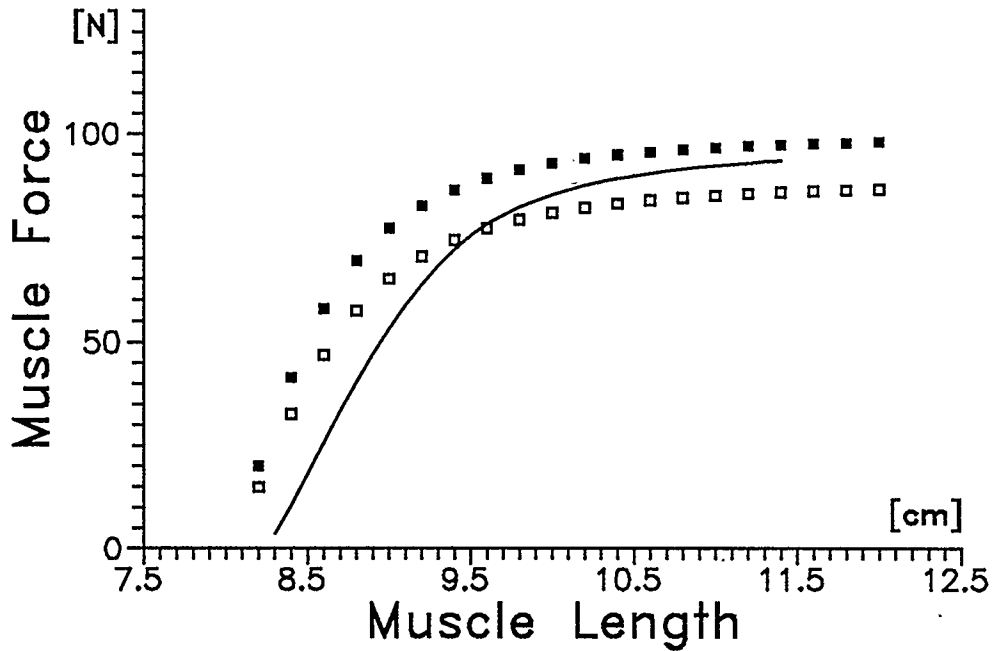


Figure 7.3: Comparison of muscle force length curves. Results for trapezoidal CM indicated by solid line, trapezoidal SLM by hollow squares, and parallel tendon sheath SLM by filled squares.

muscle force curve approaches the one resulting from the SLM parallel tendon sheath muscle predictions. The asymptotic force value for high muscle stretches is equal to $l_t \cdot \sin \alpha_0 \cdot \hat{P} = 100 \text{ N}$ for the current CM and the SLM parallel tendon sheath muscle (with $l_t = 8 \text{ cm}$, the lower tendon sheath length, $\alpha_0 = 30^\circ$, the reference angle of pinnation, and $\hat{P} = 25 \text{ N/cm}^2$, the first Piola Kirchhoff active fibre stress magnitude). This force corresponds to the value which would be typically predicted for a fusiform muscle with a cross sectional area equal to the area perpendicular to the fibre direction in the current muscle geometry (the latter is commonly termed physiological cross-sectional area).

It follows from the preceding observations that the CM and SLM do behave differently. On the other hand, the agreement of force values at the muscle reference configuration and in the asymptotic limit reinforces the reciprocal confidence in the consistency of both models.

For the shortened muscle the SLM muscle force curves corresponding to both geometries intercept the abscissa practically at the same location. The CM curve misses this abscissa interception by about 0.2 cm. In fact, the curve displays lower force values than both SLM curves throughout the muscle shortening interval. As has been pointed out before, part of this deficiency can be attributed to the passive tissue matrix stresses. However, recalling the discussion above and realizing that the CM does behave differently than the SLM, part of the force difference is due to a dissimilar deformation behaviour of the two models. In the current CM, local equilibrium has to be attained, a concept to which the SLM is completely oblivious. Reaching equilibrium imposes "constraints" regarding suitable deformations and corresponding stresses which may inhibit the capacity of force production external to the muscle. The distinctively different configurations of the current CM at low muscle lengths to those of the parallel or trapezoidal SLM at corresponding muscle lengths reveals that the latter would not constitute equilibrium configurations of the former.

7.2 Fibre Stretch Ratio dependent Fibre Force

In contrast to the previous model where the fibre forces were assumed to be independent of the fibre stretch ratio, the models presented below include stretch ratio dependent fibre forces. The fibre force profiles number 1 and number 2, which have been introduced in Chapter 4, will be used. These profiles differ from one another in the relative locations of their active fibre force peaks within the stretch ratio intervals for which there exist positive active fibre forces, as well as in the magnitude of the depression in the total (active plus passive) fibre force-length curve for stretch ratios above unity (see Figures 4.2 and 4.3).

7.2.1 Fibre Force Profile Number 1

In agreement with Woittiez et al. [1984], the fibre force profile #1 incorporates a symmetric active fibre force-length relation. The passive component is defined for stretch ratios greater than 1 and the combined (active plus passive) force profile has a local minimum at stretch ratios greater than 1 amounting to 84% of the active fibre force peak.

Figure 7.4 presents a sequence of muscle model deformations, starting, at the top, with the fully stretched configuration and ending, at the bottom, with the contracted muscle. The fully stretched configuration corresponds to a muscle length where the fibres are stretched beyond their active range (11.4 cm), while the contracted

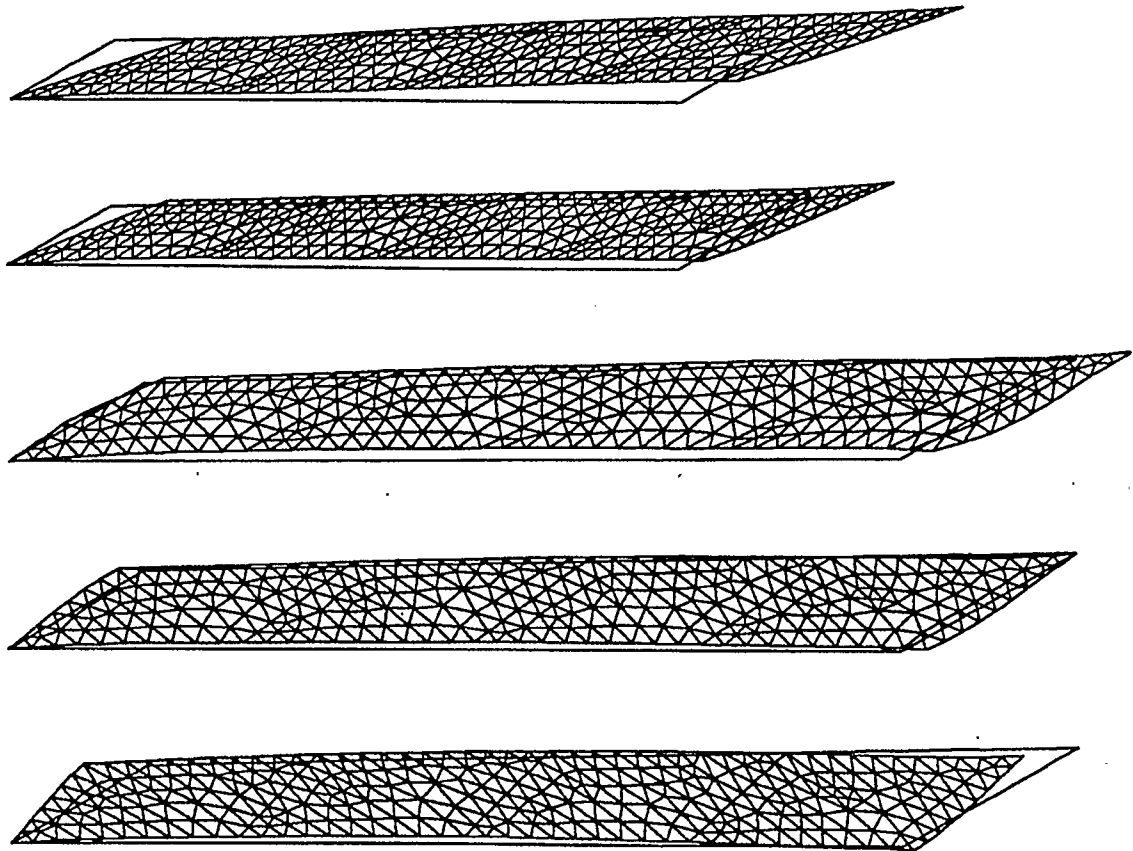


Figure 7.4: Deformations of a muscle model which is based on fibre stretch ratio dependent fibre forces. Stretched configuration at the top, contracted configuration at the bottom.

configuration corresponds to a muscle length of (9.0 cm). The muscle length at reference configuration is 9.6 cm.

The configurations at which the fibres produce a significant active force (second from top to second from bottom) show an extrusion of the muscle tissue at the muscle ends with ensuing fibre curvature, where this effect is primarily visible at the right hand boundary. This extrusion is not noticeable for the most stretched configuration (top) and barely perceptible for the most contracted configuration where the muscle force is close to zero.

In general, muscle fibres removed from the muscle end sections remain straight during muscle deformation, but the fibre directions vary slightly along the muscle length axis. The configuration displayed at the middle of Figure 7.4 constitutes an exception to the observation relating to straight fibres: close to the lower tendon sheath, fibres removed from the muscle ends become slightly curved with angles of pinnation assuming lower values compared to the predominant fibre directions. This effect becomes visible by holding a straight edge to the reference lines coinciding with the fibre directions inside the muscle. In a dissected cat gastrocnemius muscle, muscle fibres can be observed to form a S-shaped curve between the tendon sheaths. While the fibre curvature observed above for the current model assumes the corresponding tendency, it is too small to draw conclusion about the ultimate purpose of fibre curvature in physical muscles. As

far as the model is concerned, the curvature results from the requirement of local and global equilibrium of the structure.

Tendon sheaths do remain remarkably straight, with a very slight, globally convex curvature for the top and bottom tendon sheath (again, placing a straight edge on the deformation plots in Figure 7.4 clarifies this point). Except for the translation of the top tendon sheath during muscle contraction, the tendon sheaths deform only slightly. This contrasts with experimental observations, where the tendon sheath does undergo noticeable deformations after stimulation is applied, which is even true for an isometric contraction.

While the tendon sheaths do not undergo significant deformations perpendicular to their length axes, they do stretch during model contraction. This can be seen immediately by comparing the deformed geometry to the outlined geometry at reference configuration in Figure 7.4, second from bottom. The tendon stretch increases linearly over the tendon sheath lengths, with the highest stretch being located next to the muscle attachment sites. A visual representation of this fact is given in Figure 7.5, where the relative magnitude of the tendon sheath strain over the tendon sheath lengths is indicated by the lines perpendicular to the tendon sheaths.

The muscle force-length curves for the current simulation are displayed in Figure 7.6. The passive and total force-length relations, which are obtained directly from the finite element analysis, are indicated by solid lines. The active force-

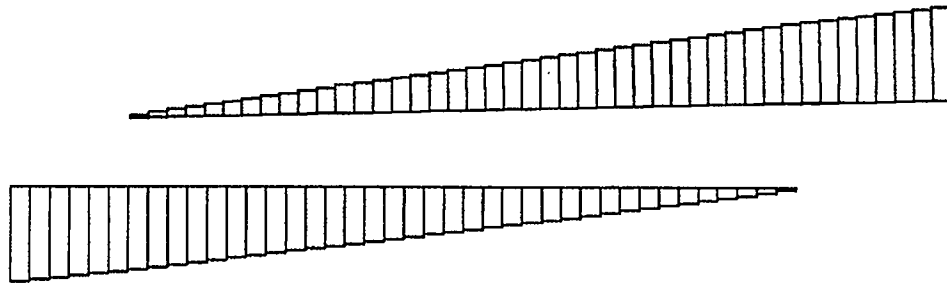


Figure 7.5: Tendon sheath strain. Horizontal lines represent top and bottom tendon sheaths, vertical lines indicate relative tendon sheath stretch.

length curve, which has been obtained by taking the difference of the former two curves, is shown by the dashed line.

For the discussion below, it will be helpful to introduce the following conventions: Referring to the active muscle force-length curve, the section having a positive slope will be called the ascending limb, and the section having a negative slope the descending limb. As for the total muscle force-length curve, the section merging into the active muscle force-length curve will be termed active branch, and the one merging into the passive muscle force-length curve passive branch.

On examining the total muscle force curve, it is striking that this curve does not feature a notable decrease in force magnitude between the active and the passive branches. While there is a small force decrease, the two branches are joined with, what could be called, a plateau region. This contrasts with the predictions of the

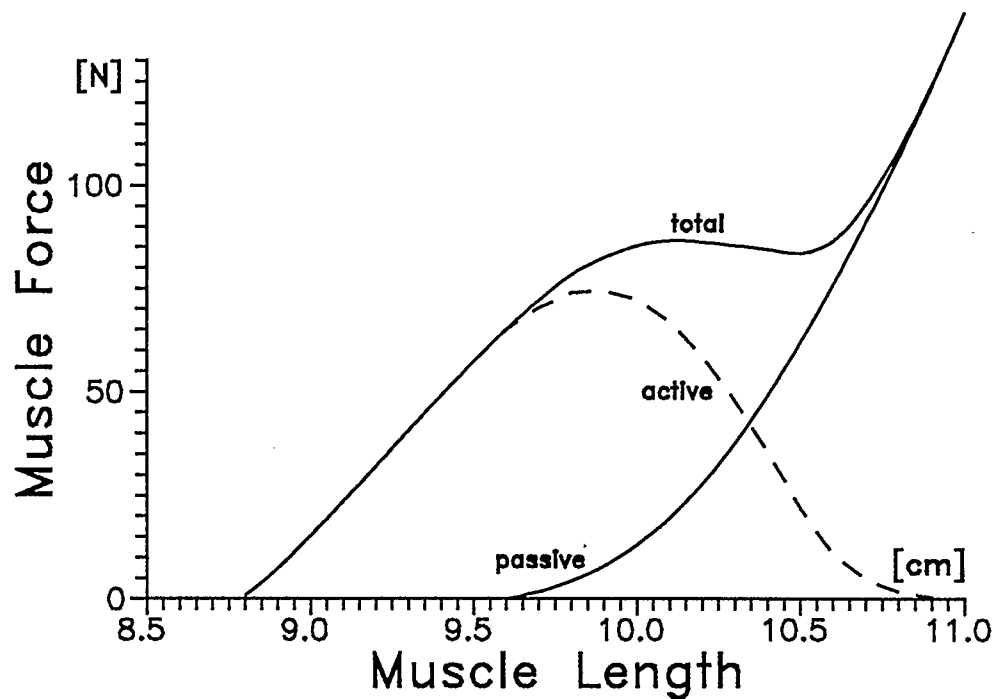


Figure 7.6: Muscle force length curves for muscle with fibre stretch ratio dependent fibre force (symmetric active force profile). Unstimulated - "passive", stimulated - "total", difference of former - "active".

SLM which show a distinctive depression in the muscle force-length curve in that region (see Figure 3.11). The total force magnitude in the plateau region is significantly higher than the active muscle force peak. This is associated with the fact that the active muscle force peak is located at a muscle length for which a passive muscle force is already manifest.

While model convergence typically results within three iterations on the passive muscle force-length curve as well as on the active and passive branches of the total force-length curve, convergence in the plateau region takes up to the order

of twenty iterations. The implications of this observation are that equilibrium configurations in the plateau region are not very sharply distinguished from neighbouring configurations; in other words, the equilibrium is indifferent in the plateau region.

The emergence of a plateau region can be examined in the context of the nonlinear fibre force-length relation whose particular features cause intrinsic difficulties to the structure in establishing equilibrium. Figure 7.7 displays a force displacement relation which is similar to the current muscle fibre characteristics. On applying a slowly increasing load to a component with such a behaviour, the displacement increases gradually up to the local maximum characterized by a horizontal tangent (the solid line of the graph is followed). Any further force increase results in an abrupt change in displacement along the dashed line, that is, a jump ensues to the displacement value at which the previous force level is attained on the right hand branch of the force displacement relation ("snap-through" effect). A similar behaviour occurs on unloading the component, except that the "snap-through" takes place when a force level corresponding to the local minimum in the graph is reached.

If the displacement instead of the applied force is increased or decreased gradually, the above snap-through effect is absent. For the current model, the displacement of the muscle insertion is imposed and the muscle origin is fully constrained. While the muscle length is controlled, the internal deformations are

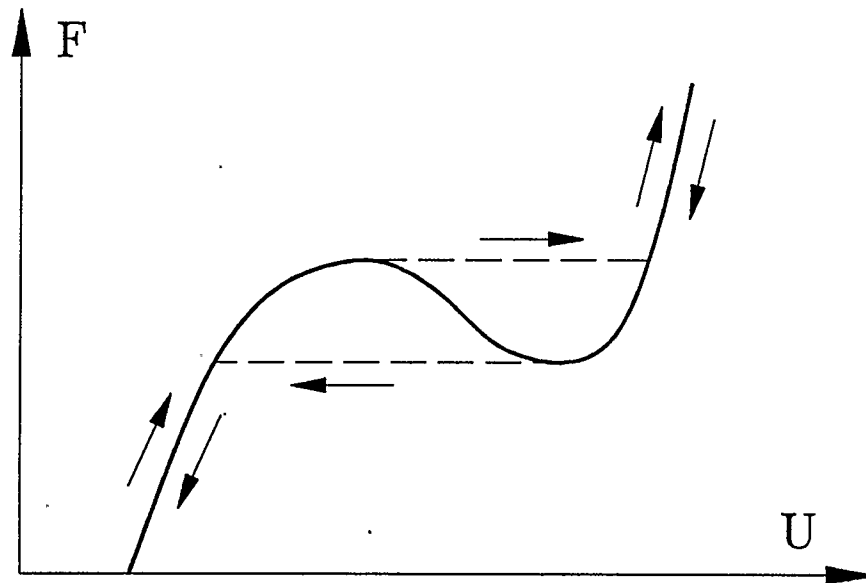


Figure 7.7: Force displacement history for a component having a nonlinear force length relation with inflection point.

free to adjust themselves according to the requirements of local and global equilibrium. It is conceivable, and will actually materialize in a case treated further below in this chapter, that effects similar to the snap-through behaviour discussed above will take place within the overall muscle structure. In contrast to the schematic one dimensional case above, this does not imply a jump in one specific characteristic length parameter, but the realization of multiple equilibrium configurations within the neighbourhood of a specific configuration, which may be a finite "distance" apart from one another. Furthermore, there is no guarantee for stability of these equilibrium conditions.

In the current model, the "snap-through" tendency is minimized by globally varying tissue deformations which equalize the muscle force within the plateau region. The varying degrees of muscle tissue deformations within the muscle body are readily apparent by looking at the configuration in Figure 7.4 which is placed third from the top. Boundary fibres are extruded. Consequently, they have higher stretch ratios than those located at the interior of the muscle. In fact, the boundary fibres are well on their passive branch of the total fibre force-length curve; the passive fibre forces limit the degree of tissue extrusion. They contain the muscle tissue and insure its form stability. If this support function of the boundary fibres is eliminated by taking the passive fibre force component out on the constitutive level, model simulations diverge. The tendon elasticity also increases the stability of the structure. Simulations with significantly increased tendon stiffness values showed an increased propensity for unstable muscle model behaviour in the plateau region.

For a more detailed discussion and in order to compare the predictions of the current CM and of the SLM, Figure 7.8 shows the active and passive muscle force-length curves for the different models in superposition. The solid curves correspond to the CM results, and the dashed lines represent SLM results for the current trapezoidal muscle geometry. The hollow squares indicate SLM results for a similar muscle geometry with parallel tendon sheaths whose volume, lower tendon sheath length and angle of pinnation are equal to the current trapezoidal

geometry. It should be reiterated that the CM passive and total muscle force-length curves result directly from the finite element analysis, while the CM active muscle force-length curve is obtained indirectly. The latter is obtained by subtracting total and passive muscle forces at corresponding muscle lengths; while this operation is performed for equal overall muscle lengths, the configurations for the stimulated and unstimulated muscles at these lengths are different in general.

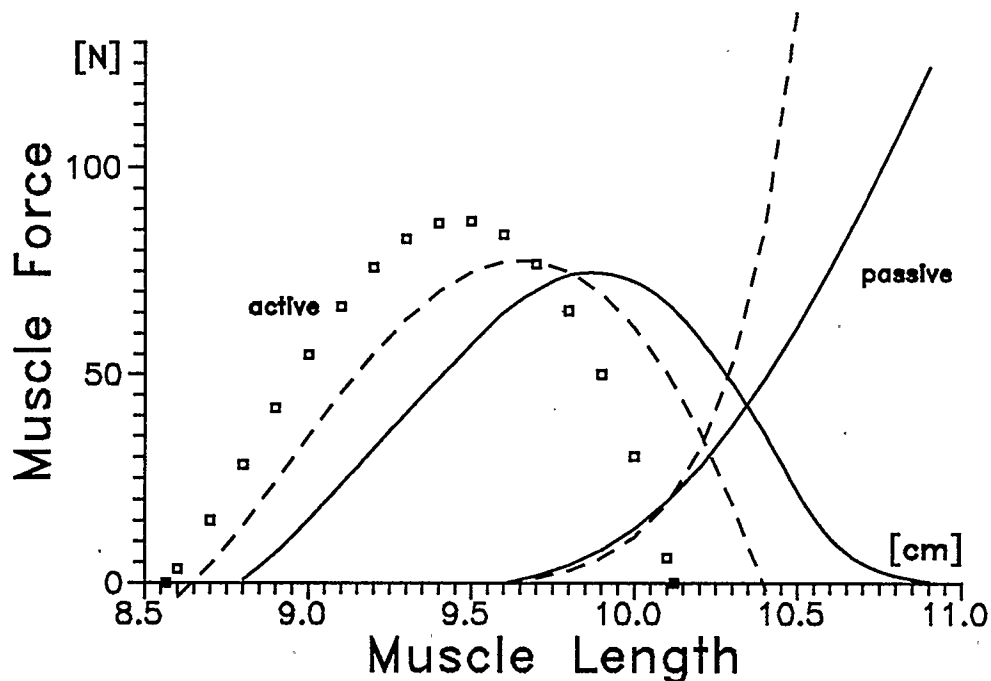


Figure 7.8: Muscle force length curves for muscle with fibre stretch ratio dependent fibre force (symmetric active force profile). Solid lines - CM results, dashed lines and hollow squares - SLM results.

The last section, based on the assumptions of constant fibre force, revealed a similar behaviour between the current trapezoidal muscle geometry and the

comparable parallel tendon sheath geometry for increased muscle stretches. Under the current assumptions of fibre stretch ratio dependent fibre forces, this correspondence has disappeared; the CM results are much closer to the trapezoidal SLM results (dashed lines) than to those of the parallel tendon sheath SLM results (hollow squares). Focusing on the two SLM active force-length curves, it is interesting to observe that they differ quite significantly in their muscle peak forces and active muscle ranges, even though the muscle geometries are very similar. This sensitivity on the muscle geometry should be kept in mind for the discussion below in the light of the differences in configurations for the stimulated and unstimulated muscle.

Comparing the CM and SLM passive muscle force curves for the trapezoidal geometry, the CM force curve initially exhibits somewhat higher force values, while forces increase far less rapidly for higher muscle stretches. As expected, both passive force curves have their origin at the muscle reference length of 9.6 cm. The initially higher CM passive forces are due to the different mode of deformation compared to the SLM. The CM mode of deformation leads right away to tendon stretches which result in additional passive forces. However, it will be demonstrated below that it is also the influence of the tendon sheath elasticities which cause the passive forces to increase less rapidly with increasing muscle stretches. The muscle model by Otten [1988] does include tendon sheath elasticities. In his model, the effect of the tendon sheath elasticities shifts the passive force curve slightly to higher muscle length. However, no changes in the

general appearance of the curve (e.g. here the observed decrease in the slope) are apparent.

Comparing the CM and SLM active muscle force curves, the CM force curve appears to be shifted to higher muscle lengths with a slightly lower peak force, a larger range, and an overall smaller slope of the ascending limb. The descending limb runs out more gradually. An element of virtual agreement between the two curves consists in the muscle force - muscle length integral, which is a measure of the work a muscle is able to perform over a complete active contraction (this work is in addition to the work regained from elastic energy storage during the passive stretch of the muscle). The CM integral evaluates to about 97% of the SLM integral, with the latter being the theoretical limit because the theory underlying the SLM does not allow for any losses and/or elastic energy storage within the muscle structure. In principle, the differences between the CM and SLM behaviour above conform with observations made by Otten [1988] in relation to his model. Compared to Otten, however, the differences observed here are far more significant in magnitude.

All the differences in the muscle force curves mentioned above follow from the inclusion of elastic tendon sheaths and from the absence of global kinematic constraints in the CM. Starting with the unstimulated muscle in reference configuration (reference muscle length, 9.6 cm) and stimulating the muscle while holding it isometrically results in a muscle deformation whose primary feature is

schematically depicted in Figure 7.9. The tendon sheaths become stretched and increase in length. This results in the muscle fibres assuming an increased angle of pinnation and a decreased length (dashed lines in Figure 7.9). A second effect is associated with the increase in absolute tendon sheath lengths; as the tendon sheaths become longer, they move closer together in order to maintain the original muscle volume. The tendon sheaths have to approach one another even further in order to compensate for the muscle tissue which is extruded at the muscle ends. The reduced distance between tendon sheaths results in a further decrease in muscle fibre lengths.

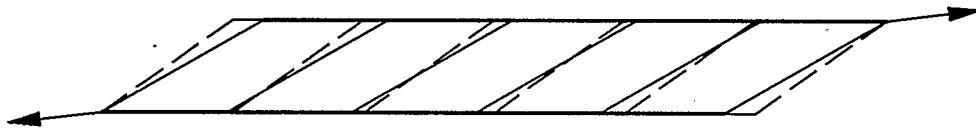


Figure 7.9: Effects of tendon stretch on fibre angle of pinnation and fibre length.

Comparing the isometrically stimulated configuration (Figure 7.4, second from bottom) to the corresponding reference configuration (Figure 7.1, top) and considering the muscle fibre at muscle mid-length reveals that the fibre has shortened from a stretch ration of $\lambda = 1.0$ to about $\lambda = 0.8$ and that its angle of

pinnation (measured against the lower tendon sheath) has increased from 30° to about 37° . Both effects combined tend to decrease the muscle force at this muscle reference length of 9.6 cm, which explains the difference in force magnitudes in Figure 7.8. between the CM and SLM predictions. Realizing that the majority of the muscle fibres in the stimulated configuration take on a stretch ratio substantially below $\lambda = 1.0$ explains the offset between the two active force-length curves; the CM's capacity to shorten from muscle reference length is decreased compared to the SLM, where the muscle fibres, by definition, maintain a stretch ratio of $\lambda = 1.0$ for the stimulated condition.

Under a passive muscle stretch, the general effects of tendon sheath stretch, that is, a fibre rearrangement which results in smaller fibre lengths and higher angles of pinnation compared to the SLM, will also occur. Consequently, the CM passive muscle force curve is less steep than SLM curve.

The input fibre force-length relation places the passive fibre force onset coinciding with the active fibre peak force. On the muscle level, the onset of the passive force and active peak force are offset considerably as a consequence of the tendon sheath elasticities and the absence of global displacement constraints. Consequently, appropriate caution should be applied when inferring fibre characteristics from experimentally determined muscle behaviour.

The lower value of the CM active force peak compared to the SLM peak force in Figure 7.8 results from a loss of synchronization in the fibre stretch ratios. The

primary effect of tendon sheath stretch, which is schematically depicted in Figure 7.9, causes a global change in relative fibre lengths and angles of pinnation. However, these changes are uniform within the muscle volume with the result that the muscle fibres are still synchronized. The muscle peak force, while occurring at a different muscle length, is expected to be equal to the force of a muscle with stiff tendon sheaths. In the current context, the extrusion of the muscle tissue at the muscle ends makes the difference. As mentioned before, this extrusion is a consequence of the internal loading and it is necessary in order to contain the muscle body. Muscle boundary fibres are stretched onto the passive branch of the fibre force-length curve until they develop enough tension to stem further deformations, while the fibres in the muscle mid-section shorten. Compared to the SLM, not all the fibres reach optimal length at the same configuration which results in a decreased active peak muscle force.

In Figure 7.8, the difference in active peak muscle force between the CM and SLM is not very significant. However, the considerations made above take on an increased importance when they are extrapolated to a fully three-dimensional muscle model. In the current model, the tissue extrusions are limited to the two muscle ends, and the tissue is contained in depth direction by the plane strain assumption. In a three-dimensional model, tissue extrusion would have to be expected all around the free muscle body boundaries which would greatly increase the effect of fibre de-synchronization and, consequently, decrease the potential active muscle force peak considerably.

The difference of 3% in the active muscle force - muscle length integral between the CM and SLM is due to elastic strain energy storage within the matrix fluid part of the muscle tissue in the shortened muscle configuration. The strain energy stored during the passive muscle stretch and the stretch of the tendon sheaths due to active fibre stresses is regained during muscle contraction. However, the shortest muscle position in Figure 7.4 constitutes a deformed, i.e. strained, configuration compared to the reference configuration. Due to the small, but finite tissue matrix elasticity, a small amount of strain energy is contained within the muscle tissue. This portion of the fibre "work potential", while it could be regained in principle during muscle relaxation in the context of the current theory (postulation of a strain energy function), is effectively lost for any system external to the muscle. Over a complete contraction of the CM the active force - length integral evaluates in the order of 3% below the value obtained for a strain energy free situation (SLM), which is rather small. However, the difference becomes more important for partial contractions, that is, for contractions ending with muscle lengths corresponding to non-zero muscle forces. In this case, the portion of the work generated by the fibres which has been converted into tendon stretch (tendon strain energy) cannot be regained for external muscle work.

Returning to the CM total force-length curve in Figure 7.6 and comparing its important features to experimental data of in-situ force measurements on the cat gastrocnemius muscle by Herzog et al. [1990], the following observations can be

made: The almost linear force increase over large portions of the active branch, the relatively small force decrease within the plateau region, and the offset between passive force onset and total force peak correspond well. However, the experiments do not show a renewed force increase for higher muscle lengths corresponding to the passive branch in the current simulation. In fact, the current model behaviour is very much influenced by, and a stable muscle behaviour is dependent on the significant passive force component in Figure 7.6. By contrast, the experiments by Herzog show an almost negligible passive force component over a muscle length interval which extended beyond the muscle's normal range of motion. A similar observation regarding low muscle passive forces has been made by Muhl [1982] who conducted muscle force-length measurements on the digastric muscle of New Zealand White rabbit.

7.2.2 Fibre Force Profile Number 2

In order to obtain some indications regarding the sensitivity of the muscle force-length relations on varying fibre force-length relations, this section presents results for model simulations based on alternate fibre characteristics. The force profile number 2 differs from the force profile number 1, which has been employed in the previous section, in that (a) the active fibre force-length relation is asymmetric and (b) the relative minimum of the total fibre force-length relation between the active and passive branch takes on a smaller value.

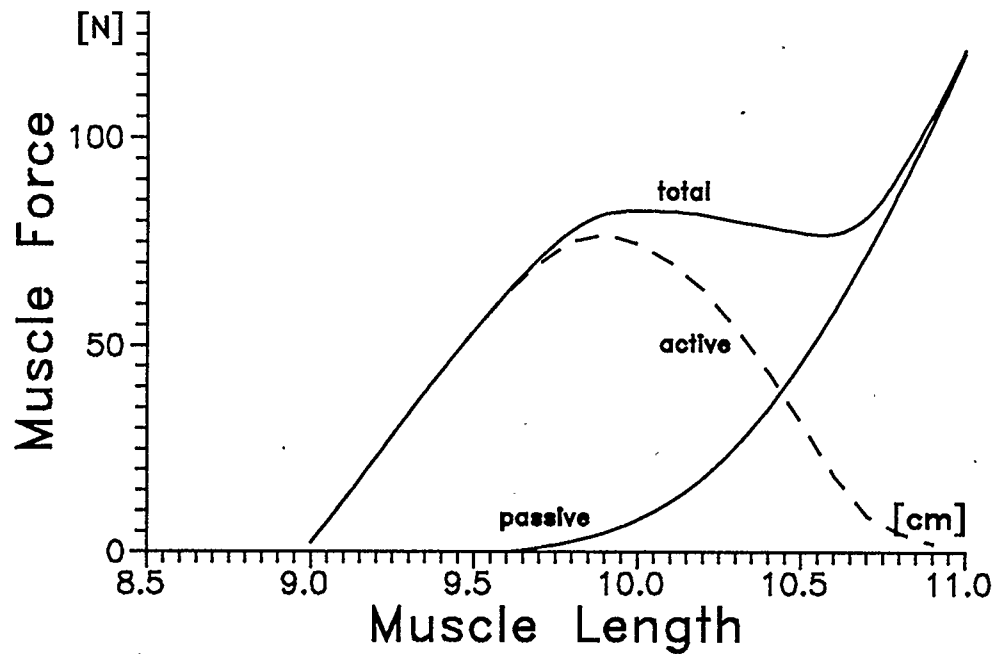


Figure 7.10: Muscle force length curves for muscle with fibre stretch ratio dependent fibre force (asymmetric active force profile). Unstimulated - "passive", stimulated - "total", difference of former - "active".

Figure 7.10 presents the muscle force-length relations for the current simulation. Comparing these results to Figure 7.6 of the previous section, the differences are not very striking. In particular, the active muscle force-length curve still shows a parabolic shape, that is, the asymmetry in the input fibre force-length relation is not apparent at muscle level. The offset between the passive muscle force onset and the peak active muscle force is virtually identical. Also, the difference in peak total muscle force and the minimum total force within the plateau region is very close in both simulations.

Differences become only apparent on closer examination: The slopes of the ascending and descending limb of the active muscle force-length curve have increased for the current simulation and the active muscle range has somewhat decreased. While the value of the active force peak is currently higher, the maximum total force in the plateau region is lower. The magnitudes of these differences are not very important. From an experimental point of view, it is doubtful whether these differences could be observed with an appropriate degree of confidence considering the usual inherent spread in experimental data. Both the symmetric and asymmetric fibre force-length curves lead to fairly symmetric muscle force-length characteristics. Starting from a muscle force-length curve, it is difficult to infer the underlying fibre characteristics with certainty.

Figure 7.11 displays the comparison between CM and SLM model results based on the current asymmetric fibre force-length profile. In principle, all the observations made in the previous section and the related discussions can be carried over. Comparing the active muscle force curves emphasized the loss of asymmetry in the case of the CM. A fairly symmetric muscle force-length curve is consistent with the experimental results of Woittiez et al. [1984] on White Wistar rat muscles [1984]. On the other hand, Muhl [1982] determined asymmetric muscle force-length relations for the digastric muscle of New Zealand White rabbits, which resemble the SLM predictions in Figure 7.11. It should be noted that both Woittiez et al. and Muhl performed muscle force-length experiments on the entire muscle-

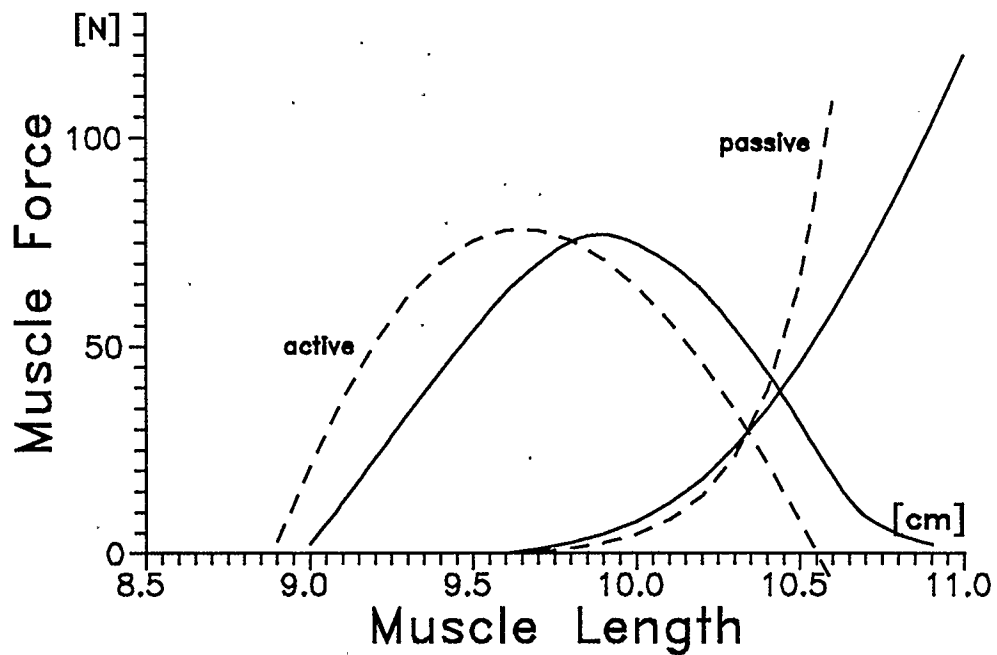


Figure 7.11: Muscle force length curves for muscle with fibre stretch ratio dependent fibre force (asymmetric active force profile). Solid lines - CM results, dashed lines - SLM results.

tendon complex. Muhl obtained two muscle force-length relations, one representing the raw experimental data, the other having been corrected for the tendon stretch. The comments above apply to the latter because this force-length relation is indicative of the muscle behaviour excluding the tendon and because the current models do not include tendons.

7.3 Curved Muscle Fibres

When a cat medial gastrocnemius muscle is dissected longitudinally from origin to insertion, muscle fibres are seen to form a characteristic S-shaped curve in a plane which is perpendicular to the tendon sheath planes. In order to investigate how the current model behaves when fibres take on varying angles of pinnation between the tendon sheaths, the trapezoidal geometry has been modified slightly. Figure 7.12 displays, at the top, the modified geometry; within the middle two quarters of the vertical distance between the tendon sheaths, the fibre angle of pinnation has, as before, the value of 30° measured against the lower tendon sheath. Within the top and bottom quarter, the angle of pinnation has been reduced to 20° . Thus, the fibre length axes take on a crude S-shaped form between the tendon sheaths with a discontinuity in the angle of pinnation at the junction of the muscle regions (or layers). Force profile number 2 will be used in the simulations below.

As far as the fibre arrangement is concerned, the modified geometry has the following consequences: if all the muscle fibres are assumed to have a constant and uniform thickness, which is the point of view adopted below, more fibres can be placed in parallel within the mid-layer than in either layer next to the tendon sheaths (compare to Chapter 3.1). This implies that a certain percentage of fibres in the mid layer terminate at the interface with the top and bottom layers.

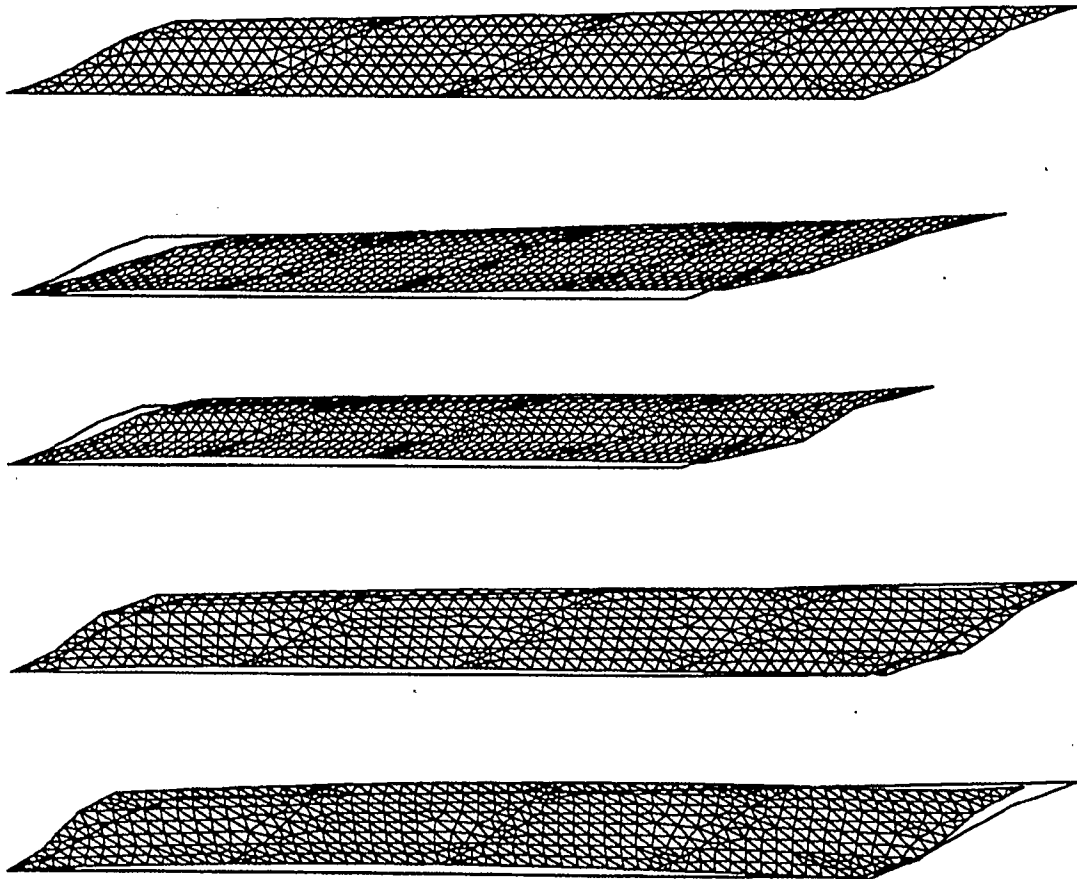


Figure 7.12: Muscle with initially curved fibres. Reference configuration - top, most stretched configuration - second from top, most contracted configuration - bottom.

Ultrasound measurements performed by Wagemans [1989] on human gastrocnemius muscles under voluntary contractions show that muscle fibres appear to be straight in the stimulated and contracted muscle. The current model behaves contrary to these observations. The plots in Figure 7.12 (second from top to bottom) show a sequence of stimulated muscle configurations from maximum stretch to maximum contraction. They reveal that the difference in angles of pinnation between the layers generally increases, rather than decreases.

While the model behaviour is certainly in contradiction with the experimental observations made by Wagemans, it is an expected consequence of the assumptions made about the constitutive characteristics of muscle tissue. Each layer may be considered as an individual muscle with its characteristic range in angles of pinnation over a complete contraction in accordance with Chapter 3. A muscle with a lower reference angle of pinnation (top and bottom layer) also has a lower angle of pinnation after a full contraction than a muscle with a higher reference angle of pinnation (middle layer). Joining the muscles together in order to form the current geometry does not change this basic consideration. Also, matching the fibre densities in the different layers in order to obtain the "same number of fibres" in parallel in all three layers does not change the model behaviour significantly as far as the relative angles of pinnation over a contraction are concerned. Furthermore, if one assumes that fibres are packed as densely as possible in the top and bottom layers, the matching of fibres would imply a less

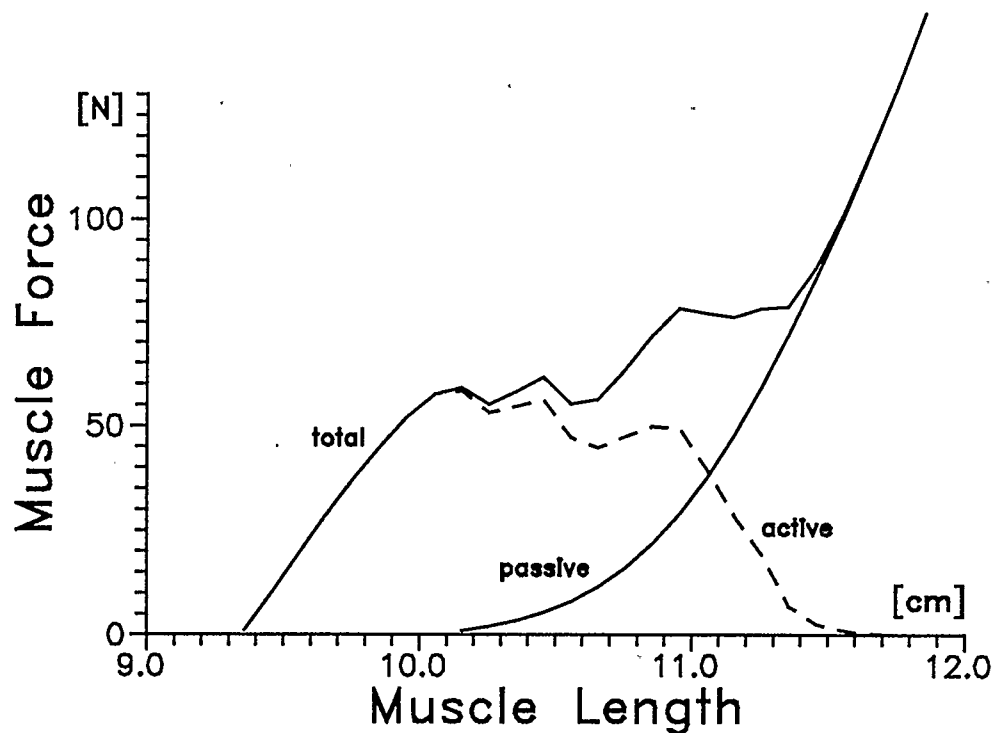


Figure 7.13: Muscle force length curves for muscle with initially curved fibres. Muscle fibres have force profile #2 characteristics. Unstimulated - "passive", stimulated - "total", difference of former - "active".

than optimal fibre packing in the mid-layer which would be a doubtful strategy from an economical point of view.

Figure 7.13 presents the muscle force-length curves for the current muscle geometry. Despite the mismatched "number of fibres" between the different layers, the passive muscle force-length curve as well as the active and passive branches of the total force-length curve have a smooth appearance, that is, the general muscle function is not disturbed by the fibre mismatch. The difference in fibre

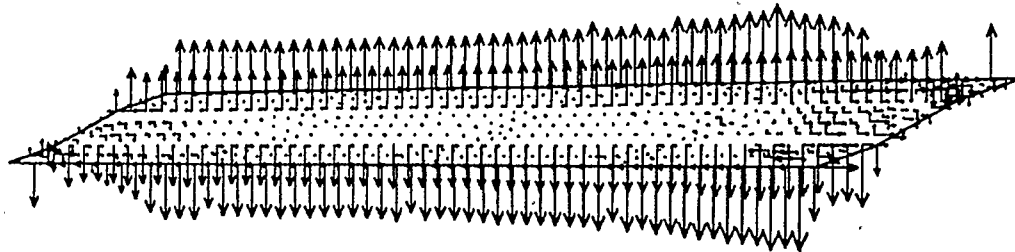


Figure 7.14: Nodal reaction forces for the muscle fluid matrix elements.

directional stresses is compensated by the tissue fluid matrix at the layer interfaces. Figure 7.14 gives an impression of this effect: it depicts the nodal reaction forces of the finite elements which represent the tissue fluid matrix. In addition to the tissue to tendon sheath interface, forces are present along the lines where the layers with different angles of pinnation are joined. These forces put the tissue fluid matrix in the mid-layer under increased pressure compared to the top and bottom layer.

The active and passive branch of the total muscle force-length curve are joined by a irregular curve, which is a result of the "snap-through" effect discussed in conjunction with Figure 7.7. At the layer junctions, the discontinuities in the angles of pinnation lead to local instabilities when the fibres take on a stretch ratio corresponding to the descending portion of the fibre force-length curve (negative

slope). The points on the irregular portion of the total force-length curve do not represent equilibrium configurations as the finite element solution iterates through "neighbouring" configurations, none of which being an equilibrium configuration. It should however be stressed that the solution does not diverge and that the configurations and muscle force values from iteration to iteration do not change too drastically. The muscle force - muscle length integral of the active force curve results in 95% of the theoretical value, which demonstrates that even the non-converged solutions have a relation to the overall performance of the muscle. Comparing the overall form of the active muscle force-length curve to those in the previous sections reveals a lower maximum force level and an increase in the muscle range over which this force level is maintained.

It should also be pointed out that the non-convergence does not constitute a failure on the part of the CM. The non-convergence is a consequence of the problematic type of the fibre force-length nonlinearity, which is compounded with the discontinuity in fibre angles of pinnation at the layer junctions. A finite element model with a greatly refined mesh which incorporates a smoother transition in angles of pinnation would be expected to behave better as far as model convergence is concerned. The general model behaviour (maintenance of different angles of pinnation in different layers) is, however, not expected to change.

Muscle fibres are usually seen to pass on forces between their origins and insertions from sarcomere to sarcomere with the implication that when one

sarcomere within a fibre fails, the whole fibre would become dysfunctional. As outlined above, the current geometry may be interpreted to contain fibres which extend over the mid-layer only. In other words, they are not connected to the tendon sheaths and should be considered dysfunctional according to the point of view above. The simulation results showing a normal muscle behaviour for a large portion of the contraction history and the reasonable value for the active muscle force - muscle length integral indicate that this disfunction simply does not occur. Not the fibre forces passed on along the muscle fibres, but the global stress state control the muscle behaviour. While the stress state changes locally if a fibre is severed, the global stress state hardly changes. Consequently, a localized fibre damage is not expected to render the entire fibre useless.

Chapter 8

Finite Element Simulations: Gastrocnemius Geometry

Straight line models similar to the one presented in Chapter 3 limit the degree of details in muscular geometry which can be represented and analyzed. In order to permit a comparison between the present Continuum Model (CM) and the Straight Line Model (SLM), the simulations in the previous chapter were based on geometries appropriate for SLM analyses. However, one advantage of the CM over the SLM is that more involved geometries can be treated. In taking advantage of the CM's increased flexibility, the simulations in this chapter will be based on a geometry which approaches the shape of the cat medial gastrocnemius muscle.

The interpretation of simulations in the previous sections have been focused very much on the muscle behaviour as it is characterized by the muscle force-length relation. In the second part of this chapter, the focus will be shifted to the aspect

of structural integrity. An alternate mode of muscular contraction will be presumed and its consequences on muscle deformation and stress state will be outlined.

8.1 Fibre Force Profile Number 2

The following simulations are based on the gastrocnemius geometry as presented in Chapter 5 and reproduced in Figure 8.1, top. This geometry is characterized by a slender "neck" section at the left end and a thickened "head" section at the right end of the geometry. Tendon sheaths run along the extent of both the upper and lower geometry boundaries. Fibre angles of pinnation take on a value of 30° relative to adjoining tendon sheaths. This results in discontinuously changing fibre directions within the head section similar to those in Chapter 7.3. Continuous lines (formed by the edges of the triangular elements) at regular intervals over the muscle length, which coincide with the local fibre direction, make the fibre directions apparent. Material parameters are identical to those in the previous chapter (matrix material constants, $A = B = 0.125 \text{ N/cm}^2$, $\nu = 0.4995$, tendonal stiffness, 1200 N/cm^2 , and active fibre stress, $\hat{P} = 25 \text{ N/cm}^2$). The fibre force profile number 2 will be used for the simulations in this section. The muscle origin at the top-left is fully constrained, while the muscle insertion at the bottom-right is displaced along the line of action of the muscle for the deforming muscle. Deformation plots in Figure 8.1 are not uniformly scaled. In order to provide a point of reference, outlines of the muscle geometry at reference configuration are superimposed to the deformed geometries.

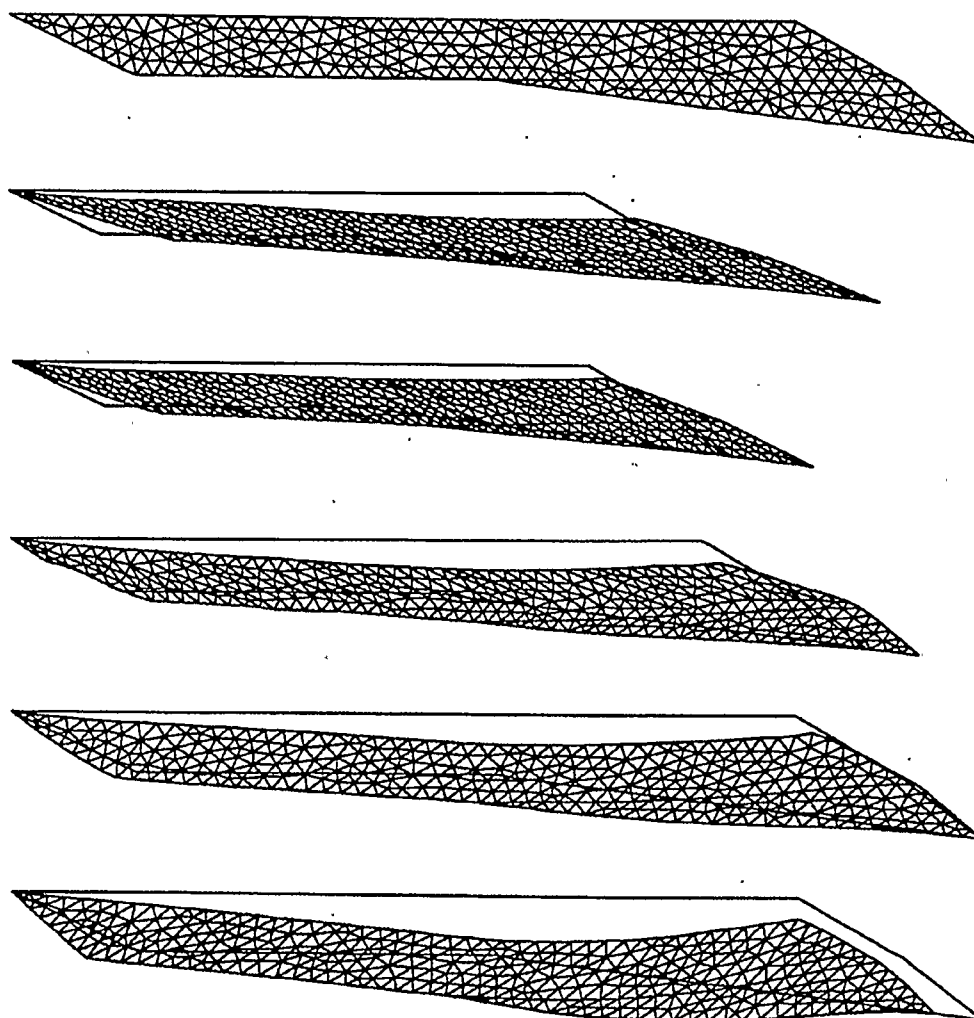


Figure 8.1: Medial gastrocnemius muscle geometry and deformations. Displayed are the initial muscle geometry (top) and a sequence of configurations from most stretched (second from top) to fully contracted (bottom).

Within the deformed configurations in Figure 8.1, initially straight muscle fibres remain straight except for minor curvatures at the two free boundaries next to the origin and insertion. A minor degree of fibre curvature can also be observed in the neck section of the moderately stretched configuration (fourth from top). For all configurations, the relative change in fibre directions within the head section persists. In fact, the degree of the fibre direction change along the line of the fibre angle discontinuity in reference configuration is amplified for the configurations shown in Figure 8.1, fourth from top to bottom. The latter conforms with the observations made in Chapter 7.3, and the discussion can be carried over.

Furthermore, the muscle force-length relation for the current simulation is similar to the one presented in Chapter 7.3. In particular, the irregularity of the total muscle force curve over the plateau region has the same degree of severity and is due to the instabilities forming inside the muscle geometry along the line of the fibre angle discontinuity within the head section.

The stimulated muscle undergoes a significant deformation perpendicular to the muscle's line of action. This deformation mode is especially apparent for shorter muscle lengths and results in a bending of the whole muscle for the shortest configuration. While the general tendency of deformation can be observed when one stretches an isolated cat medial gastrocnemius muscle, the degree of deformation resulting from the current simulation appears too high.

However, it is important to realize that the here observed deformation mode is restricted within the biological system. The lower boundary of the muscle geometry in Figure 8.1 coincides with the location of another muscle, i.e. the plantaris muscle. The plantaris muscle prevents the medial gastrocnemius from deforming in the downwards vertical direction of Figure 8.1. In order to mimic the effects of the plantaris muscle on the medial gastrocnemius muscle, the boundary conditions over the extent of the lower tendon sheath will be modified in the following manner: nonlinear gap boundary elements are applied along the lower tendon sheath boundary which prevent the muscle from deforming downwards in vertical direction. Nodes on the lower tendon sheath boundary remain unconstrained in their horizontal and upwards vertical direction. To conform with these new boundary conditions, the muscle is stretched and contracted by moving its insertion in horizontal direction.

Figure 8.2 presents the muscle deformations obtained for a simulation with the modified boundary conditions described above. Because of the boundary conditions an overall bending of the muscle is absent. In the shortest muscle configuration (bottom) most of the nonlinear gap boundary elements on the lower tendon sheath boundary within the muscle head section are active, that is, the gap is closed and the muscle is supported at these locations. Along the neck section and close to the muscle insertion, however, the gap elements are open, which corresponds to a lifting of the gastrocnemius muscle away from the plantaris

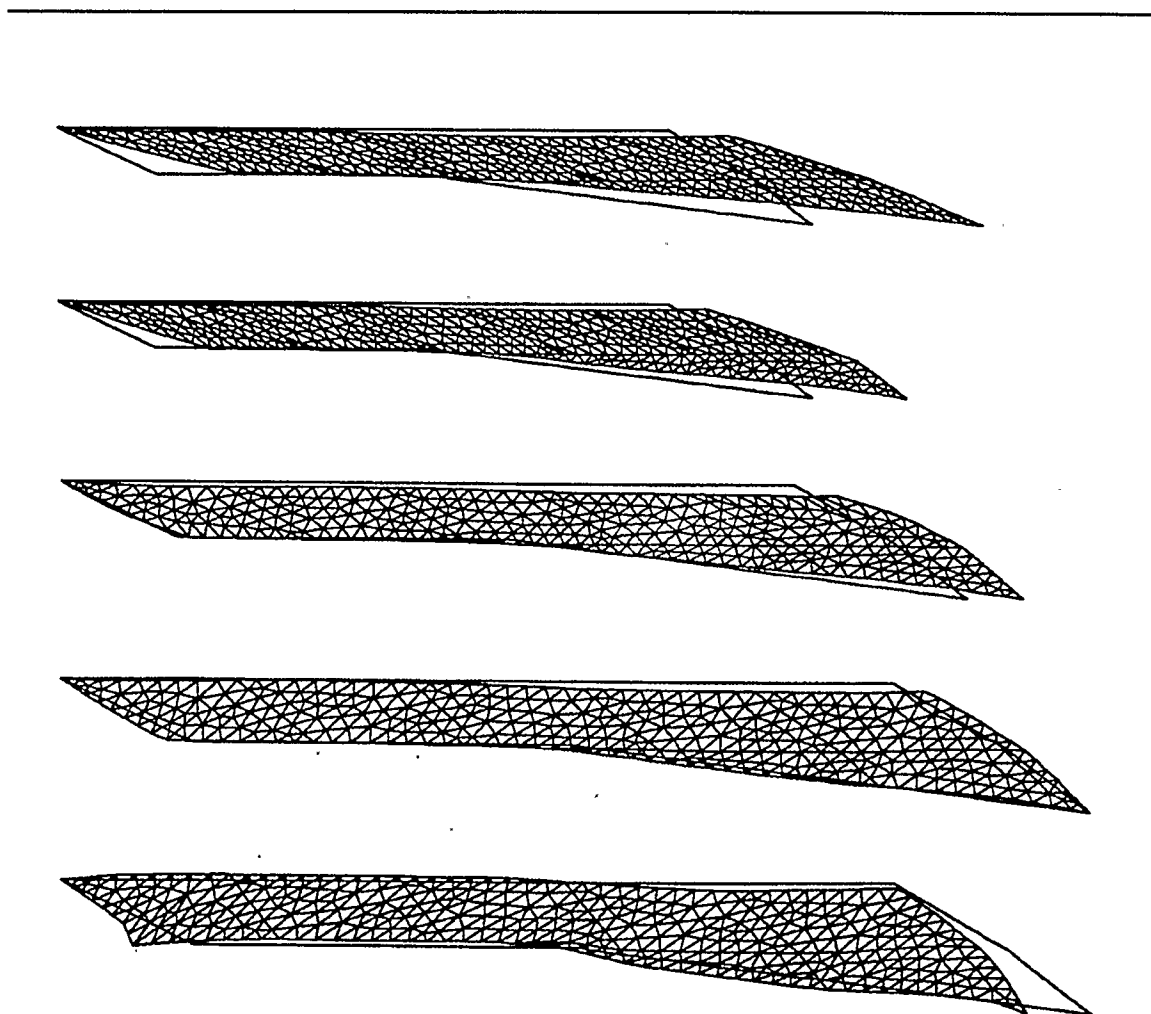


Figure 8.2: Medial gastrocnemius muscle deformations for supported lower tendon sheath boundary. A sequence of deformations is displayed from most stretched (top) to fully contracted (bottom).

muscle. Muscle fibres inside the muscle geometry remain mostly straight. Contrary to the previous simulation however, the degree of fibre angle change along the line of the fibre angle discontinuity within the head section has decreased. This aspect corresponds better to the observations made by Wagemans of straight muscle fibres within the contracted human gastrocnemius muscle [1989]. The free muscle boundary adjacent to the muscle insertion has a rounder and smoother appearance which comes closer to anatomical observations than that of the previous simulation (Figure 8.1, bottom). The free muscle boundary adjacent to the muscle origin takes on a notch-shaped form. This general shape has been observed on serial sections of the medial gastrocnemius muscle of the cat.

Figure 8.3 presents the muscle force-length curves for the current simulation. As before, the curve labelled "passive" corresponds to muscle elongations without stimulation (stimulation parameter $\Theta = 0$), the curve labelled "total" corresponds to muscle deformations for fully stimulated fibres ($\Theta = 1$), and the curve labelled "active" constitutes the difference of the former two curves. Compared to the results of Chapter 7.3, the total force-length curve shows a lesser degree of irregularity within the plateau region joining the active and passive branch. On the other hand, the curve has some degree of irregularity well onto its passive branch. The active force-length curve has, in contrast to the results in Chapter 7, a clearly asymmetric shape with a steep ascending limb and a more gradual descending limb. In its asymmetric shape, the active curve resembles the general shape obtained by Muhl in experiments on the digastric muscle of New Zealand White

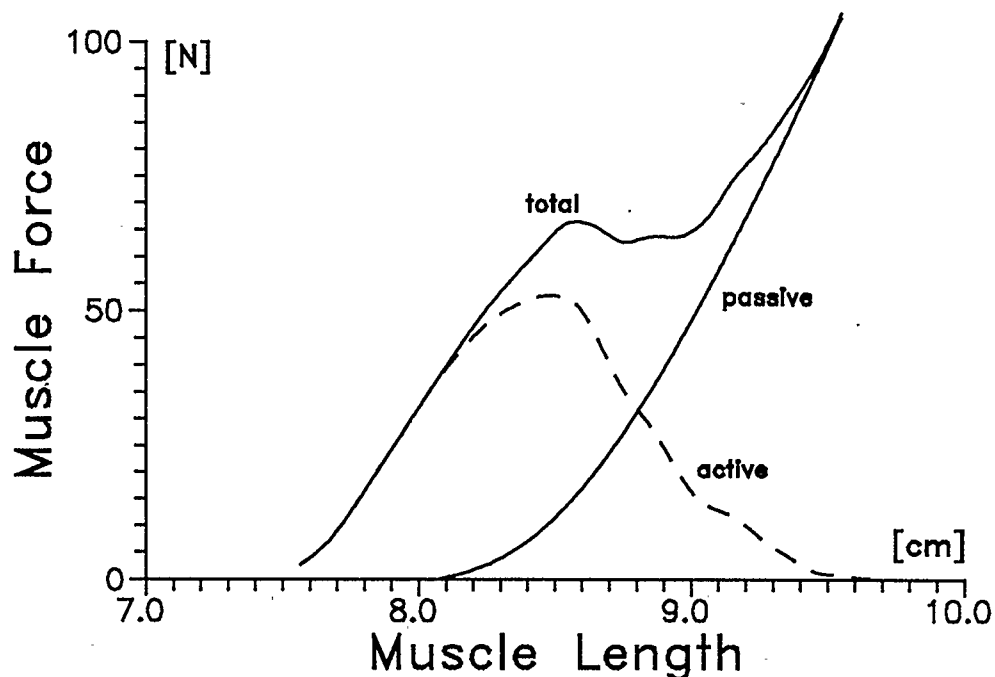


Figure 8.3: Muscle force length curves for medial gastrocnemius muscle with supported lower tendon sheath. Unstimulated - "passive", stimulated - "total", difference of former - "active".

rabbit [1982]. In the digastric muscle, muscle fibres connect directly to the bone of the jaw, that is, the digastric muscle has only one free tendon sheath. The current model, with its lower tendon sheath supported, approaches the aspect of the digastric muscle. It must however be stressed that Woittiez et al. [1984] obtained a close to symmetric muscle force-length curve for the medial gastrocnemius muscles of Wistar rats whose geometry is presumably more closely approximated by the current model than that of the digastric muscle. As has already been observed throughout Chapter 7, the onset of the passive force

occurring at significantly lower muscle lengths than muscle optimal length differs both from Muhl and Woittiez. The magnitude of the passive muscle force over the active muscle range appears too high compared to Muhl [1982], Woittiez et al. [1984], and Herzog et al. [1990]. Judging by the data of Herzog the cat gastrocnemius muscle seems to function mostly on the ascending limb and a little bit beyond the active force peak which translates to a muscle working range of about 2 cm. The current model predicts a corresponding range of only about 1 cm. This deficiency in range has already been observed in the context of the Straight Line Model in Chapter 3 as well as in the simulations of Chapter 7.

It must be reiterated that the model predictions are a direct consequence of the assumptions about muscle tissue characteristics and muscle geometry, all of which being reasonable when taken by themselves. Having the global muscle model behave more closely to experimental muscle data requires that the underlying assumptions have to be changed, and this change may have to be done in a way which is not supported by currently accepted perceptions about muscle fibre and muscle tissue characteristics.

8.2 Alternate Mode of Muscular Contraction

Muscle force-length relations resulting from the simulations so far exhibit the main characteristics of experimental observations, even though the model predictions and experimental data are not in complete agreement. More importantly, the model results are consistent with the underlying assumptions concerning muscle tissue

characteristics. In addition to the force-length relations, the current continuum muscle model also provides predictions about muscle deformations and stress state. Unfortunately, no or only scant experimental data relating to general muscle deformations and tissue stresses are available for comparison. One may, however, make the following observations: Free tendon sheaths, i.e. tendon sheaths which are not supported by neighbouring structures, usually take on a convex shape during contraction, even if the curvature is minute; the current model predicts a concave curvature. Some pennate muscles, with the cat gastrocnemius muscle being an example, do have curved fibres when they are not stimulated. Wagemans [1989] has shown that, at least for the human gastrocnemius muscle, this curvature disappears under stimulation and contraction; the current model preserves and, for certain cases, even magnifies any initial fibre curvature under stimulation. Muscle pressure measurements by Otten [1988] resulted in a smooth pressure distribution within the muscle; the current model predictions result in irregular pressure distributions with local pressure concentrations (as seen in Figure 6.6). In the current model, the interaction between muscle tissue and tendon sheath, which is visualized by the nodal reaction forces in Figure 6.7, is irregular and leads to model instabilities when the stimulation parameter, Θ , is changed too rapidly between iterations. Calling on engineering judgement, neither the pressure distribution nor the muscle tissue to tendon sheath interactions generated by the model conform with what would be expected from a balanced structure.

In an attempt to alleviate the incongruities listed above, the continuum model has been modified by introducing an alternate mode of muscular contraction which consists of: (a) the muscle tissue is given some degree of compressibility (or expansivity), and (b) the fibre contractile property has been removed and substituted by a tissue tendency to expand isotropically. The fibre passive characteristics have not been changed. The current modifications are remotely related to the suggestions of Vain [1990] who proposed a thickening tendency of muscle fibres.

Figure 8.4 presents the muscle deformation, tissue to tendon sheath interaction and muscle tissue matrix pressure distribution for a simulation based on the changed tissue characteristics. The gastrocnemius geometry with supported lower tendon sheath boundary has been used for the simulation. The free, that is, unsupported tendon sheath at the top of the muscle geometry deforms now into a convex shape. Furthermore, the initially present discontinuities in fibre directions within the muscle head section have disappeared completely. Both the tissue to tendon sheath interaction and the pressure distribution take on a much smoother pattern compared to Figures 6.6 and 6.7. They correspond better to a balanced structure. Finally, the model converges even for significant changes of the stimulation parameter, Θ , between iterations. It should also be mentioned that the muscle does generate a tensile force matching previous results, even though the modified tissue characteristics have the tissue expand under stimulation.

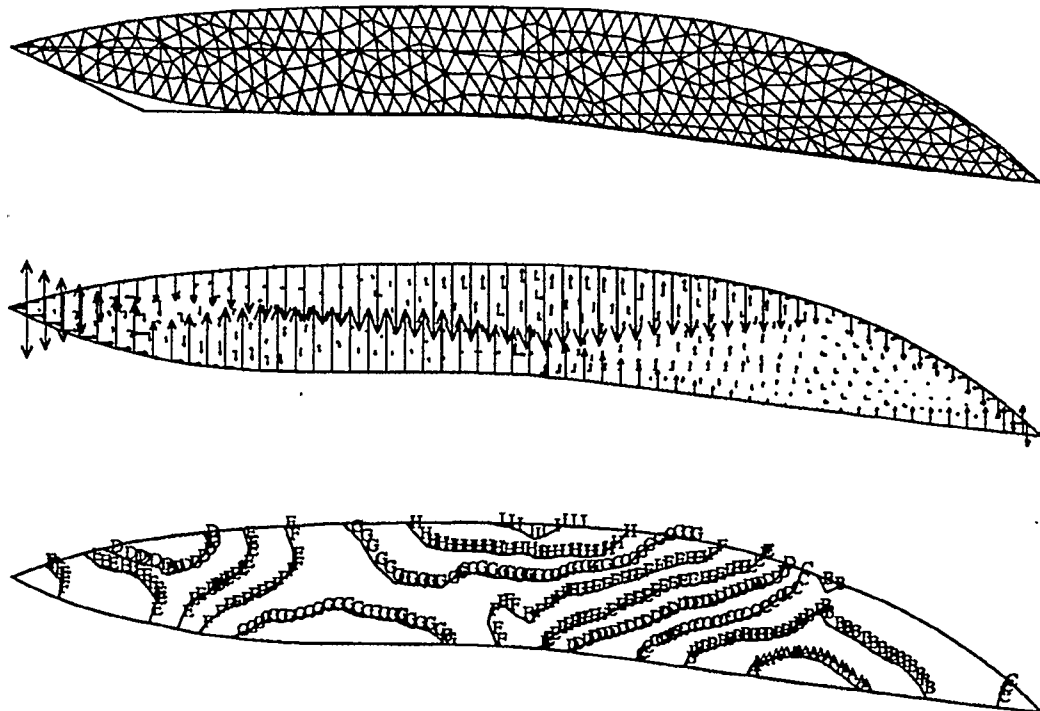


Figure 8.4: Muscle deformation, tissue - tendon sheath interaction, and tissue matrix pressure distribution based on the alternate mode of muscular contraction.

Certainly, the improved structural model behaviour has been obtained by making changes to the muscle tissue description which contradict physiological evidence. Muscle tissue has been shown to be incompressible, e.g. Abbott et al. [1962], and it is unquestionable that muscle fibres do contract. The point to be made here is that a more balanced structural behaviour can be achieved by modifying the assumptions about tissue characteristics. The modifications implemented above are too radical; more subtle modifications which conform with physiological

observations would obviously be desirable, but could not be found with the current model. Bound by the original decisions regarding exclusively contracting and independent muscle fibre behaviour, possible changes to the material model are limited without reworking the whole muscle model from the beginning. For now, the modifications made to the material description above may serve to inspire a change in perspective with regard to the perceived muscle tissue behaviour and to indicate new directions for further research.

It should also be mentioned that a structurally more satisfying muscle behaviour can be obtained by increasing the passive characteristics of the muscle tissue description. In the context of the current model, this can be simply achieved by increasing the constants A and B in the muscle tissue matrix description. This approach provides the tissue with additional shear rigidity and eliminates all the problems of convergence in Chapter 7.3 as well as some of the incongruities listed at the outset of this section. One might favour this approach as it does not immediately contradict physiological facts. However, any increase in the passive components of the tissue description would result in more strain energy storage for muscle deformations with an associated decrease in available muscle work external to the muscle, which translates into a smaller muscle peak force and an reduced muscle range. While the muscle force-length curve can be patched up by changing the muscle fibre force profile accordingly, this does not change the fact that a larger amount of work generated by the fibres will be transformed into strain energy rather than external muscle work.

The function of skeletal muscle consists in generating work on the skeletal system. It may be expected that nature accomplishes this efficiently, i.e. without wasting energy on internal (strain) energy storage which would be lost for all practical purposes. Only further research can tell whether modifications to the material description presented in Chapter 4 are necessary. If they are, it appears more sensible for these modifications to affect the active tissue characteristics than the passive ones.

Chapter 9

Summary and Conclusions

Two mechanical models of muscular contraction have been presented in the context of this thesis. Keeping with the presently accepted view of muscle structure and function, the assumptions underlying both models are that muscle fibres are one-dimensional entities and that the mechanical muscle behaviour is a reflection of the active and passive muscle fibre characteristics exclusively.

The Straight Line muscle Model (SLM) has been based on kinematic constrained muscle deformation modes, similar to the treatment by other authors. Paying special attention to physical consistency and simplicity, the SLM is founded on consistent equilibrium considerations which relate the internal fibre forces to the external muscle force, and the equations describing the model are expressed by a closed set of nonlinear algebraic equations. The changing number of muscle fibres acting in parallel as a function of the geometrical parameters, most notably the reference angle of pinnation, is taken into account by the model.

The Continuum muscle Model (CM) has been based on constitutive relations for muscle tissue. No kinematic constraints have been applied, except for anatomically justifiable boundary conditions, and the model formulation allows for a natural inclusion of tendon sheath elasticities. Overall muscle deformations are not preordained, but result from the solution of the structural problem. In addition to the muscle force-length relation, the internal stress state of the muscle becomes accessible. The CM has the potential of representing more complicated muscle geometries, muscle fibre curvature, varying muscle fibre densities, etc. Furthermore, the concepts underlying the model are transferrable to a three-dimensional modelling approach.

The unifying factor of both models consists in the active and passive Muscle Tissue Energy Density function (MTED)¹. Given the active MTED function and the volume of a muscle, the amount of work this muscle can produce over a complete contraction, expressed by the integral of the active muscle force over the active muscle range, is determined and equal for both muscle models. However, the actual shape of the muscle force-length relations show a notable dependency on the parameters describing the muscle geometry at reference configuration and, in the case of the CM, on the boundary conditions. Therefore, most experimentally obtained muscle force-length relations could probably be reproduced using the

¹The constitutive treatment of the CM is based on the MTED function. The SLM also uses the MTED function but in a less rigorous manner.

presented models in their current implementation². A more detailed model description, which might include a three-dimensional geometry, different fibre densities and orientations throughout the structure, etc., appears dispensable.

Muscle force-length relations constitute the majority of quantified experimental data pertaining to mechanical muscle characteristics, and they certainly describe one of the most important aspects of muscular function in the musculo-skeletal system. However, they do not describe all aspects of muscular contraction. The presented models do allow for additional considerations which have led to the following incongruities: Although the fibre angle of pinnation predicted by the model for maximum muscle force is in agreement with the experimental observations by Wagemans [1989], the values of the angles of pinnation over the extent of a complete contraction are significantly different. Contrary to experimental observations, muscle deformations obtained from CM simulations result in a globally concave curvature of unsupported tendon sheaths. Furthermore, the resulting stress state within the muscle does not conform to a balanced structure.

These incongruities cannot be resolved by adjusting the geometrical parameters or by changing the functional form of the input fibre force-length relation. Rather, they are a reflection of the initial model assumptions about muscle tissue behaviour, and changes to the model have to be made at that level. It is, therefore,

²In addition to the parameters describing the muscle geometry, the scaling factor for active fibre stress, \hat{P} , may have to be adjusted to this end. Given the variations in magnitude for fibre stresses listed in the literature however, good arguments can be made for using greatly varying values.

felt that further work should be concerned with the reexamination and modification of these assumptions, even if this should require to step beyond the bounds of currently established experimental ground. Realizing that desirable experiments on muscles and muscle tissue are at times difficult, if not impossible to perform, models similar to the presented CM may prove themselves to be invaluable tools in obtaining indications about the validity of modified assumptions.

Bibliography

- Abbott, B.C., Wilkie, D.R. (1953) The relation between velocity of shortening and the tension-length curve of skeletal muscle. *Journal of Physiology*, 120: 214-223.
- Abbott, B.C., Baskin, R.J., (1962) Volume changes in frog muscle during contraction. *Journal of Physiology (London)*. 161: 379-391.
- Alexander, R.McN. (1975) The mechanics of hopping by kangaroos (macropodidae) *Journal of Zoology (London)*. 177: 265-303.
- Anton, M.G., Epstein, M. (1989) Continuum model of skeleton muscle tissue. *European Society for Biomaterials, Proceedings of the 8th European Conference on Biomaterials, Heidelberg*.
- Anton, M.G., Nigg, B.M. (1990) An optimal control model for running. *Canadian Society for Biomechanics. Proceedings of the sixth biennial conference, Quebec*.
- Audu, M.L., Davy, D.T. (1985) The influence of muscle model complexity in musculoskeletal motion modeling. *Journal of Biomechanical Engineering*, 107: 147-157.
- Becker, E., Bürger, W. (1975) *Kontinuumsmechanik*. Teubner Verlag, Stuttgart.
- Benninghoff, A., Rollhäuser, H. (1952) Zur inneren Mechanik des gefiederten Muskels. *Pflügers Archiv für die gesamte Physiologie*, 254: 527-548.

- Blickhan, R. (1989) The spring-mass model for running and hopping. *Journal of Biomechanics*, 22: 1217-1227.
- Demer, L.L., Yin, F.C.P. (1983) Passive biaxial properties of isolated canine myocardium. *Journal of Physiology*, 339: 615-630.
- Fung, Y.C. (1970) Mechanics of the heart muscle. *Journal of Biomechanics*, 3: 381-404.
- Fung, Y.C., (1981) *Biomechanics: Mechanical properties of living tissues*. Springer-Verlag New York.
- Gans, C., Bock, W.J. (1965) The functional significance of muscle architecture - a theoretical analysis. *Ergebnisse der Anatomie und Entwicklungsgeschichte*, 38: 115-142.
- Gans, C. (1982) Fiber architecture and muscle function. *Exercise and Sport Sciences Reviews*, 10: 160-207.
- Gordon, A.M., Huxley, A.F., Julian, F.J. (1966) The variation in isometric tension with sarcomere length in vertebrate muscle fibres. *Journal of Physiology*, 184: 170-192.
- Greene P.R., McMahon, T.A. (1979) Reflex stiffness of man's anti-gravity muscles during knee bends while carrying extra weights. *Journal of Biomechanics*, 12: 881-891.
- Hatze, H. (1976) The complete optimization of the human motion. *Mathematical Biosciences*, 28: 99-135.
- Herzog, W. (1987) Individual muscle force estimates using a non-linear optimal design. *Journal of Neuroscience Methods*, 21: 167-179.
- Herzog, W., Leonard, T.R., Renaud, J.M., Wallace, J.L., Chaki, G., (1990) Force-length relations of in-situ cat gastrocnemius muscles. *Canadian Society for Biomechanics. Proceedings of the sixth biennial conference, Quebec*.
- Herzog, W. (1991) Analysis of experimental data from Wagemans [1989]. University of Calgary, Department of Physical Education. Private communication.
- Heukelom, B., van der Stelt, A., Diegenbach, P.C. (1979) A simple anatomical model of muscle and the effects of internal pressure. *Bulletin of Mathematical Biology*, 41: 791-802.

- Hill, A.V., (1938) The heat of shortening and the dynamic constants of muscle. *Proceedings of the Royal Society of London. Series B: Biological Sciences* (London), 126: 136-195.
- Hill, A.V. (1970) *First and last experiments in muscle mechanics*. At the University Press, Cambridge.
- Huxley, A.F., (1957) Muscle structure and theories of contraction. *Progress in Biophysics and Biophysical Chemistry*, 7: 255-318.
- Huxley, A.F., (1974) Muscular contraction. *Journal of Physiology*, 243: 1-43.
- Kardel, T. (1990) Niels Stensen's geometrical theory of muscle contraction (1667): A reappraisal. *Journal of Biomechanics*, 23: 953-965.
- Kaufman, K.R., An, K.-N., Chao, E.Y.S. (1989) Incorporation of muscle architecture into the muscle length-tension relationship. *Journal of Biomechanics*, 22: 943-948.
- Kaufman, K.R., An, K.-N., Litchy, W.J., Chao, E.Y.S. (1991) Physiological prediction of muscle forces - I. Theoretical formulation. *Neuroscience*, 40: 781-792.
- Kohnke, P.C. (1989) *ANSYS Theoretical Manual*. Swanson Analysis Systems, Inc., Houston.
- Lanir, Y., (1983) Constitutive equations for fibrous connective tissues. *Journal of Biomechanics*, 16: 1-12.
- Lanir, Y., Yin, F.C.P., Perl, M., Sheinman, I. and Strumpf, R.K. (1988) Structural three-dimensional constitutive law for the passive myocardium. *Journal of Biomechanical Engineering*, 110: 200-207.
- Malvern, L.E. (1969) *Introduction to the mechanics of a continuous medium*. Prentice-Hall, Inc. New Jersey.
- McMahon, T.A., Greene, P.R. (1979) The influence of track compliance on running. *Journal of Biomechanics*, 12: 893-904.
- Mooney, M. (1940) A theory of large elastic deformation. *Journal of Applied Physics*, 6: 582-592.
- Muhl, Z.E. (1982) Active length-tension relation and the effect of muscle pinnation on fiber lengthening. *Journal of Morphology*, 173: 285-292.

- Otten, E. (1985) Morphometrics and force-length relations of skeletal muscles. In A. Winter et al. (eds.) International Series on Biomechanics (ISB), Biomechanics, Volume IX-A. Champaign, Ill.: Human Kinetic Publishers. pp. 27-32.
- Otten, E. (1987a) Optimal design of vertebrate and insect sarcomers. *Journal of Morphology*, 191: 49-62.
- Otten, E. (1987b) A myocybernetic model of the jaw system of the rat. *Journal of Neuroscience Methods*, 21: 287-302.
- Otten, E. (1988) Concepts and models of functional architecture in skeletal muscle. *Exercise and Sport Sciences Reviews*, 16: 89-137.
- Petrofsky, J.S., Hendershot, D.M. (1984) The interrelationship between blood pressure, intramuscular pressure, and isometric endurance in fast and slow twitch skeletal muscle in the cat. *European Journal for Applied Physiology*, 53: 106-111.
- Scott, S.H., Winter, D.A. (1991) A comparison of three muscle pennation assumptions and their effect on isometric and isotonic force. *Journal of Biomechanics*, 24: 163-167.
- Spencer, A.J.M. (1984) Continuum theory of the mechanics of fibre-reinforced composites. Courses and Lectures No. 282, Springer-Verlag Wien-New-York.
- Truesdell, C. (1965) The elements of continuum mechanics. Springer-Verlag, New-York.
- Truong, X.T., (1974) Viscoelastic wave propagation and rheologic properties of skeletal muscle. *American Journal of Physiology*, 226: 256-265.
- Vain, A. (1990) On the phenomenon of mechanical stress transmission in skeletal muscles. Research Group on Microprocessor Technology and Biomechanical Diagnostics, Tartu University, Estonia.
- Wagemans, E. (1989) Relations between architecture and the function of pennate muscles during an isometric plantar flexion of the ankle. PhD Thesis, University of Leuven, Belgium.
- Wickiewicz, T.L., Roy, R.R., Powell, P.L., Egerton, V.R. (1983) Muscle architecture of the lower limb. *Clinical Orthopaedics and Related Research*. 179: 275-283.

- Woittiez, R.D., Huijing, P.A., Rozendal R.H. (1983) Influence of muscle architecture on the length-force diagram: a model and its verification. *Pflügers Archiv für die gesamte Physiologie*, 397: 73-74.
- Woittiez, R.D., Huijing, P.A., Boom, H.B.K., Rozendal, R.H. (1984) A three dimensional muscle model: a quantified relation between form and function of skeletal muscles. *Journal of Morphology*, 182: 95-113.
- Woledge, R.C., Curtin, N.A., Homsher, E. (1985) Energetic aspects of muscle contraction. Monographs of the Physiological Society, No. 41. Academic Press, London.
- Yamada, H., (1970) Strength of biological materials. The Williams and Wilkins Company, Baltimore.
- Yin, F.C.P., Strumpf, R.K., Chew, P.H. and Zeger S.L., (1987) Quantification of the mechanical properties of noncontracting canine myocardium under simultaneous biaxial loading. *J. Biomechanics*, 20: 577-589.
- Zajac, F.E. (1989) Muscle and tendon: Properties, models, scaling, and application to biomechanics and motor control. *CRC Critical Reviews in Biomedical Engineering*, 17: 359-411.